AN ABSTRACT OF THE THESIS OF

NENG CHUN G. YAO for the Doctor of Philosophy
(Name) (Degree)

in OCEANOGRAPHY presented on February 26, 1974
(Major) (Date)

TITLE: BISPECTRAL AND CROSS-BISPECTRAL ANALYSIS OF WIND AND CURRENTS OFF OREGON COAST

Redacted for Privacy

Abstract approved: _____
Dr. Steve Neshyba

Third order spectra computed from the rotary components of winds and currents at the TOTEM buoy site off the Oregon coast provide an insight to the nonlinear, quadratic interactions within and between these vector fields. The topography of bispectra and cross-bispectra as displayed on four tri-frequency planes shows that significant non-linear interaction takes place between triples of oscillatory components over wide ranges of frequencies.

A quantitative evaluation of the energy transferred linearly and non-linearly from wind to current is obtained through the development of a set of general, complex-valued transfer functions for two-dimensional vector random processes.

Using a postulated "cause-effect" relation between measured surface wind stress and current at 14 m (within the mixed layer), the inertial frequency energy in the current field is attributed solely to

the non-linear transfer of momentum from the wind field. The transfer occurs from multiple pairs of frequencies (in the intermediate frequency range) in the wind field, with the dominant transform attributed to the wind stress oscillations at half-day and quarter-day periods. In the intermediate frequency range, 63% of the total kinetic energy in the 14 m current is derived from the wind stress through nonlinear processes, but only about 7% of the total kinetic energy in the current at 34 m, below the mixed layer, is related indirectly to this source.

Bispectral and Cross-bispectral Analysis of Wind and Currents off the Oregon Coast

by

Neng-chun G. Yao

A THESIS

submitted to

Oregon State University

in partial fulfillment of
the requirements for the
degree of

Doctor of Philosophy

June 1974

APPROVED:

Redacted for Privacy

Associate Professor of Oceanography
in charge of major

Redacted for Privacy

Dean of School of Oceanography

Redacted for Privacy

Dean of Graduate School

Date thesis is presented February 26, 1974

Typed by Suelynn Williams for Neng-Chun G. Yao

ACKNOWLEDGMENTS

This dissertation is one of the results from the TOTEM buoy research project of the School of Oceanography, Oregon State University. All the members of this project contributed in one way or another to this study. Special acknowledgment is due to Dr. Steve Neshyba, my major professor. Without his extraordinary guidance and encouragement, this study would never have been successful.

Acknowledgment is also due to my committee members, Dr. Henry Crew, Dr. Norbert A. Hartman Jr. and Dr. Lloyd W. Gay. Their guidance and assistance were vital to the success of this study. I deeply appreciate their help and understanding.

The occasional discussions with Dr. Christopher N. K. Mooers were rewarding and valuable in the development of the rotary bispectral and rotary cross-bispectral analyses techniques. For his assistance I am grateful.

I wish to extend my gratitude to Mr. Godfrey Watson and Mr. Joseph Bottero for their assistance in computer programming, and to Mr. Edwin Sobey for his assistance in proofreading this text.

Credit also should be given to the PDP-15 computer of the TOTEM project. With its limited capacity, it faithfully carried the heavy burden of the development of the new spectral analysis techniques and the data analysis work.

The understanding and encouragement of my wife, Shiu-chin, in Taiwan during the long period of my study in the United States, is highly appreciated.

My studies in the past three years have been supported by the Ministry of National Defense, Republic of China.

TABLE OF CONTENTS

TABLE OF CONTENTS CONTINUED

Chapter

LIST OF FIGURES

LIST OF FIGURES CONTINUED

LIST OF TABLES

BISPECTRAL AND CROSS-BISPECTRAL ANALYSIS OF WIND AND CURRENTS OFF OREGON COAST

I. INTRODUCTION

The inertial oscillation in the ocean is an important phenomenon of the response of the ocean to the transient applied wind stress (E. B. Krauss, 1972). It is necessary to study its characteristics and the mechanisms governing its generation and dissipation for understanding the problems concerning the atmosphere-ocean interactions. This introduction gives the definition of the inertial oscillation and a brief review of the previous published studies of this subject. It also discusses the need for new analysis techniques to investigate certain questions concerning the inertial oscillation that have not yet been answered by the previous studies.

Theoretically, if a horizontal motion is set forth inertially in the ocean, the direction of the motion will continuously turn to the right in the northern hemisphere (left in the southern hemisphere) due to the effects of the earth's rotation, until the motion becomes a circular one whose centrifugal force balances the Coriolis force caused by earth's rotation. The circular motion has a period of a half pendulum day, or a frequency equivalent to the Coriolis

paramenter, i.e., $2\Omega \sin\theta$ where the Ω is the angular velocity of the earth' rotation and θ is the latitude. The frequency of the circular motion is called inertial frequency, and the motion itself is called inertial-period motion or inertial oscillation. Since it is usually superimposed on some large scale horizontal motions to cause wave-like features, it is also called an inertial wave.

Inertial-period motions have been observed over a range of latitudes and depth in the ocean since the early thirties. Published reports up to 1967 are summarized by Webster (1968). He finds the following general agreements:

1) Horizontal "inertial" currents rotating at a rate about 2 sin (latitude) revolutions per day do exist in the ocean at various depths.

2) Typical velocities are a few centimeters per sec (cm/sec). The oscillations are intermittent but, when they do occur, the frequency is generally slightly higher than the expected frequency at the observed latitude.

3) Whenever simultaneous measurements are made at nearby locations, the records appear remarkably dissimilar except at the prominent inertial frequency. This is true for either horizontal or vertical separation of stations.

4) The occurrences do not seem to be functions of depth, bottom topography, or latitude, but their association with wind stress variation is quite obvious.

Webster (1968) thinks that inertial oscillations are essentially transient phenomena of thin vertical extent and of limited horizontal extent. He finds that the coherence of inertial motions is as high as 0.7 for stations separated by 3 kilometers but only in the neighborhood of 0.2 for sensors at the same station but with a vertical separation of more than 100 meters. He also points out that the amplitude of an inertial oscillation generated by the surface winds might be expected to diminish with depth; he states, however, that current measured by moored meters do not support such expectation. He states further that, at great depth, inertial oscillations have been observed with amplitudes comparable to those found near the surface. Perkins (1970) also finds the existence of inertial oscillations at great depth in Mediterranean, and he shows that such inertial oscillations are not relatable to the local events at ocean surface (which can produce inertial oscillation).

Inertial oscillations are found to be associated with storm passages by Collins (1968). Pollard and Millard (1970) examined the wind and current records obtained from the same location and show that, in the upper layer, the inertial oscillations responds to a sudden change in direction of high-speed wind, and they decay and drift out of phase with the wind during the period of low wind. They also show that the amplitudes of the oscillations drop sharply from 10 meters to 50 meters depth, are remarkably

independent of depth between 50 and 500 m, and decrease gradually with depth below 500 m. Thus, they do not agree with Webster (1968) about the features of inertial oscillations in deep ocean. Sakou (1970) showed that the inertial motions are well correlated with the local wind-stress variation and that the build-up and decay of the motion is accomplished over relative short periods. Analyzing moored current meter data, Sakou and Neshyba (1972) showed that the temporal variation in amplitudes of the inertial-period motion is not related to that of the semidiurnal tide and is characterized by intermittency while the tide varies more slowly in amplitude. They also find that the spatial structure of inertial motions is comparable to that found by Webster (1968).

The above observations give strong support to the hypothesis that inertial oscillations in the upper layer of the ocean are locally generated by wind. But what mechanisms determine the observed features of these oscillatory currents, such as spatial coherence and intermittency, remains to be explained.

Theoretical study of wind-generated inertial oscillations has always been fair game for many investigators. As long ago as 1905, Ekman showed that a change in wind stress would generate inertial waves as well as non-oscillatory currents. Subsequent studies on the problem of the response of ocean to the transient applied wind stress have been re-examined by Veronis (1956). He extended the

study of the transitory Ekman boundary layers with more general conditions on the duration and strength of the applied stress, and considered the partition of energy between geostrophic and non-geostrophic motions when a two-layer ocean is acted on by a body force in the upper layer for lengths of time up to one inertial period. He also considered the adjustment of the system as the inertial waves propagated horizontally away from the forced region. His theory, as the previous ones, is not able to explain in detail the spatial and temporal structure of the oscillations.

Because of the complicated structure of the wind stress variations and of inertial oscillations in the ocean, recent investigators consider these phenomena as random fields and apply random function theory for their study. Belyaev and Kolesnikov (1966) studied the spectral density of the velocity distribution on a pure drift current in a homogeneous sea of finite depth and showed that the transmission functions for the spectrum of horizontal components of current velocity had their maximum at the frequency close to the inertial frequency. They expected that a resonance, with peak intensity 10 db above surrounding level, would occur in the current spectrum within a narrow bandwidth of ± 1% of the inertial frequency. With additional considerations such as the spatial irregularity of wind field and gradient flow velocity component, Belyeav (1967) theorized that except in a rather shallow sea (say, 5 meters in the area of 30 degree of latitude), the

transfer of wind energy has little dependence on the space scales of the inhomogeneous wind field but indeed depends to a considerable extent on time scale. Fomin (1968) studied the spectral density of the distribution of the drift current components in the ocean as a function of the tangential wind stress spectrum. He concluded that the amplitudes of horizontal waves in the drift current decrease exponentially with depth, the intensity of their damping depending on the scale of non-uniformities in the wind field; hence, spatial structure is also important. The random process approach seems to be able to derive transmission functions quite well but the validity of the assumption of Gaussian processes has to be proved. While these authors show that inertial oscillations are generated by wind stress variations, their conclusion differs from those given in previous studies by suggesting that the maximum transmission of wind energy to the drift current occurs at the inertial frequency. The relationship of the vertical distribution of inertial oscillations and the spatial wind structure (Fomin, 1968) is also new. They fail to account for the observed intermittency in inertial currents.

Faller and Kaylor (1969) studied the harmonic solution of the transitory Ekman problem with a simple model. They assumed that the variations of wind stress were arbitrary and Gaussian. Their numerical model considered two cases of wind and surface stress: (1) constant eddy viscosity with surface wind stress linearly

proportional to wind speed and (2) quadratic viscosity with stress proportional to wind speed. In both cases, they showed that a large inertial oscillation develops rapidly in response to transients in the wind stress not only at the inertial frequency but also at higher frequencies. They omitted consideration of horizontal and vertical fluxes of inertial energy, and did not provide a satisfactory explanation of the observed features in inertial oscillation.

A numerical model based on the heat balance in the navifacial boundary layer has been given by Pandolfo (1969). This theory is also local, in that, it omits the effects of vertical transfer processes on horizontal variations in the dependent variables, but it does allow effects inthe reverse direction. Without considering the tide-generating force, he shows two versions of the model. In the first version, the navifacial temperature is considered to be constant in time; in the second version, it is computed from a navifacial heat budget balance condition under diurnally varying radiation input. The first version shows a persistent inertial oscillation with significant amplitude in the ocean and relatively smaller amplitude of inertial oscillation in the atmosphere. The second version shows that the dominant energy-containing modes of the flow are the inertial mode in the current and the diurnal mode with its harmonics in the wind. No diurnal mode is evident in the ocean, even though there is a diurnal source term. His results are qualitatively

consistent with the observational results of Fofonoff (1967, cited in Pandolfo, 1969). This particular result makes one doubt whether the inertial oscillations in the ocean are mainly caused by the wind stress variation at the inertial frequency.

Pollard (1970) used an analytical model similar to Veronis' (1956) but with a continuously stratified ocean. In his study the wind stress is also considered as having Gaussian characteristics. He thinks the inertial oscillations are primarily forced directly by the body force in the mixed layer, and not by its curl or divergence. The amount of energy put into the inertial period motion by such fluctuations is primarily dependent on the depth of the mixed layer and is very little affected by the stratification of the ocean or the horizontal scale of the wind stress. Thus, wind generated inertial oscillations are strongly confined to the top 100 meters or so of the ocean and decrease very rapidly with depth below the mixed layer. He concludes (1) that inertial oscillations at great depth are not generated by the action of a single storm on the surface, (2) inertial oscillations are not intensified by the variation of the Coriolis parameter with latitude as mentioned by Webster (1968) and Munk and Phillips (1968) and (3) the intermittency is due to the wind stress which can destroy as well as create the inertial oscillations. He considers that there is no transfer of energy from one mode to another. His hypothesis has been partly supported by observations

(Pollard and Millard, 1970) which show that inertial motion, once generated, decays very slowly by dispersion. They think of the new, inertially-rotating current vector as the sum of the old inertial current plus a newly wind-induced inertial current. Both the phase and amplitude of the new current depend crucially on the phase of the old current if the new wind-induced current is small; otherwise, the phase of the old current is not important. Pollard's model shows clearly that the inertial oscillations are predominantly locally generated by surface wind. The other claims remained to be verified.

Endoh and Nitta (1971) investigate analytically the response of Ekman boundary layer to an oscillating wind stress as an initial value problem. They use the time-dependent equations of motion to show that, in general, the amplitude of the response of the Ekman boundary layer to the transitory wind stress is smaller than that to the steady wind stress except for the case where the frequency of the forcing wind stress is the inertial frequency. In this case, when the resonance phenomenon occurs, the magnitude of the oscillatory velocity component increases proportionally as the square root of the time elapsed. They also think that horizontal variations of the wind stress due to the travelling atmospheric disturbances do not change the characteristics of the response. Their study strongly supports the resonance theory given by random process approach.

Very recently, W. Kraus (1972) extends the model used by Belyaev (1967) to a stratified ocean and also incorporates the variation in the air pressure. His solution shows that the velocity and sea surface response due to wind stress is more significant than that due to the air pressure; however, response to air pressure variation is evident in the low frequency range. It also shows that the inertial waves are the dominant features of the velocity response in shallow water as well as in deep water, and that they occur at all wave numbers smaller than ca. 10^{-5} cycles per meter (wave lengths larger than ca. 100 kilometers). He also shows that internal and very long surface waves are more important than the quasistatic response which corresponds to the current derived from steady-state. He concludes that both inertial and internal waves are caused mainly by the wind, and that the dispersion lines for internal, inertial and surface waves act like windows through which energy is transmitted from the sea surface into the entire water column. This model does not consider that the inertial oscillations in the ocean are locally generated, but it does support the resonance theory. It explains the high spatial coherences at the inertial frequency by indicating that the wave lengths of the inertial oscillation are larger than 100 kilometers.

In summary, most theoretical work supports the idea that inertial oscillations in the ocean are locally generated as shown by observed data. The strong arguments that these oscillations are due

to the resonance response of the drift current to the wind stress at the inertial frequency are based on the assumption of random Gaussian processes. But, how valid is this assumption? The fact that, near the sea surface, there may be no significant energy contained in the inertial frequency components of the wind stress spectrum raises the question of whether the energy contained in other components of the spectrum can be thought of as energy sources for the inertial oscillation in the ocean? The interesting new suggestion (Pollard, 1970) that decay or enhancement of the inertial oscillations depends on the phase relationship between the old and the newly-formed oscillations brings about another question of whether there are any phase-lock phenomena existing among the inertial oscillations themselves? However, the analysis of observed data has not yet been able to provide enough information to answer these questions. It is the purpose of this study to investigate some new techniques of data analysis so that such needed information can be obtained.

II. REVIEW OF EXISTING DATA ANALYSIS METHODS

The data analysis methods used in previous inertial oscillation studies are Progressive Vector Diagrams (PVD), Complex demodulation, and Spectral Analysis. A brief review of their procedures, functions, and applicabilities are given in the following sections.

A. Progressive Vector Diagrams (PVD)

The progressive vector diagram is constructed by vector addition, beginning with the initial observation at the reference point and adding successively a vector representing each ensuing observation of velocity. Such a PVD does not represent the actual path of the particle unless there is homogeneous flow. It can only show the general trend of the mean flow. The life history of the periodic motion can be traced on the PVD, but it is rather difficult to distinguish inertial oscillations from tidal oscillations. It is also impossible to assess the real values of the amplitude variations and phase relationship of the periodic motion from the PVD. However, PVD have been employed by most investigators to show the indication of inertial oscillations in a time series current record (Webster, 1968; Pollard and Millard, 1970; Sakou and Neshyba, 1972;

Pillsbury, 1972).

B. Complex Demodulation

Complex demodulation can be considered to be a method of producing a low-frequency "image" of a more or less gross-frequency component of a time series. Computationally, each frequency band of interest is shifted to zero and the result runs through a low pass filter. If $x(t)$ is the original series, the frequency-shifted series is

$$\tilde{\tilde{x}}_{\lambda}(t) = x(t)\, e^{-i\lambda t} \quad . \tag{1}$$

Where λ is the frequency of interest, and the filtered complex demodulate is the complex-valued time series

$$Z_{\lambda}(t) = \sum_{s=-m}^{m} w(s)\tilde{\tilde{x}}_{\lambda}(t+s) \quad . \tag{2}$$

Where w is the weighted factors of the low pass window. $Z_{\lambda}(t)$, being complex, may also be expressed in polar form as

$$Z_{\lambda}(t) = \left| Z_{\lambda}(t) \right| e^{-i\phi_{\lambda}(t)} \quad . \tag{3}$$

Where $\left| Z_{\lambda}(t) \right|$ and $\phi_{\lambda}(t)$ are now the amplitude and phase of $Z_{\lambda}(t)$. This technique has been discussed in detail by Granger and Hatanaka (1964), Bingam, Godfrey, and Tukey (1967). It has been widely used by various investigators (Webster, 1968; Pollard and Millard, 1970; Sakou, 1970; Sakou and Neshyba, 1972; Pillsbury, 1972).

However, as inertial oscillations are really quasi-periodic processes imbedded in a continuum of processes of all scales, a fairly long record is necessary to separate them from the "noise" of the processes. For instance, at a place of 45° of latitude such as off the Oregon coast, there are at least two other oscillations whose frequencies are very close to that of inertial oscillations. They are the diurnal and semidiurnal tides. The difference in frequency between inertial and semidiurnal tidal oscillations is 0.0025 cycles per hour (CPH) and that between the inertial and diurnal tidal oscillation is 0.017 CPH. In order to separate them clearly, a very narrow filter is required. A symmetrical window with 241 hours weights has provided satisfactory results (Pillsbury, 1972); it requires information from five days before and five days after any given time. If an oscillation lasts only one period, the demodulation output would show that the amplitude begins to change five days before the oscillation, and the changes continue for five days after the oscillation stopped. If an effort is made to resolve the generation and decay times, a short window should be used, but the frequency resolution is rather poor. Even so, the length of data necessary to resolve the inertial oscillation may still be larger than the life time of the oscillation. As a consequence, the results of complex-demodulation in dealing with the inertial oscillation are subjected to either inaccurate estimation or strong tidal contamination.

C. Spectral Analysis

Spectral analysis is the most useful technique. It is a means of summarizing and presenting in condensed form some basic properties of a long and complicated sampled function. It is deemed to be the basic tool in studying oceanographic and geophysical problems (Tukey, 1961).

The most common spectral analyses are 1) Auto-spectral analysis -- spectral analysis of a single time series and 2) Cross-spectral analysis -- spectral analysis of a pair of time series. The spectra are generally estimated through the intermediate step of computing lagged correlation and cross correlation functions; these are transformed from the time domain to the frequency domain. Then the contributions of the sample variance of a single time series at each frequency are given in form of the power density spectrum; the coherence and phase relation of the paired time series at each frequency are given as the cospectrum and quadratic spectrum or, more explicitly, coherence and phase spectra. The basic assumption for these two forms of analysis is that the processes governing the time series are Gaussian and stationary, i.e., the time series is then a linear superposition of infinite number of statistically independent Fourier components.

Two important characteristics of the spectral estimates are the shape of the spectral window and the spectral reliability. The spectral

window is the Fourier transform of the lag window by which the correlation functions are tapered (to reduce the variance of spectral estimates) and the reliability is specified by the equivalent degrees of freedom (EDF). If the elementary frequency bandwidth of a time series of N data points is $\Delta f = 1/N$ CPD (cycles per data interval), the resolved frequency bandwidth of the spectral estimates is ΔF, taking the width of the rectangle having the same maximum height and area as the spectral window, then, relationship among them is given as $EDF = 2\,\Delta F/\Delta f$. One can see that, for a definite length of time series, there exists a basic conflict between the quality of the frequency resolutions and the reliability of the estimated spectra. The real improvement one can make is to obtain a sufficiently long data record of a stationary process. The theory and methods of the spectral analysis have been discussed, for example by Jenkins and Watts (1968). They have also been used in study of inertial oscillations (Webster, 1968; Sakou and Neshyba, 1972).

Modified versions of the spectral analysis have been given by Mooers (1970, 1973). His rotary spectral spectral analysis extends auto- and cross-spectra into negative frequency range with the assumption that the positive and negative frequencies are associated with counter-clockwise and clockwise rotations respectively, and the coherence and phase for the polarized components (counter-clockwise and clockwise components) can be estimated with pairs of two-

dimensional complex-valued time series in general. One obvious advantage of this analysis is the invariance of coherence under coordinate rotation. They are also used by later investigators (Perkins, 1970; Gonella, 1972; Pillsbury, 1972), and they will be used in this study also. Details of this new technique will be discussed in the next chapter.

The problems of using spectral analysis in studying inertial oscillation are the same as those of using complex demodulation. The additional restriction is the assumption of Gaussian processes. There is evidence that most geophysical processes are not Gaussian (Tukey, 1961). For example, TOTEM wind data shows that the distribution of wind components off Oregon coast fail the normality test in most cases (Plutchak, 1972).

In view of the limitations of the above mentioned data analysis methods, and the additional information needed for the study of inertial oscillations, some other techniques are required. Bispectral and Cross-bispectral analyses suggested by Tukey (1961) appear to be useful. Their definitions, procedures and applicability will be discussed in more detail in the next chapter where a new technique for analyzing two dimensional non-Gaussian random process is developed.

III. DEVELOPMENT OF THE TECHNIQUE FOR ANALYZING TWO DIMENSIONAL NON-GAUSSIAN RANDOM PROCESSES

Most physical processes in the atmosphere and in the ocean are not strictly Gaussian in nature (Tukey, 1961) and the classical spectral analysis is not able to discern any correlation and any energy transform due to nonlinear interactions. Higher order spectral analysis techniques are needed to address such a problem. Existing techniques of bispectral and cross-bispectral analysis are particularly useful for studying the quadratic interactions (lowest order of non-linear interactions). However, they have been developed along the assumption that all the processes are real (see next section for references). For studying vector random processes, such as wind and ocean current velocity, one is forced to resolve them into scalar quantities along certain rectangular coordinates. The results of the spectral analysis from the resolved data not only depend highly on the choice of the coordinates but also are very difficult to interpret (Fofonoff, 1969; Mooers, 1970).

A new version of bispectral and cross-bispectral analysis, based on the rotary component concept given by Mooers (1970), is developed by this author to deal specifically with this particular problem. The development of the new technique and the comparison

between it and existing ones are given in the following sections. An energy transfer equation in terms of rotary spectral parameters is also given. It will show the certain amount of energy transformed due to particular quadratic interactions involved. A brief review of bispectral and cross-bispectral analysis as well as the rotary components spectral analysis will be given before the detail of the development of the new technique is presented. The newly developed technique will be used to study the quadratic interactions between the atmospheric wind and the near-surface ocean current.

A. Bispectral and Cross-bispectral Analysis

Since the suggestion made by Tukey (1961), several theorectical studies of the estimation of higher order spectra have been given (Rosenblatt and Van Ness, 1965; Van Ness, 1966; Brillinger and Rosenblatt, 1966b; Hinich and Clay, 1968; and Nagata, 1970). Bispectral analysis has been applied to the study of non-Gaussian processes in geophysical problems (Hasselmann, Munk, McDonald, 1963; McDonald, 1963; Haubrich, 1965; Murty and Henry, 1972) as well as in the other fields (Godfrey, 1965; Hasselmann, 1966; Barnett, Johnson, Naitoh, Hicks and Nute, 1971; Huber, Kleiner, Gasser and Dumermuth, 1971). Application of cross-bispectral analysis has been given by Hasselmann's (1966) study of nonlinear ship motion, and by Roden and Bendiner's (1973) study of oceanic parameters.

Higher order spectral, such as the trispectrum, have not yet been used in practical problems because they require large amounts of computing time (Nagata, 1970). Even bispectral and cross-bispectral analysis are relatively new. However, they are useful in studying the low order nonlinear interacting phenomenon associated with non-Gaussian processes.

A brief review of the definitions concerning their various functions and their physical meaning will be given in the following section. Comparisons with ordinary spectral functions are made for better understanding. An effort is made to emphasize the difference between the spectral density function of a frequency and the part of spectrum contained in a resolved frequency band around that particular frequency.[1]

1. Definitions of Bispectral Density, Biphase and Bicoherence

The spectral and bispectral density of a random process are

---

[1] The physical meaning of spectral density and the part of the spectrum contained in a resolved frequency band centered at that particular frequency are obviously different. However, in most literature, a distinction between these two quantities has not been established, and the definition of the spectral density by Jenkins and Watts (1968) adds further confusion. They define the spectral density function as the normalized power spectrum (i.e., the part of the spectrum in a resolved frequency band divided by the total variance of the random process). For the sake of consistency, their definition will not be used in this study.

defined as the frequency decomposition of the random processes second and third moment respectively (Hasselmann, et al., 1963). For example, if $\zeta(t)$ is a stationary random function of time (or distance) with zero mean, the spectral density $F(\lambda)$ and bispectral density $B(\lambda_1, \lambda_2)$ of $\zeta(t)$ are obtained from the Fourier transforms of $\zeta(t)$'s mean second- and third-order products:

$$F(\lambda) = \frac{1}{2\pi} \int_{-\infty}^{\infty} R(\tau)\, e^{-i2\pi\lambda\tau} d\tau \tag{4}$$

where $R(\tau) = \langle \zeta(t)\zeta(t+\tau) \rangle$, and

$$B(\lambda_1, \lambda_2) = \frac{1}{(2\pi)^2} \int\int_{-\infty}^{\infty} S(\tau_1, \tau_2) e^{-i2\pi(\lambda_1\tau_1 + \lambda_2\tau_2)} d\tau_1 d\tau_2 \tag{5}$$

where $S(\tau_1, \tau_2) = \langle \zeta(t)\zeta(t+\tau_1)\zeta(t+\tau_2) \rangle$.

$R(\tau)$ and $S(\tau_1, \tau_2)$ are called the covariance and bicovariance of $\zeta(t)$ respectively. τ is the time lag (or distance lag), and λ is the frequency (wave number in case that τ is the distance lag). The brackets $\langle\ \rangle$ denote means. The inverse relations of (4), (5) are

$$R(\tau) = \int_{-\infty}^{\infty} F(\lambda) e^{i2\pi\lambda\tau} d\lambda \tag{6}$$

$$S(\tau_1, \tau_2) = \int\int_{-\infty}^{\infty} B(\lambda_1, \lambda_2) e^{i2\pi(\lambda_1\tau_1 + \lambda_2\tau_2)} d\lambda_1 d\lambda_2 \tag{7}$$

For real $\zeta(t)$,

$$F(\lambda) = F^{*}(-\lambda) \tag{8}$$

$$B(\lambda_1, \lambda_2) = B^{*}(-\lambda_1, -\lambda_2) \tag{9}$$

Here * denotes the conjugate of the quantity. As $\zeta(t)$ is assumed to be stationary with real-valued components, the known symmetry relations

$$R(\tau) = R(-\tau) \tag{10}$$

$$S(\tau_1, \tau_2) = S(\tau_2, \tau_1) = S(-\tau_2, \tau_1 - \tau_2)$$

$$= S(\tau_1 - \tau_2, -\tau_2) = S(-\tau_1, \tau_2 - \tau_1) = S(\tau_2 - \tau_1, \tau_1) \tag{11}$$

follow (Hasselmann et al., 1963; Brillinger and Rosenblatt, 1966a, b). In terms of the spectral and bispectral densities, (10) and (11) become

$$F(\lambda) = F(-\lambda) \tag{12}$$

$$B(\lambda_1, \lambda_2) = B(\lambda_2, \lambda_1) = B(\lambda_1, -\lambda_1 - \lambda_2)$$

$$= B(-\lambda_1 - \lambda_2, \lambda_1) = B(\lambda_2, \lambda_1 - \lambda_2) = B(-\lambda_1 - \lambda_2, \lambda_2) \tag{13}$$

From (8), (9), (12) and (13), it follows that the spectrum density is real and is determined by its value on a half line, whereas the bispectrum density is not real (see below) but can be determined by

its values in an octant; for example

$$0 \leq \lambda_2 \leq \infty \ , \quad 0 \leq \lambda_1 \leq \lambda_2 \ .$$

The spectral density and bispectral density of a random process can also be expressed in terms of the components $dZ(\lambda)$ of the Fourier-Stieltjes representation of the random process $\zeta(t)$ as follows:

$$\zeta(t) = \int_{-\infty}^{\infty} dZ(\lambda) e^{i2\pi\lambda t}$$

$$\begin{aligned} \langle dZ(\lambda_1) dZ(\lambda_2) \rangle &= F(\lambda_1) d\lambda_1 \quad \text{if } \lambda_1 + \lambda_2 = 0 \\ &= 0 \qquad\qquad \text{if } \lambda_1 + \lambda_2 \neq 0 \end{aligned} \tag{14}$$

i.e., $\langle dZ(\lambda_1) dZ^*(\lambda_1) \rangle = F(\lambda_1) d\lambda_1$

$$\begin{aligned} \langle dZ(\lambda_1) dZ(\lambda_2) dZ(\lambda_3) \rangle &= B(\lambda_1, \lambda_2) d\lambda_1 d\lambda_2 \quad \text{if } \lambda_1 + \lambda_2 + \lambda_3 = 0 \\ &= 0 \qquad\qquad\qquad\qquad \text{if } \lambda_1 + \lambda_2 + \lambda_3 \neq 0 \end{aligned} \tag{15}$$

i.e., $\langle dZ(\lambda_1) dZ(\lambda_2) dZ^*(\lambda_1 + \lambda_2) \rangle = B(\lambda_1, \lambda_2) d\lambda_1 d\lambda_2$

(Hasselmann et al., 1963; MacDonald, 1963; Huber et al., 1971). These expressions not only provide an alternative computational procedure for estimating the spectral and bispectral densities but also suggest some physical interpretations of them. From equation (14), one can see that $F(\lambda_1) d\lambda_1$, the part of spectrum in the resolved

frequency band centered at λ_1, represents the contribution to the mean square of the random process, $\overline{\zeta^2(t)}$, from the products of its Fourier components of frequencies λ_1 and $-\lambda_1$. From equation (15) one finds that $B(\lambda_1, \lambda_2)d\lambda_1 d\lambda_2$ the part of bispectrum in the two-dimensional frequency domain bounded by the resolved frequency bands centered at λ_1 and λ_2 respectively, represents the contribution to the mean cube of the random process, $\overline{\zeta^3(t)}$, from the product of its three Fourier components of frequency λ_1, λ_2 and $-(\lambda_1+\lambda_2)$ respectively. It is interesting to note that bispectral density is a function of two independent frequencies only. Since the mean cube, or third moment, of a random process generally results from a second order interaction (Nagata, 1970), $B(\lambda_1, \lambda_2)$ is a measure of the amount of such interaction involving the random processes components whose frequencies are λ_1, λ_2 and $-(\lambda_1+\lambda_2)$ respectively. Since $B(\lambda_1, \lambda_2)$ is a complex function, (as shown by equation (15)), the interpretation of the interactions among the components would be clearer if $B(\lambda_1, \lambda_2)$ is expressed in polar form.

$$B(\lambda_1, \lambda_2) = \left| B(\lambda_1, \lambda_2) \right| e^{i\phi(\lambda_1, \lambda_2)}$$

$$\phi(\lambda_1, \lambda_2) = \tan^{-1} \frac{\mathrm{Im}[B(\lambda_1, \lambda_2)]}{\mathrm{Re}[B(\lambda_1, \lambda_2)]} \qquad (16)$$

$$-\pi \leq \phi(\lambda_1, \lambda_2) \leq \pi$$

$|B(\lambda_1, \lambda_2)|$ is the amplitude of the bispectral density. If it is not significantly larger than zero, there are no interactions among the components of the three frequencies. $\phi(\lambda_1, \lambda_2)$ is the phase of the bispectral density. It is determined by the ratio of the imaginary part of the bispectral density to the real part of it, and was formally called biphase by Barnett et al. (1971).

A third function which is derived from the normalization of the bispectrum has been given various names in literature. Hasselmann et al. (1963) relates the normalized bispectrum to the skewness with the following dimensionless equation

$$\frac{<\zeta_1 \zeta_2 \zeta_3>}{[<\zeta_1^2><\zeta_2^2><\zeta_3^2>]^{\frac{1}{2}}} = \frac{B(\lambda_1, \lambda_2)d\lambda^2}{[F(\lambda_1)F(\lambda_2)F(\lambda_3)d\lambda^3]^{\frac{1}{2}}} \qquad (17)$$

where ζ_1, ζ_2, ζ_3 are the frequency components of $\zeta(t)$ obtained by passing it through three filters centered on λ_1, λ_2, $\lambda_3 = -\lambda_1 - \lambda_2$ and of bandwidth $d\lambda$. Godfrey (1965) calls the result of the same equation the bispectral coefficient. Since it is a measure of skewness of the random process, it is also called the bispectral skewness (Hinich and Clay, 1968). The name bicoherence also appears in the published papers (Haubrich, 1965; Barnett et al., 1971; Huber et al., 1971), but it has been defined rather inconsistently by various authors. Haubrich (1965) and Barnett et al. (1971) show

$$bic^2(\lambda_1, \lambda_2) = \frac{\left| B(\lambda_1, \lambda_2) \right|^2}{< \left| X(\lambda_1) \right|^2 \left| X(\lambda_2) \right|^2 \left| X(\lambda_1 + \lambda_2)^2 \right| >} \qquad (18)$$

where $bic(\lambda_1, \lambda_2)$ is the bicoherence. Here $(B(\lambda_1, \lambda_2)$ is defined as bispectrum (rather than bispectral density) and $B(\lambda_1, \lambda_2) = < X(\lambda_1) \cdot X(\lambda_2) X^*(\lambda_1 + \lambda_2) >$ and $X(\lambda_j)$ is the Fourier coefficient of the random process obtained from discrete Fourier transform.

Equation (18) is essentially the same one with which Hinich and Clay (1968) used to define the bispectral skewness, except they explicitly express as the spectrum over the resolved band centered at frequency λ. Equation (18) appears differently from equation (17) given by Hasselmann et al. (1963) because different scales of Fourier transform parameters are used. (See Hinich and Clay (1968) for details.) Physically, however, they are the same. Thus by definition, the bicoherence or bispectral skewness is a dimensionless real value with a range from zero to one.

A definition given by Huber et al. (1971) seems different. He also calls the bicoherence the normalized bispectrum, but he gives a mathematical relationship as

$$bic(\lambda_1, \lambda_2) = \frac{B(\lambda_1, \lambda_2)}{(F(\lambda_1)F(\lambda_2)F(\lambda_3))^{\frac{1}{2}}} \qquad (19)$$

where $B(\lambda_1, \lambda_2)$ is the bispectral density and $F(\lambda_j)$ is the spectral

density as defined by equations (13) and (14). Bicoherence such defined has a dimension of $(d\lambda)^{-\frac{1}{2}}$ and is not a real value. The amplitude varies from zero to $(d\lambda)^{-\frac{1}{2}}$. For the sake of consistency, this definition of bicoherence will not be used. In this study, bicoherence will be considered as the dimensionless absolute value of the normalized bispectrum or bispectral skewness defined in equation (17).

Hinich and Clay (1968) show that if the component at $\lambda_1 + \lambda_2$ is basically due to a multiplicative interaction between the components of the random process at λ_1 and λ_2, then the value of bicoherence is equal to one and the biphase is the phase lag of the nonlinear process.

$$\phi(\lambda_1, \lambda_2) = \phi(\lambda_1) + \phi(\lambda_2) - \phi(\lambda_3) \tag{20}$$

where $\phi(\lambda_j)$ are the phases of the interacting components of the random process. The case, in which $\phi(\lambda_1, \lambda_2) = 0$ or π is called phase locking by Barnett et al. (1971).

2. Definitions of Cross-bispectral Density, Cross-biphase, and Cross-bicoherence

The definitions concerning cross-bispectrum have been derived following the same line of the bispectral analysis by Hasselmann (1966) and Roden and Bendiner (1973). For stationary random functions of time (or distance) with zero mean, say $x(t)$, $y(t)$, $z(t)$, the cross-

spectral density $F_{xy}(\lambda)$ and cross-bispectral density $B_{xyz}(\lambda_1, \lambda_2)$ are defined respectively as the Fourier transforms of $R_{xy}(\tau)$, covariance of $x(t)$ and $y(t)$; and $S_{xyz}(\tau_1, \tau_2)$, cross-bicovariance of $x(t)$, $y(t)$ and $z(t)$:

$$F_{xy}(\lambda) = \frac{1}{2\pi} \int_{-\infty}^{\infty} R_{xy}(\tau) e^{-i2\pi\lambda\tau} d\tau \tag{21}$$

where

$$R_{xy}(\tau) = < x(t+\tau) y(t) > , \tag{22}$$

$$B_{xyz}(\lambda_1, \lambda_2) = \frac{1}{(2\pi)^2} \iint_{-\infty}^{\infty} S_{xyz}(\tau_1, \tau_2) e^{-2\pi(\lambda_1\tau_1 + \lambda_2\tau_2)} d\tau_1 d\tau_2 \tag{23}$$

where

$$S_{xyz}(\tau_1, \tau_2) = < x(t+\tau_1) y(t+\tau_2) z(t) > . \tag{24}$$

In terms of the components of the Fourier Stietjes representation of

$$x(t) = \int_{-\infty}^{\infty} dZ_x(\lambda) e^{i2\pi\lambda t}$$

$$y(t) = \int_{-\infty}^{\infty} dZ_y(\lambda) e^{i2\pi\lambda t}$$

$$z(t) = \int_{-\infty}^{\infty} dZ_z(\lambda) e^{i2\pi\lambda t}$$

then

$$< dZ_x(\lambda_1) dZ_y(\lambda_2) > = F_{xy}(\lambda_1) d\lambda_1, \text{ if } \lambda_1 + \lambda_2 = 0$$

$$= 0 \quad \text{if } \lambda_1 + \lambda_2 \neq 0 \tag{25}$$

$$\text{i.e. } \langle dZ_x(\lambda_1) dZ_y^*(\lambda_1) \rangle = F_{xy}(Y_1) d\lambda_1$$

$$\langle dZ_x(\lambda_1) dZ_y(\lambda_2) dZ(\lambda_3) \rangle = B_{xyz}(\lambda_1, \lambda_2) d\lambda_1 d\lambda_2 \text{ if } \lambda_1 + \lambda_2 + \lambda_3 = 0$$

$$= 0 \quad \text{if } \lambda_1 + \lambda_2 + \lambda_3 \neq 0 \tag{26}$$

$$\langle dZ_x(\lambda_1) dZ_y(\lambda_2) dZ_z^*(\lambda_1 + \lambda_2) \rangle = B_{xyz}(\lambda_1, \lambda_2) d\lambda_1 d\lambda_2 .$$

The symmetry relations are

$$R_{xy}(\tau) = R_{yx}(-\tau) \tag{27}$$

$$S_{xyz}(\tau_1, \tau_2) = S_{yxz}(\tau_2, \tau_1) = S_{yzx}(\tau_2 - \tau_1, -\tau_1)$$

$$= S_{zyx}(-\tau_2, \tau_1 - \tau_2) \tag{28}$$

and hence

$$F_{xy}(\lambda) = F_{yx}(-\lambda) \tag{29}$$

$$B_{xyz}(\lambda_1, \lambda_2) = B_{yxz}(\lambda_2, \lambda_1) = B_{yzx}(\lambda_2, -\lambda_1 - \lambda_2)$$

$$= B_{zyx}(-\lambda_1 - \lambda_2, \lambda_1) . \tag{30}$$

The physical meaning of cross-spectral density is well known. It is a complex quantity. Its amplitude shows whether a frequency component in one random process (say x(t)) is associated with larger or smaller amplitudes at the same frequency in other random process (say y(t)). The phase shows whether the frequency component in one

random process lags or leads the component at the same frequency in the other random process. As pointed out by Roden and Bendiner (1973), the cross-bicorrelation measures the joint interaction between three sets of variables displaced relative to each other in the time domain and gives an indication of the persistence of the interaction. The cross-bispectral density is a measure of such interaction in frequency domain. If any two of the three random processes are the same, then the cross-bispectral density gives the measure of the quadratic interaction between two frequency components, say λ_1, λ_2 in one random process, and the frequency component of $-(\lambda_1+\lambda_2)$ in the other random process. If all three are the same process, the cross-bispectral density is just the bispectral density of the process; subsequently, all the subscripts in the formula can be dropped.

Cross-bispectral density is also a complex function. Its phase can be defined the same way as the biphase:

$$\phi_{xyz}(\lambda_1, \lambda_2) = \tan^{-1} \frac{\mathrm{Im}[\, B_{xyz}(\lambda_1, \lambda_2)\,]}{\mathrm{Re}[\, B_{xyz}(\lambda_1, \lambda_2)]} \tag{31}$$

where $\phi_{xyz}(\lambda_1, \lambda_2)$ is called cross-biphase by Roden and Bendiner (1973).

By the same analogy, the cross-bicoherence can be defined as

$$\mathrm{bic}^2_{xyz}(\lambda_1, \lambda_2) = \frac{\left| B_{xyz}(\lambda_1, \lambda_2)d\lambda_1 d\lambda_2 \right|^2}{(F_x(\lambda_1)F_y(\lambda_2)F_z(\lambda_3)d\lambda^3)}$$

where $bic_{xyz}(\lambda_1, \lambda_2)$ is the cross-bicoherence, $B_{xyz}(\lambda_1, \lambda_2)$ is the cross-bispectral density and $F_x(\lambda_1), F_y(\lambda_2), F_z(\lambda_3)$ are the spectral densities of random processes $x(t)$, $y(t)$ and $z(t)$ at frequencies λ_1, λ_2, λ_3 respectively. The cross-bicoherence is, by definition, a real valued quantity equal to or larger than zero. In cases where the nonlinear process is due to quadratic interaction between the independent frequencies λ_1 and λ_2 such that the component at $\lambda_1 + \lambda_2$ is equal to or proportional to the product of the components at λ_1 and λ_2, the cross-bicoherence (and also the bicoherence) is unity. It follows, therefore, that if the cross-bicoherence differs from unity significantly, the nonlinear processes cannot be of the simple type (Roden and Bendiner, 1973).

The interpretation of cross-biphase can also be obtained by the analogy to that of biphase. In general, one can consider that the bispectral analysis is the special case of the cross-bispectral analysis.

B. Derivation of Rotary Bispectral and Rotary Cross-bispectral Functions

1. Fourier Representation of Rotary Components of a Two-dimensional Vector Random Process

The idea of rotary components was introduced by Mooers (1970). His method is based on a decomposition of the complex-valued series into polarized components. For a two-dimensional velocity vector

expressed as a complex valued quantity, oscillatory elements execute periodic, elliptical orbits in the hodograph plane. The trajectory of the velocity vector in this plane then is composed of a superposition of those ellipses of all oscillatory elements. The velocity vector series can be decomposed, for each frequency, into two counter-rotating circular components. Each component has its own amplitude and phase. The counter-clockwise rotating components correspond to oscillatory motions at positive frequencies; the clockwise rotating components correspond to those at negative frequencies. In other words, the oscillatory element at each frequency is composed of two counter rotating components which have angular velocities equal to the positive and negative angular frequencies respectively (Gonella, 1972).

The oscillatory elements can be represented as the Fourier components of the velocity vector series (Perkins, 1970). Gonella (1972) gives the Fourier transform, for the angular velocity ω of the complex time series $\vec{u}(t)$ as

$$U(\omega) = \frac{1}{T}\int_0^T \vec{u}(t)e^{-i\omega t}dt$$

and

$$U(\omega) = \left| U(\omega)\right| e^{i\Phi\omega} \tag{33}$$

where T is the duration of the complex time series $\vec{u}(t)$, and

$$\vec{u}(t) = u_1(t) + iu_2(t)$$

u_1 and u_2 are the scalar components of $\vec{u}$ along horizontal rectangular axes $0x_1, 0x_2$. The complex coefficient $U(\omega)$ gives the amplitude $|U(\omega)|$ and phase Φ_ω at the initial time, of the rotary components with an angular velocity ω. The angular velocity ω will be an integral multiple, positive or negative, of $2\pi/T$. $U(\omega)$ can be readily obtained in terms of the sine and cosine Fourier coefficients of $u_1(t)$ and $u_2(t)$ corresponding to the angular frequency $\sigma = |\omega|$,

$$U(\omega) = \frac{1}{T}\int_0^T [u_1(t) + iu_2(t)][\cos\omega t - i \sin \omega t]\, dt$$

$$= [A_1(\omega) + B_2(\omega)] + i[A_2(\omega) - B_1(\omega)] \qquad (34)$$

where

$$A_j(\omega) = \frac{1}{T}\int_0^T u_j(t)\cos\omega t dt$$

$$B_j(\omega) = \frac{1}{T}\int_0^T u_j(t)\sin\omega t dt$$

A_j and B_j are the sine and cosine Fourier coefficients of $u_j(t)$.

Let $$U_+(\sigma) = U(\omega) \text{ if } \omega = \sigma$$

$$U_-(\sigma) = U(\omega) \text{ if } \omega = -\sigma$$

Then
$$U_+(\sigma) = [A_1(\sigma) + B_2(\sigma)] + i[A_2(\sigma) - B_1(\sigma)]$$
$$U_-(\sigma) = [A_1(\sigma) - B_2(\sigma)] + i[A_2(\sigma) + B_1(\sigma)] \qquad (35)$$

$U_+(\sigma)$, $U_-(\sigma)$ are complex quantities. They represent the amplitude and the phase of the rotary components of angular frequencies $+\sigma$ and $-\sigma$ respectively. They are called rotary Fourier coefficients in this study. It is obvious that the rotary Fourier coefficient of $(+\sigma)$ does not necessarily equal the conjugate of the rotary Fourier coefficient of $(-\sigma)$.

The inverse of Fourier transform will be

$$u(t) = u_1(t) + iu_2(t) = \sum_{n=-\infty}^{+\infty} U(\omega)e^{i\omega t} \tag{36}$$

where $$\omega = \frac{2\pi n}{T} \quad .$$

In terms of rotary Fourier coefficient

$$u_1(t) + iu_2(t) = \sum_{\sigma=0}^{\infty} U_+(\sigma)e^{i\sigma t} + U_-(\sigma)e^{-i\sigma t} \quad . \tag{37}$$

If $u_{1\sigma}(t)$, $u_{2\sigma}(t)$ represent the scalar components of the oscillatory element with angular frequency σ, then the ellipse equation is

$$u_{1\sigma}(t) + iu_{2\sigma}(t) = U_+(\sigma)e^{+i\sigma t} + U_-(\sigma)e^{-i\sigma t} \tag{38}$$

By equation (35), one can see[2]

---

[2]The amplitude of rotary component derived in this study is twice of that given by Gonella (1972).

$$u_{1\sigma}(t) = 2[A_1(\sigma)\cos\sigma t + B_1(\sigma)\sin\sigma t]$$
$$u_{2\sigma}(t) = 2[A_2(\sigma)\cos\sigma t + B_2(\sigma)\sin\sigma t] \quad (39)$$

The rotary Fourier coefficients derived here are the linear functions of the sine and cosine coefficients of the scalar components of the vector time series. Since the scalar components are resolved along an arbitrary chosen rectanglar axes, their Fourier coefficients are not independent of the coordinates. In fact, if one rotates the coordinate, the Fourier coefficients will obey the same coordinate transform as the scalar components (Fofonoff, 1969), i.e.:

$$A_1' = A_1 \cos\theta + A_2 \sin\theta$$
$$A_2' = -A_1 \sin\theta + A_2 \cos\theta$$
$$B_1' = B_1 \cos\theta + B_2 \sin\theta \quad (40)$$
$$B_2' = -B_1 \sin\theta + B_2 \cos\theta$$

where θ is the angle (measured counterclockwise) between the primed and unprimed axes. Substituting equation (40) into equation (35) yields

$$U_+'(\sigma) = U_+(\sigma)e^{-i\theta}$$
$$U_-'(\sigma) = U_-(\sigma)e^{-i\theta} \quad (41)$$

From equation (41), it is obvious that the amplitude of the rotary

Fourier coefficient is invariant under the coordinate rotation but the phase does change by an amount equal to the angle of the rotation; i.e.

$$\left| U_{\pm}'(\sigma) \right| = \left| U_{\pm}(\sigma) \right|$$

$$\Phi'_{\pm\sigma} = \Phi_{\pm\sigma} - \theta \tag{42}$$

In the terminology of an ellipse, $\left| \left| U_{+}(\sigma) \right| + \left| U_{-}(\sigma) \right| \right|$ is the length of semimajor axis of the ellipse, and $\left| \left| U_{+}(\sigma) \right| - \left| U_{-}(\sigma) \right| \right|$ is the length of its semiminor axis. The orientation of the major axes, from the data coordinate system, is

$$\frac{\Phi_{\sigma_+} - \Phi_{\sigma_-}}{2}$$

and that of the minor axes is

$$\frac{\Phi_{\sigma_+} + \Phi_{\sigma_-}}{2}$$

(Mooers, 1970). Therefore, if $\left| U_{+}(\sigma) \right|$ equals $\left| U_{-}(\sigma) \right|$ the oscillatory element is in unidirectional oscillation; if either $\left| U_{+}(\sigma) \right|$ or $\left| U_{-}(\sigma) \right|$ is zero, the oscillatory element describes pure circular motion rotating in the direction of the non-zero component. For a scalar random process, the rotary Fourier coefficients will be the same as the ordinary Fourier coefficients (see equation 35). In this case,

$$U_{+}(\sigma) = U_{-}^{*}(\sigma), \tag{43}$$

it is a special unidirectional oscillation.

2. Advantages of Using Rotary Component Method for Spectral Analysis of Two Dimensional Vector Random Processes

For a two-dimensional vector random process, spectral analysis can be conducted on the scalar component series resolved along rectangular coordinates. The spectral functions generated from the two scalar series are dependent upon the orientation of the coordinates along which the observations were made or analyzed. Also, the two component series are not independent. These problems were noted by Fofonoff (1969). He proposes that, for each frequency, a normal set of coordinates can be introduced such that the non-invariant cospectrum between the scalar component series vanishes. This is a tedious method for analyzing one set of such vector random process alone, to say nothing of analyzing a pair of them. The rotary component method can overcome these problems as shown by Perkins (1970), Mooers (1970, 1973) and Gonella (1972).

Since certain oscillatory components in the ocean current are expected to have regular motion with one sense of rotation, for instance inertial oscillation and tidal oscillations, this method appears more adequate to analyze the oceanic current velocity data than the resolved scalar component series method. The rotary spectral functions and rotary cross-spectral functions have been well defined and discussed by Gonella (1972) and Mooers (1973). Some of these functions will be reviewed briefly in the next section,

while the rotary component method is extended to third order spectral analysis.

3. Rotary Spectral- and Rotary Bispectral-Functions

In earlier sections, the spectral and bispectral densities have been defined as the frequency decomposition of a real random process' second and third moments respectively. For a vector random process, the same operations yield general second and third-order spectral densities (Brillinger and Rosenblatt, 1966b). If the decomposition is carried out in terms of angular velocities on the covariance and bicovariance functions of a two dimensional random process, the results are defined as the rotary spectral density and the rotary bispectral density respectively. Let $\vec{u}(t)$ be the stationary two-dimensional vector random process. Its covariance is defined as

$$\begin{aligned} \vec{R}(\tau) &= < \vec{u}^{*}(t)\vec{u}(t + \tau) > \\ &= < \vec{u}(t)\vec{u}^{*}(t - \tau) > \end{aligned} \tag{44}$$

(Bendat and Piersol, 1966). By the same token, its bicovariance is defined as

$$\begin{aligned} \vec{S}(\tau_1, \tau_2) &= < \vec{u}^{*}(t)\vec{u}(t + \tau_1)\vec{u}(t, + \tau_2) > \\ &= < \vec{u}^{*}(t)\vec{u}(t + \tau_2)\vec{u}(t + \tau_1) > . \end{aligned} \tag{45}$$

The second and third-order spectral densities of $\vec{u}(t)$ are then

$$P(\omega) = \frac{1}{2\pi}\int_{-\infty}^{\infty} \vec{R}(\tau)e^{-i\omega\tau}d\tau \qquad (46)$$

and

$$RB(\omega_1, \omega_2) = \frac{1}{(2\pi)^2}\iint_{-\infty}^{\infty} \vec{S}(\tau_1, \tau_2)e^{-i(\omega_1\tau_1+\omega_2\tau_2)}d\tau_1 d\tau_2 \qquad (47)$$

where ω is the angular velocity of an oscillatory component.

Expressed in terms of the Fourier-Stieltjes representations,

$$\vec{u}(t) = \sum_{n=-\infty}^{\infty} U(\omega)e^{i\omega t}, \text{ with}^3\ \omega = \frac{2\pi n}{T}$$

$$< U(\omega_1)\, U^*(\omega_2) > = P(\omega)d\omega \quad \text{if } \omega_1 = \omega_2$$

$$= 0 \qquad \text{if } \omega_1 \neq \omega_2 \qquad (48)$$

and

$$< U(\omega_1)\, U(\omega_2)\, U^*(\omega_3) > = RB(\omega_1, \omega_2)d\omega^2 \quad \text{if } \omega_1+\omega_2 = \omega_3$$

$$= 0 \qquad \text{if } \omega_1+\omega_2 \neq \omega_3 . \qquad (49)$$

For $\omega = \pm\sigma$, equation (48) is rewritten as

$$P_{u\pm u\pm}(\sigma)d\sigma = <U_\pm(\sigma)U_\pm^*(\sigma)> = <\left|U_\pm(\sigma)\right|^2> \qquad (50)$$

where $P_{u+u+}(\sigma)$ and $P_{u-u-}(\sigma)$ are the rotary spectral densities of

---

[3] In practice, is limited by the Nyquist frequency, Ny i.e.,

$$\frac{-1}{2\Delta t} \leq \frac{n}{T} \leq \frac{1}{2\Delta t}, \quad -\frac{\pi}{\Delta t} \leq \omega \leq \frac{\pi}{\Delta t}$$

where Δt is the data interval.

u(t) for positive and negative angular velocities respectively. In view of the characteristics of the rotary Fourier coefficients given in the previous section, it is obvious that

1) $P_{u+u+}(\sigma)$, $P_{u-u-}(\sigma)$ are independent of the coordinates along which the scalar components of u(t) are measured.

2) $P_{u+u+}(\sigma)$ is not equal to $P_{u-u-}(\sigma)$ in general except when the angular frequency is zero or when the oxcillatory element at this frequency is unidirectional. Also the sum of $P_{u+u+}(\sigma)d\sigma$ and $P_{u-u-}(\sigma)d\sigma$ is the contribution to the total variance of u(t) from the oscillatory element of the frequency[4] σ.

In case of the third-order spectral density, all three angular velocities can have both positive and negative values. The constraint relationships of ω_j, j = 1, 2, 3, have eight permutations:

---

[4]Gonella (1972) gives a complete set of functions of the rotary component method for spectral and cross-spectral analysis. $P_{u\pm u\pm}(\sigma)d\sigma$ defined here is twice the value of his mean kinetic energy spectrum $S_{\pm}(\sigma)$:

$$S_{\pm}(\sigma) = \tfrac{1}{2} < U_{\pm}(\sigma)U_{\pm}^{*}(\sigma) >.$$

He also shows that all the rotary spectral- and rotary cross spectral functions can be related linearly to the ordinary spectral- and cross spectral functions of the resolved scalar component series.

It should also be noted that common usage in spectral analysis is to refer to the second order spectral estimates as "energy" even though the described quantity does not have "energy" dimensions. This conventional terminology is also adopted in this study, e.g., the energy spectrum of wind stress.

$$
\begin{array}{ll}
|\sigma_2| > |\sigma_1| & |\sigma_2| < |\sigma_1| \\
1)\ \sigma_1 + \sigma_2 = \sigma_3 & 2)\ \sigma_1 + \sigma_2 = \sigma_3 \\
3)\ -\sigma_1 + \sigma_2 = \sigma_3 & 4)\ \sigma_1 - \sigma_2 = \sigma_3 \\
5)\ \sigma_1 - \sigma_2 = -\sigma_3 & 6)\ -\sigma_1 + \sigma_2 = -\sigma_3 \\
7)\ -\sigma_1 - \sigma_2 = -\sigma_2 & 8)\ -\sigma_1 - \sigma_2 = -\sigma_3
\end{array}
\tag{51}
$$

The sum of these permutations can be seen clearer in a frequency domain diagram of Euclidean representation (Fig. 1).

Due to the symmetric relation of ω_1 and ω_2 (Equation 49) there are only four independent permutations, i.e., the third spectral density of a two-dimensional vector random process can be defined in the half-plane of the frequency domain.[5] Correspondingly, the rotary bispectral densities covering the four independent sections in the frequency domain are

---

[5] The third order spectral density of the two dimensional vector random processes can also be represented by the linear combination of ordinary bispectral density and cross-bispectral density of the vector's resolved scalar component series. (See Appendix I for details.) There are six independent bispectral and cross-bispectral densities for each such combination. (In case of three different vector processes, the independent functions are eight cross-bispectral densities among the various scalar component series of the different vector processes.) It is not only very tedious to compute them but also very difficult to interpret them.

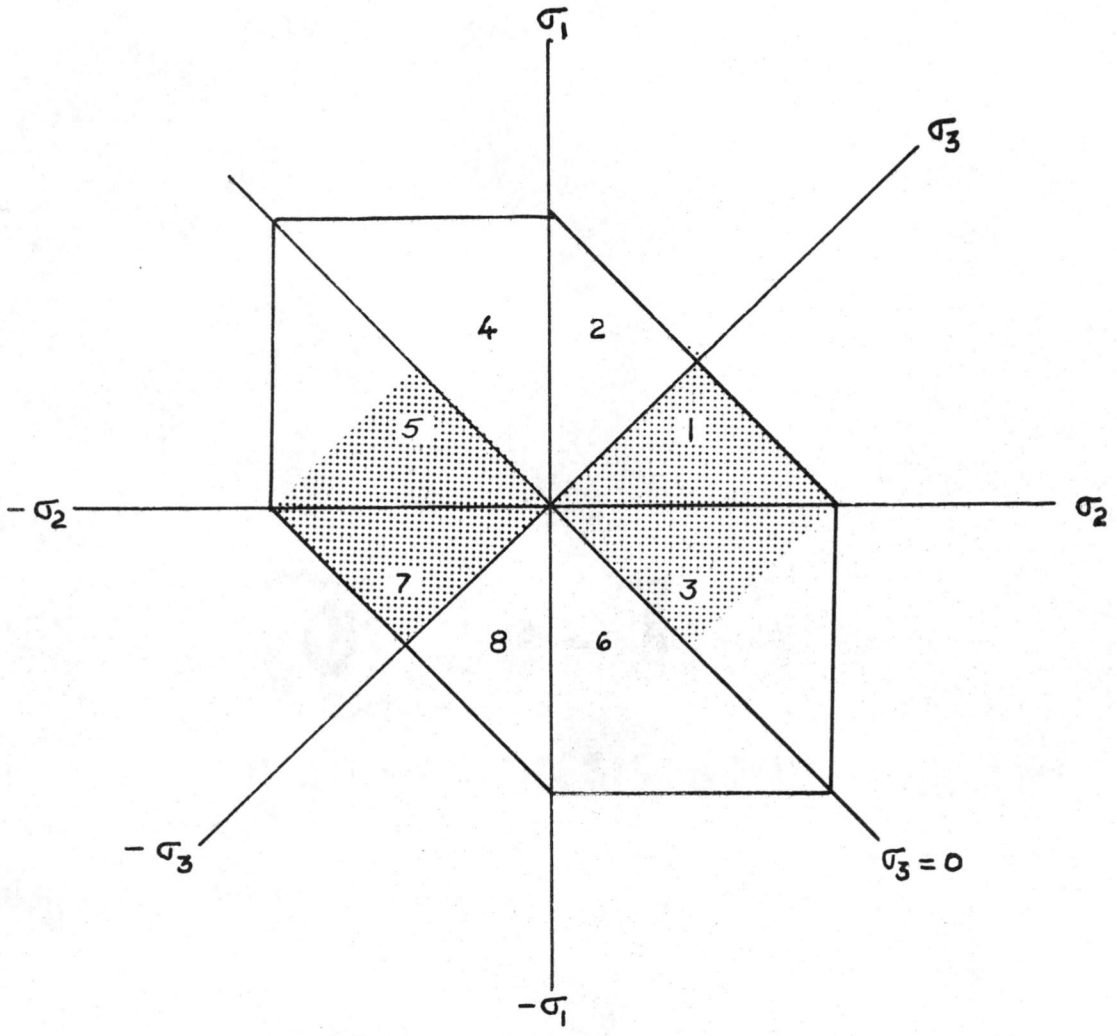

$$0 \leq \sigma_j \leq Ny \ , \ j = 1, \ 2, \ 3$$

$$\text{and } [\pm \sigma_1] + [\pm \sigma_2] = [\pm \sigma_3]$$

Figure 1. Frequency domain of the rotary bispectrum and rotary cross-bispectrum. The symmetric sections are 1 and 2; 3 and 4; 5 and 6; 7 and 8. (The shaded areas comprise the portions of the half-plane which will be examined; in this study; the unshaded portions of 3 and 5 would involve interactions between frequency components which are found statistically not significant.)

$$RB(\sigma_1,\sigma_2)d\sigma^2 = < U_+(\sigma_1)U_+(\sigma_2)U_+^*(\sigma_3)>,\ \sigma_1+\sigma_2=\sigma_3$$

$$RB(-\sigma_1,\sigma_2)d\sigma^2 = < U_-(\sigma_1)U_+(\sigma_2)U_+^*(\sigma_3)>,\ -\sigma_1+\sigma_2=\sigma_3$$

$$|\sigma_2|>|\sigma_1|$$

$$RB(\sigma_1,-\sigma_2)d\sigma^2 = < U_+(\sigma_1)U_-(\sigma_2)U_-^*(\sigma_3)>,\ \sigma_1-\sigma_2=\sigma_3$$

$$|\sigma_2|>|\sigma_1|$$

$$RB(-\sigma_1,-\sigma_2)d\sigma^2 = < U_-(\sigma_1)U_-(\sigma_2)U_-^*(\sigma_3)>,\ -\sigma_1-\sigma_2=-\sigma_3$$

Since the rotary bispectral density is a complex quantity, it can be expressed in polar form, for instance:

$$RB(\sigma_1,\sigma_2) = \left| RB(\sigma_1,\sigma_2)\right| e^{iR\phi(\sigma_1,\sigma_2)} \tag{53}$$

where $R\phi(\sigma_1,\sigma_2)$ is defined as rotary biphase:

$$R\phi(\sigma_1,\sigma_2) = \tan^{-1}\frac{Im[RB(\sigma_1,\sigma_2)]}{Re[RB(\sigma_1,\sigma_2)]}. \tag{54}$$

The corresponding bicoherence is defined as the rotary bicoherence, $Rbic(\sigma_1,\sigma_2)$:

$$Rbic^2(\sigma_1,\sigma_2) = \frac{\left| RB(\sigma_1,\sigma_2)d\sigma^2\right|^2}{(P_{u+u+}(\sigma_1)P_{u+u+}(\sigma_2)P_{u+u+}(\sigma_3)d\sigma^3)} \tag{55}$$

It is easy to see that the amplitude of the rotary bispectral density and the rotary bicoherence are independent of the rectangular

coordinates along which the scalar components of the vector random process are measured. However, the rotary biphase is not an independent quantity. If the coordinate system is rotated by some angle, the value of the rotary biphase will change the same amount in the direction opposite to that of the coordinate rotation. This can be verified by using equations (41), (52), (53) and (54).

The rotary bispectrum is then the measure of low order nonlinear interactions among the rotary components of the oscillatory elements.

4. Rotary Cross-spectral Functions and Rotary Cross-bispectral Functions

The rotary cross-spectral function and rotary cross-bispectral functions are obtained here following the same line of reasoning as in the previous section. Let $\vec{x}(t)$, $\vec{y}(t)$ and $\vec{z}(t)$ be the stationary two-dimensional random processes. The cross-covariance is defined as (Bendat and Piersol, 1966).

$$\vec{R}_{xy}(\tau) = < \vec{x}^{*}(t)\vec{y}(t+\tau) > = < \vec{x}(t)\vec{y}^{*}(t-\tau) > \tag{56}$$

and the cross-bicovariance is then

$$\begin{aligned} \vec{S}_{xyz}(\tau_1, \tau_2) &= < \vec{x}^{*}(t)\vec{y}(t+\tau_1)\vec{z}(t+\tau_2) > \\ &= < \vec{x}^{*}(t)\vec{z}(t+\tau_2)\vec{y}(t+\tau_1) > \\ &= \vec{S}_{xzy}(\tau_2, \tau_1) \end{aligned} \tag{57}$$

$$P_{xy}(\omega) = \frac{1}{2\pi}\int_{-\infty}^{\infty} \vec{R}_{xy}(\tau)e^{-i\omega\tau}d\tau \tag{58}$$

$$RB_{xyz}(\omega_1, \omega_2) = \frac{1}{(2\pi)^2}\int\int_{-\infty}^{\infty} \vec{S}_{xyz}(\tau_1, \tau_2)e^{-i(\omega_1\tau_1+\omega_2\tau_2)}d\tau_1 d\tau_2 \tag{59}$$

where $P_{xy}(\omega)$ is the cross-spectral density between $\vec{x}(t)$ and $\vec{y}(t)$, and $RB_{xyz}(\omega_1, \omega_2)$ is the cross-bispectral density among $\vec{x}(t)$, $\vec{y}(t)$ and $\vec{z}(t)$.

Expressed in terms of the Fourier-Stieltjes representations

$$\begin{aligned}
\vec{x}(t) &= \sum_{n=-\infty}^{\infty} U_x(\omega)e^{i\omega t} \\
\vec{y}(t) &= \sum_{n=-\infty}^{\infty} U_y(\omega)e^{i\omega t} \\
\vec{z}(t) &= \sum_{n=-\infty}^{\infty} U_z(\omega)e^{i\omega t}
\end{aligned} \tag{60}$$

$$\begin{aligned}
< U_x(\omega_1)U_y^*(\omega_2) > &= P_{xy}(\omega_1)d\omega \quad \text{if } \omega_1 = \omega_2 \\
&= 0 \qquad\qquad\quad \text{if } \omega_1 \neq \omega_2
\end{aligned} \tag{61}$$

$$\begin{aligned}
< U_x(\omega_1)U_y(\omega_2)U_z^*(\omega_3) > &= RB_{xyz}(\omega_1, \omega_2)d\omega^2 \quad \text{if } \omega_1+\omega_2 = \omega_3 \\
&= 0 \qquad\qquad\qquad\quad \text{if } \omega_1+\omega_2 \neq \omega_3
\end{aligned} \tag{62}$$

it is obvious that,

$$P_{xy}(\omega) = P^*_{yx}(\omega)$$

and

$$RB_{xyz}(\omega_1, \omega_2) = RB_{xzy}(\omega_2, \omega_1) \tag{63}$$

For $\omega = \pm\sigma$, equation (59) is rewritten as

$$P_{x\pm y\pm}(\sigma)d\sigma = \langle U_{x\pm}(\sigma)U_{y\pm}^{*}(\sigma)\rangle \tag{64}$$

where $P_{x+y+}(\sigma)$ and $P_{x-y-}(\sigma)$ are the rotary cross spectral densities between x(t) and y(t) for the positive and negative angular frequencies respectively.

In the case of rotary cross-bispectral density, the permutation and symmetric relations are the same as those for rotary bispectral density. There,

$$RB_{xyz}(\sigma_1,\sigma_2)d\sigma^2 = \langle U_{x+}(\sigma_1)U_{y+}(\sigma_2)U_{z+}^{*}(\sigma_3)\rangle$$

$$\sigma_1+\sigma_2=\sigma_3$$

$$RB_{xyz}(-\sigma_1,\sigma_2)d\sigma^2 = \langle U_{x-}(\sigma_1)U_{y+}(\sigma_2)U_{z+}^{*}(\sigma_3)\rangle$$

$$-\sigma_1+\sigma_2=\sigma_3 \quad |\sigma_2|>|\sigma_1|$$

$$RB_{xyz}(\sigma_1,-\sigma_2)d\sigma^2 = \langle U_{x+}(\sigma_1)U_{y-}(\sigma_2)U_{z-}^{*}(\sigma_3)\rangle \tag{65}$$

$$\sigma_1-\sigma_2=-\sigma_3 \quad |\sigma_2|>|\sigma_1|$$

$$RB_{xyz}(-\sigma_1,-\sigma_2)d\sigma^2 = \langle U_{x-}(\sigma_1)U_{y-}(\sigma_2)U_{z-}^{*}(\sigma_3)\rangle$$

$$-\sigma_1-\sigma_2=-\sigma_3$$

and

$$RB_{xyz}(\sigma_1,\sigma_2) = \left|RB_{xyz}(\sigma_1,\sigma_2)\right| e^{iR\phi_{xyz}(\sigma_1,\sigma_2)} \tag{66}$$

where $R\phi_{xyz}(\sigma_1, \sigma_2)$ is defined as rotary cross-biphase

$$R\phi_{xyz}(\sigma_1, \sigma_2) = \tan^{-1} \frac{Im[RB_{xyz}(\sigma_1, \sigma_2)]}{Re[RB_{xyz}(\sigma_1, \sigma_2)]} . \tag{67}$$

Correspondingly, the rotary cross-bicoherence is

$$Rbic^2_{xyz}(\sigma_1, \sigma_2) = \frac{\left| RB_{xyz}(\sigma_1, \sigma_2) d\sigma^2 \right|^2}{(P_{x+x+}(\sigma_1) P_{y+y+}(\sigma_2) P_{z+z+}(\sigma_3) d\sigma^3)} . \tag{68}$$

Again, one can see that the rotary bispectral functions are the special cases of the rotary cross-bispectral functions. If all three vector random processes are identical, all the subscripts, x, y, z, can be dropped, and one has a set of rotary bispectral functions. But the rotary cross-biphase has a higher dependence on the coordinates. It is easy to see

$$R'\phi_{xyz} = R\phi_{xyz} - \theta_x - \theta_y + \theta_z \tag{69}$$

where θ_x, θ_y, θ_z are the amount of rotation of which the coordinates of $\vec{x}(t)$, $\vec{y}(t)$, $\vec{z}(t)$ undertake respectively.

The rotary cross-bispectrum is the measure of low order non-linear interactions among the rotary components of the different vector random processes. If the first two processes are identical, then the rotary cross bispectrum is the measure of quadratic inter-actions between the two different processes.

5. Estimation Procedure

The rotary bispectral and rotary cross-bispectral functions can be easily estimated with the rotary Fourier coefficients of the respective two-dimensional vector random processes. The algorithm is readily supplied by the related equations given in the previous sections. The proposed procedures are outlined and given in Appendix II.

6. Applicability

The rotary bispectrum is a reliable tool for examining the non-Gaussian nature of a vector random process. Being independent of the rectangular coordinates along which the scalar components of the process are described, the amplitude of the rotary bispectral density gives the unique measure of the low-order nonlinear interactions (the quadratic interactions) internal to the process itself. However, the amplitude does not show the cause and effect of the quadratic interaction as it is only a measure of the contribution to third moment of the process by combinations of three oscillatory interacting components whose frequencies are related in the manner described by equation (51), i.e., one frequency is the algebraic sum of the other two frequencies. It does not show explicitly the amount of internal energy transferred among the oscillatory components (e.g., the third moment of a current series has dimension of L^3/T^3, which is

not an energy dimension). The rotary biphase shows the phase lag of the quadratic interaction. Since the rotary biphase is not a unique quantity, i.e., not independent of the coordinates, it does not yield meaningful information if considered alone.

The amplitude of the rotary cross-bispectral density, a quantity also independent of coordinate description, gives a unique measure of the quadratic interactions among three different vector processes at the triple frequencies of which one is the algebraic sum of the other two. If a pair of the three processes are the same process, then the measure is of quadratic interaction between the two independent processes (in this case, two of the three oscillatory elements belong to one process). Since the rotary cross-bispectral analysis involves two or three different vector process, the role of the cause and effect of the quadratic interactions may be assigned to each process by examining the physical nature of the interacting process. One assigns the "cause" to the two oscillatory components and the "effect" to that component whose frequency is the algebraic sum of the frequencies of the "cause" components. The possible combinations of such an assignment are illustrated in Fig. 2.

In this study, the quadratic interactions to be examined are the effect of two interacting oscillating wind stress components upon the energy contained in an ocean current at the third frequency. Thus, one can postulate the relation

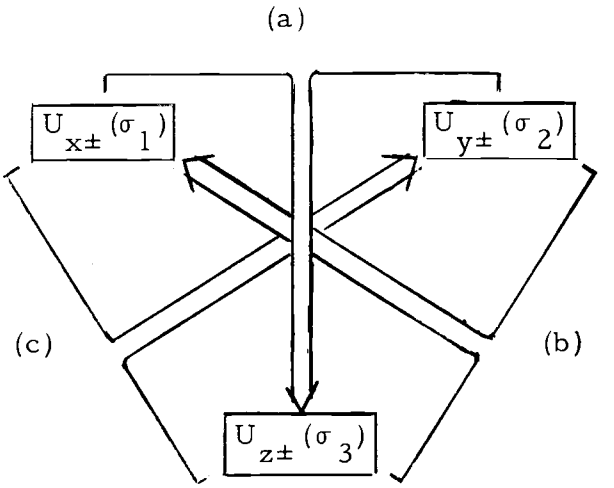

a) $[\pm\sigma_1]+[\pm\sigma_2]=[\pm\sigma_3]$ b) $[\pm\sigma_2]+[\pm\sigma_3]=[\pm\sigma_1]$ c) $[\pm\sigma_1]+[\pm\sigma_3]=[\pm\sigma_2]$

$$0 \leq \sigma_1 \leq N_y \qquad 0 \leq \sigma_2 \leq N_y \qquad 0 \leq \sigma_3 \leq N_y$$

Figure 2. Possible combinations of cause and effect for quadratic interactions shown by the rotary cross-bispectrum.

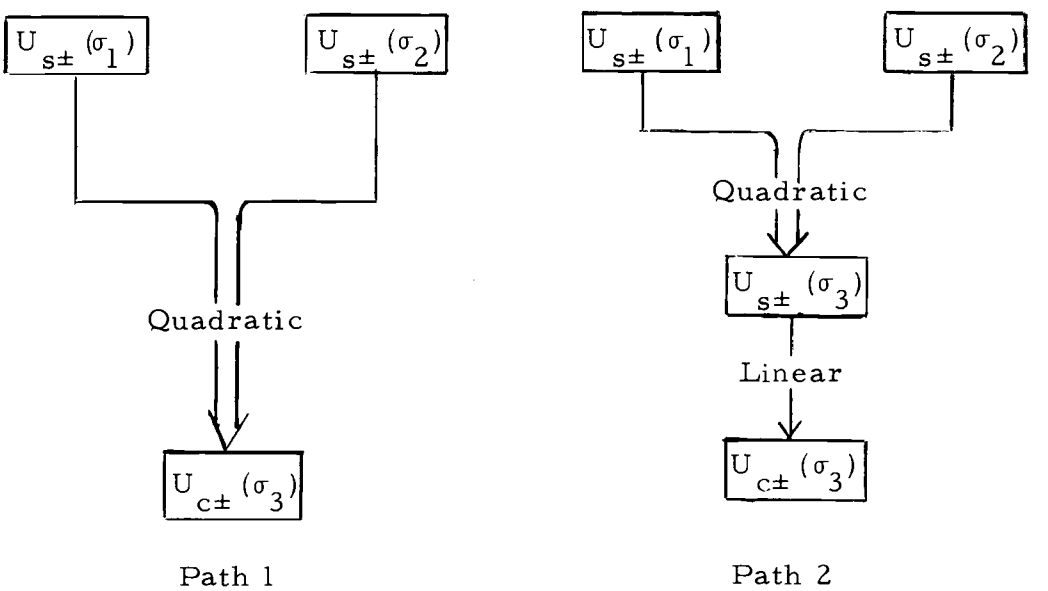

Figure 3. Quadratic energy transfer paths from process s to process c.

$$\vec{c}(t) = a\vec{s}(t) + b\vec{s}^{2}(t) \qquad (70)$$

where $\vec{s}(t)$ and $\vec{c}(t)$ are the wind stress and current fields respectively, a is the coefficient of the linear dependence term and b is the coefficient of the quadratic, nonlinear dependence of current on the wind stress. Two cases are examined: 1) wind stress vs. current at 14 m, and 2) wind stress vs. current at 34 m. In a similar manner, quadratic interactions between the ocean currents at 14 m and 34 m levels are examined (in this case, the left hand side of the equation (70) will denote current field at 34 m and the right hand side will denote current field at 14 m). Thus, the rotary cross-bispectral analysis involves only two processes of which, in case of wind stress vs. current, the wind stress field is assigned the role of "cause", and, in case of current vs. current, the current field at 14 m is assigned that of "cause" process.[6]

The amount of energy transferred still cannot be shown quantitatively as the rotary cross-bispectral density only shows the amount of common cube shared by the three interacting components, and its dimension is the product of the energy of the "cause" process and the

---

[6] Different method for examining the nonlinear relationship is given by Dewan (1969). However, his method only deals with the interaction among the two components with same frequency in one process and third component in another process, whose frequency is either zero or twice of that of the other two components. Thus, it only covers the axes of $\sigma_3 = 0$, $\sigma_1 = \sigma_2$ in the frequency domain shown by Fig. 1.

half power of the "effect" process. Besides, the energy transformed quadratically from one process to another can take two paths: 1) direct quadratic interaction among the two components in the "cause" process and the interacted component in the "effect" process, 2) linear interaction between an "effect" component and a "cause" component which is itself produced by quadratic interaction internal to the "cause" process. These two paths are shown in Fig. 3. They may both exist in nature but the cross-bispectrum cannot show the latter even qualitatively, in order to assess the amount of energy transformed quadratically from one process to another, an additional scheme is developed in the following section.

C. Energy Transfer Functions between a Pair of Two-dimensional Vector Random Processes

1. Rotary Fourier Representation of Quadratic Interaction between Two Different Vector Random Processes

Hasselmann (1966) developed a Fourier representation of the quadratic interactions between two random processes. A modification makes it useful for the rotary component representation of two different vector random processes. The rotary Fourier coefficients previously defined are used in place of the Fourier Stieltjes representations. Also, where Hasselmann used the ordinary conjugate to denote a function of negative frequency, the rotary component method

requires use of the function of negative frequency itself. With this modification, Hasselmann's equation (7) is applied to the rotary component analysis, as

$$\vec{u}_c(t) = \sum_{\sigma} [U_{c+}(\sigma)e^{i\sigma t} + U_{c-}(\sigma)e^{-i\sigma t}]$$

$$= \sum_{\sigma} [T_+(\sigma)U_{s+}(\sigma)e^{i\sigma t} + T_-(\sigma)U_{s-}(\sigma)e^{-i\sigma t}]$$

$$+ \sum_{\sigma_1}\sum_{\sigma_2} [K_+(\sigma_1+\sigma_2)U_{s+}(\sigma_1)U_{s+}(\sigma_2)e^{i(\sigma_1+\sigma_2)t}$$

$$+ K_-(\sigma_1+\sigma_2)U_{s-}(\sigma_1)U_{s-}(\sigma_2)e^{-i(\sigma_1+\sigma_2)t}$$

$$+ V(\sigma_1-\sigma_2)U_{s+}(\sigma_1)U_{s-}(\sigma_2)e^{i(\sigma_1-\sigma_2)t}$$

$$+ V(-\sigma_2+\sigma_1)U_{s-}(\sigma_1)U_{s+}(\sigma_2)e^{i(-\sigma_1+\sigma_2)t}] \quad (71)$$

where

1) $U_{s\pm}(\sigma)$, $U_{c\pm}(\sigma)$ are the rotary Fourier coefficients of random processes $\vec{s}(t)$, $\vec{u}(t)$ respectively, e.g. wind stress and current velocity.

2) σ is the frequency with a range of $0 < \sigma < \infty$. For the discrete time series, the upper limit of σ is the Nyquist frequency.

3) $T_\pm(\sigma)$ are the time-independent linear transfer function, and $T_\pm(\sigma) \neq T_\pm^*(\sigma)$ in general.

4) $K_{\pm}(\sigma_1+\sigma_2)$ are the time-independent quadratic sum transfer functions and

$$K_{\pm}(\sigma_1+\sigma_2) = K_{\pm}(\sigma_2+\sigma_1)$$

but $K_{\pm}(\sigma_1+\sigma_2) \neq K_{\pm}^{*}(\sigma_1+\sigma_2)$ in general.

5) $V(\sigma_1-\sigma_2)$ and $V(-\sigma_1+\sigma_2)$ are the time independent quadratic difference transfer functions.

$$V(\sigma_1-\sigma_2) = V_{+}(\sigma_1-\sigma_2) \quad \text{if } \sigma_1-\sigma_2 > 0$$

$$= V_{-}(\sigma_1-\sigma_2) \quad \text{if } \sigma_1-\sigma_2 < 0$$

$$V(-\sigma_1+\sigma_2) = V_{+}(-\sigma_1-\sigma_2) \quad \text{if } -\sigma_1+\sigma_2 > 0$$

$$= V_{-}(-\sigma_1+\sigma_2) \quad \text{if } -\sigma_1+\sigma_2 < 0$$

Thus it is obvious

$$V_{\pm}(\sigma_1-\sigma_2) = V_{\pm}(-\sigma_2+\sigma_1)$$

and $V_{+}(\sigma_1-\sigma_2) \neq V_{-}^{*}(\sigma_1-\sigma_2)$ in general.

For any particular frequency σ_3 equation (72) can be separated into two different equations concerning positive angular velocity $\omega_3 = \sigma_3$ and negative angular velocity $\omega = -\sigma$ components. Thus if $|\sigma_2| \geq |\sigma_1|$

$$U_{c+}(\sigma_3)e^{i\sigma_3 t} = T_{+}(\sigma_3)U_{s+}(\sigma_3)e^{i\sigma_3 t} + 2\sum_{\sigma_1}\sum_{\sigma_2} K_{+}(\sigma_1+\sigma_2)U_{s+}(\sigma_1)\,U_{s+}(\sigma_2)e^{i(\sigma_1+\sigma_2)t} \times \delta\left[(-\sigma_1+\sigma_2)-\sigma_3\right]$$

$$+ 2 \sum_{\sigma_1} \sum_{\sigma_2} V_+(-\sigma_1 + \sigma_2) U_{s-}(\sigma_1) U_{s+}(\sigma_2) e^{i(-\sigma_1 + \sigma_2)t} \times \delta[(-\sigma_1 + \sigma_2) - \sigma_3] \quad (72)$$

and

$$U_{c-}(\sigma_3) e^{-\sigma 3 t} = T_-(\sigma_3) U_{s-}(\sigma_3) e^{-i\sigma 3 t} + 2 \sum_{\sigma_1} \sum_{\sigma_2} K_-(\sigma_1 + \sigma_2) U_{s-}(\sigma_1) U_{s-}(\sigma_2) \times e^{-i(\sigma_1 + \sigma_2)t} \delta[-(\sigma_1 + \sigma_2) + \sigma_3]$$

$$+ 2 \sum_{\sigma} \sum_{\sigma} V_-(\sigma_1 - \sigma) U_{s+}(\sigma_1) U_{s-}(\sigma_2) e^{-i(\sigma_1 - \sigma_2)t} \times \delta[-(\sigma_1 - \sigma_2) + \sigma_3] \quad (73)$$

where $\delta[\ ]$ is the Dirac's Delta function serving as a constraint device for the double summation e.g., $\delta[(\sigma_1 + \sigma_2) - \sigma_3]$ implies the summations only cover the range $\sigma_1 + \sigma_2 = \sigma_3$. Because of this constraint, these two equations can be simplified as

$$U_{c\pm}(\sigma_3) = T_\pm(\sigma_3) \quad s\pm(\sigma_3) + 2 \sum_{\sigma_1} \sum_{\sigma_2} K_\pm(\sigma_1 + \sigma_2) U_{s\pm}(\sigma_1) U_{s\pm}(\sigma_2) \times \delta[\pm(\sigma_1 + \sigma_2) \pm \sigma_3]$$

$$+ 2 \sum_{\sigma_1} \sum_{\sigma_2} V_\pm(\pm \sigma_1 \pm \sigma_2) U_{s\pm}(\sigma_1) U_{s\pm}(\sigma_2) \times \delta[\pm(\sigma_1 - \sigma_2) \pm \sigma_3] \quad (74)$$

where[7]

$$|\sigma_1| \leq |\sigma_2|$$

One has to notice also that each $U_{s\pm}(\sigma_3)$ may be expressed in equation (74) form if there are any quadratic interactions existing in $\vec{u}_s(t)$. However, for simplicity, it will be assumed that $\vec{u}_s(t)$ is a Gaussian process. But this assumption shall be corrected later when the quadratic transform functions K and V are defined (see Hasselmann, 1966).

2. The Transfer Functions

The transfer functions T, K, V, can be defined in terms of the Rotary spectral parameters.

a. Linear Transfer Functions $T_{\pm}(\sigma)$

The linear transfer function is given by Hasselmann (1966) as the ratio of the cross-spectral density between the driving process and the responding process, to the spectral density of the driving process. For rotary spectral expression, one has

---

[7] Dimensional wise. $[T_{\pm}(\sigma)] = [U_{c\pm}(\sigma)U_{s\pm}(\sigma)^{-1}]$

$[K_{\pm}(\sigma_1+\sigma_2)] = [V_{\pm}(\pm\sigma_1 \pm \sigma_2)] = [U_{c\pm}(\sigma_3)U_{s\pm}(\sigma_1)^{-1}U_{s\pm}(\sigma_2)^{-1}]$

$$T_{+}(\sigma) = \frac{P^{*}_{s+c+}(\sigma)}{P_{s+s+}(\sigma)} \tag{75}$$

and

$$T_{-}(\sigma) = \frac{P^{*}_{s-c-}(\sigma)}{P_{s-s-}(\sigma)} \tag{76}$$

b. Quadratic Sum Transfer Functions, $K_{\pm}(\sigma_1 + \sigma_2)$

Multiplying the positive frequency equation of equation (74) by $U^{*}_{s+}(\sigma_1)$ and $U^{*}_{s-}(\sigma_2)$, with $\sigma_1 + \sigma_2 = \sigma_3$, and taking the ensemble average, one has[8]

$$RB^{*}_{ssc}(\sigma_1, \sigma_2)d\sigma^2 = T_{+}(\sigma_3)RB^{*}_{sss}(\sigma_1 + \sigma_2)d\sigma^2 + 2K_{+}(\sigma_1 + \sigma_2)P_{s+s+}(\sigma_1)P_{s+s+}(\sigma_2)d\sigma^2 \tag{77}$$

If σ is zero frequency, $\sigma_3 = \sigma_0 = 0$. Then

$$RB^{*}_{ssc}(\sigma_0, \sigma_2)d\sigma^2 = T_{+}(\sigma_3)RB^{*}_{sss}(\sigma_0, \sigma_2)d\sigma^2 + 4K_{+}(\sigma_0 + \sigma_2)P_{s+s+}(\sigma_0)P_{s+s+}(\sigma_2)d\sigma^2 \tag{78}$$

---

[8] In a manner analogous to that given in Hasselmann (1966),

$$< U_s(\omega_1)\, U_s(\omega_2) U_s^{*}(\omega_3) U_s^{*}(\omega_4) > = 0$$

unless $\omega_1 = \omega_3$, $\omega_2 = \omega_4$. If, for the rotary component method $\omega_2 = \omega_4 = -\sigma_2$, $\omega_1 = \omega_3 = \sigma_1$, then

$$< U_{s+}(\sigma_1)\, U_{s-}(\sigma_2)\, U_{s+}^{*}(\sigma_1)\, U_{s-}^{*}(\sigma_2) > = P_{s+s+}(\sigma_1)P_{s-s-}(\sigma_2)d\sigma^2$$

as $K_+(\sigma_0+\sigma_2) = V_+(-\sigma_0+\sigma_2)$ and $P_{s+s+}(\sigma_0) = P_{s-s-}(\sigma_0)$. Here the rotary bispectral density $RB^*_{sss}(\sigma_1, \sigma_2)$ is included to account for the non-Gaussian nature of the u(t) process itself. Solving for the quadratic sum transfer function, one obtains

$$K_+(\sigma_1+\sigma_2) = \frac{RB^*_{ssc}(\sigma_1,\sigma_2)}{2\,P_{s+s+}(\sigma_1)P_{s+s+}(\sigma_2)} - T_+(\sigma_3)\frac{RB^*_{sss}(\sigma_1,\sigma_2)}{2\,P_{s+s+}(\sigma_1)P_{s+s+}(\sigma_2)},$$

$$\sigma_1+\sigma_2=\sigma_3 . \tag{79}$$

The first and second terms on the right hand side of equation (79) account for the path 1 and path 2 illustrated in Fig. 3. If $\vec{u}(t)$ is indeed a Gaussian process, then the second term does not exist because $RB^*_{sss}(\sigma_1, \sigma_2)$ will not be significantly greater than zero. On the other hand, if there are no quadratic interactions between the two random processes, but the driving process has its own internal quadratic interaction, then the σ_3 component of the responding process still will be affected by σ_1, σ_2 components in the driving process provided that the linear transfer function $T_+(\sigma_3)$ is significant. The quadratic sum transfer function is then

$$K_+(\sigma_1+\sigma_2) = -T_+(\sigma_3)\frac{RB^*_{sss}(\sigma_1,\sigma_2)}{2P_{s+s+}(\sigma_1)P_{s+s+}(\sigma_2)}$$

This interaction is not explicit. The same relation also holds for negative components.

$$K_{-}(\sigma_1+\sigma_2) = \frac{RB^{*}_{ssc}(-\sigma_1, -\sigma_2)}{2P_{s-s-}(\sigma_1)P_{s-s-}(\sigma_2)}$$

$$- T_{-}(\sigma_3)\frac{RB^{*}_{sss}(-\sigma_1, -\sigma_2)}{2P_{s-s-}(\sigma_1)P_{s-s-}(\sigma_2)} \qquad (80)$$

c. Quadratic Difference Transfer Functions, $V_{\pm}(\mp\sigma_1 \pm \sigma_2)$

The quadratic difference transfer functions can be derived the same way as the quadratic sum transfer functions. Thus

$$V_{\pm}(\mp\sigma_1 \pm \sigma_2) = \frac{RB^{*}_{ssc}(\mp\sigma_1, \pm\sigma_2)}{2P_{s\mp s\mp}(\sigma_1)P_{s\pm s\pm}(\sigma_2)}$$

$$- T_{\pm}(\sigma_3)\frac{RB^{*}_{sss}(\mp\sigma_1, \pm\sigma_2)}{2P_{s\mp s\mp}(\sigma_1)P_{s\pm s\pm}(\sigma_2)} . \qquad (81)$$

3. The Energy Transfer Equation

The energy transfer equation between a pair of two dimensional vector random processes can be readily obtained from equation (74). As $P_{c\pm c\pm}(\sigma_3)d\sigma = \langle U_{c\pm}(\sigma_3)\, U_{c\pm}{}^{*}(\sigma_3)\rangle$, one has[9]

$$P_{c\pm c\pm}(\sigma_3)d\sigma = \left|T_{\pm}(\sigma_3)\right|^2 P_{s\pm s\pm}(\sigma_3)d\sigma +$$

---

[9] Mathematically, there should be a factor of four in the second and third terms on the right hand side of equation (82) to account for the permutations of each pair of the interacting frequency components. The factor of four is not included in this equation as only one of the permutations represents the true energy process.

$$+\sum_{\sigma_1}\sum_{\sigma_2}\left|K_{\pm}(\sigma_1+\sigma_2)\right|^2 P_{s\pm s\pm}(\sigma_1)P_{s\pm s\pm}(\sigma_2)d\sigma^2\cdot\delta[(\pm\sigma_1\pm\sigma_2)\mp\sigma_3]$$

$$+\sum_{\sigma_1}\sum_{\sigma_2}\left|V_{\pm}(\mp\sigma_1\pm\sigma_2)\right|^2 P_{s\mp s\mp}(\sigma_1)P_{s\pm s\pm}(\sigma_2)d\sigma^2\cdot\delta[(\mp\sigma_1\pm\sigma_2)\mp\sigma_3] \quad (82)$$

where $|\sigma_2|\geq|\sigma_1|$.

The first term on the right hand side of the equation denotes the amount of energy being transformed from the driving process to the responding process through linear action. The second and third terms denote the amount of energy being transformed through quadratic interactions.

D. Statistical Considerations

The development of this proposed technique is based on two hypotheses; first that the random processes are not normally distributed (non-Gaussian), and second that the random processes are stationary. Therefore, any set of data used for this analysis should first pass a statistical test of these hypotheses. Since this analysis is carried out on a limited sample, significance test should also be applied to function extimates such as rotary cross-spectral density, rotary bispectral density and rotary cross-bispectral density. The estimates should be significantly greater than zero to yield any useful information. These tests are discussed in the following sections. Detailed testing procedures are referred to appropriate literature.

1. Normality test

The well known χ^2 test for goodness of fit of normality is chosen as the main testing scheme. It has been well documented (Crow, Davis and Maxfield, 1960), and the proper computer programs needed for the test are also available (Bevington, 1969). A complimentary testing scheme using Cornu ratio and skewness (Crew and Bodvarsson, 1971) will also be used for comparison. The tests are applied to the scalar component series for the two dimensional vector random process. If both of the scalar component series fail all of the tests then this vector random process is not normally distributed (Jenkins and Watts, 1968).

2. Stationarity test

For practical reasons, the rigorous testing of stationarity of a random process is not feasible (Bendat and Piersol, 1966). However, in this proposed analysis, all of the data series used must satisfy the condition of weak stationarity, to second order, as a minimum condition. This is due to the fact that all the functions defined here are derived directly or indirectly from the Fourier coefficients of the scalar component series. It is rather important to ensure that the Fourier representation of the series is valid.

Haubrich (1965) gives such a test in detail, based on the idea that the coherence squared between the Fourier coefficients at

different frequencies will be significantly greater than zero if the random process is not stationary. This idea has been further proven by Lumley (1970). He states that, for a stationary process, Fourier components at two different frequencies are uncorrelated, though not statistically independent.

Therefore, the stationarity test by Haubrich (1965) is utilized for this analysis for the sake of compatibility and practicality. It will be conducted on each resolved scalar data series to ensure that its Fourier representation is valid.

3. Significance Test of the Rotary Cross-spectral Estimates

The rotary cross-spectral density is meaningful only when its corresponding coherence estimate is significantly greater than zero. The rotary coherence $\gamma_{12}(\pm\sigma)$ is defined as (Mooers, 1973)

$$\gamma_{12}^{2}(\pm\sigma) = \frac{P_{1\pm 2\pm}(\sigma)^{2}}{P_{1\pm 1\pm}(\sigma)\, P_{2\pm 2\pm}(\sigma)} \tag{83}$$

where

$$0 \leq \gamma_{12}^{2} \leq 1 ,$$

and $P_{1\pm 1\pm}(\sigma)$ is the rotary cross-spectral density between processes 1 and 2, and $P_{1\pm 1\pm}(\sigma)$, $P_{2\pm 2\pm}(\sigma)$ are rotary spectral densities of processes 1 and 2 at $\pm\sigma$. It provides a non-dimensional measure of the correlation between two time series as a function of frequency.

Jenkins and Watts (1968) give a simple significance test scheme for such correlation based on least squares analysis in the frequency domain. They show that the random variable

$$\frac{(EDF-2)\,\hat{\gamma}_{12}^{2}(\sigma)}{2(1-\hat{\gamma}_{12}^{2}(\sigma))} \tag{84}$$

is distributed approximately as the $F_{2,\,(EDF-2)}$ where EDF is the equivalent degree of freedom of the spectral estimates. $F_{2,\,(EDF-2)}$ is the Fisher F distribution with 2 and (EDF-2) degrees of freedom, and $\hat{\gamma}_{12}$ is the estimated value of the coherence squared. Thus,

$$\frac{(EDF-2)\,\hat{\gamma}_{12}^{2}(\sigma)}{2(1-\hat{\gamma}_{12}^{2}(\sigma))} \leq f_{2,\,(EDF-2)}(1-\alpha) \tag{85}$$

then γ_{12}^{2} is not greater than zero at the α significance level.

This test is derived from ordinary spectral and cross-spectral functions. It can also be applied to the rotary component spectral functions by following the same analogy.

4. Significance Test of the Rotary Bispectral and Rotary Cross-bispectral Estimates

The third order spectral estimates of a random process (vector-valued or real-valued) are asymptotically unbiased and asymptotically

normal under mild conditions (Brillinger and Rosenblatt, 1966a). Thus the estimates of the coherence squared asymptotically has a χ^2 distribution with two degrees of freedom since it is sum of squares of two terms each of which is asymptotically normally distributed. Haubrich (1965) gives that the expected values of the estimate of the bicoherence squared, obtained from truncated data, is approximately 2/EDF if its corresponding bispectral density estimates have true vanishing value.

Therefore, the bispectral density estimates will be significantly greater than zero at 5% level if its corresponding estimates of the bicoherence squared is greater than or equal to 6/EDF. This testing criterion can also be applied to the cross-bispectral estimates which have been shown as the general case of the bispectral estimates in earlier section. By the same analogy, it can also be applied to the rotary bispectral and cross-bispectral estimates. Thus, if the estimate of the rotary bicoherence squared is less than 6/EDF, the corresponding rotary bispectral density is not significantly greater than zero at 5% level. The same rule holds for rotary cross-bispectral density.

Due to the fact that the bicoherence can only be estimated when the three interacting components all have a reasonable amount of spectral density (Hinich and Clay, 1968), a significance test should be applied to the spectral density estimates of the rotary components

before their bispectral density are tested for significance. One can see that this requirement is also true for the significance test of the rotary cross-bispectral density estimates.

5. Significance Test of the Rotary Spectral Density Estimates

For a discrete time series, the spectral density estimates should decrease to zero before the Nyquist frequency. If the spectral density estimate at the Nyquist frequency appears greater than zero, this estimated value is the noise introduced by aliasing of the frequency components above the Nyquist frequency. This noise cannot be completely eliminated in practice. Heuristically, the noise is regarded as the systematical error for the true zero spectral density estimate, and it can be used as a threshold value for testing other non-zero spectral estimates. The confidence limits for spectral density estimate at certain significance level can be easily obtained with the estimate, its equivalent degrees of freedom, and variable associated with the significance level (Jenkins and Watts, 1968). A simple test is then proposed in this study to compare the lower limit of any rotary spectral density estimate against the upper limit of that at the Nyquist frequency. If the former value is less than the latter, the tested rotary spectral density is considered not to be significantly greater than zero at that certain level.

It is obvious that all of the significance tests are essential to

the reliability of this proposed analyzing technique. Thus, in order to have valid result, all the interpretations and calculations should only be based on the rotary spectral parameters which have passed these tests.

IV. DESCRIPTION OF THE DATA

A. The Data Source

The TOTEM buoy developed by Oregon State University, School of Oceanography provides a stable platform for monitoring wind stress and near surface ocean current system (Plutchak, 1972; Burt, 1973). The buoy was located at 44°59.6' N, 124°44.7' W, a position of about 35 miles northwest of Newport, Oregon (Figure 4). The buoy site is near the upper edge of the continental slope, and the depth of the ocean at that location is about 500 meters.

From 1110 July 20 to 0410 August 13, 1971, continuous surface wind (10 meters above the sea surface) and ocean currents at 14 and 34 meter depths were recorded simultaneously and stored on magnetic tape as three data series. Each series has 3424 data lines with data interval of 10 minutes, and each line has four quantities of speed (meter/sec), direction (degree), u and v components of the velocity (meter/sec).

B. Data Processing

Only the u, v components of the velocity of each data series are used in this study. The data interval of each data series is converted

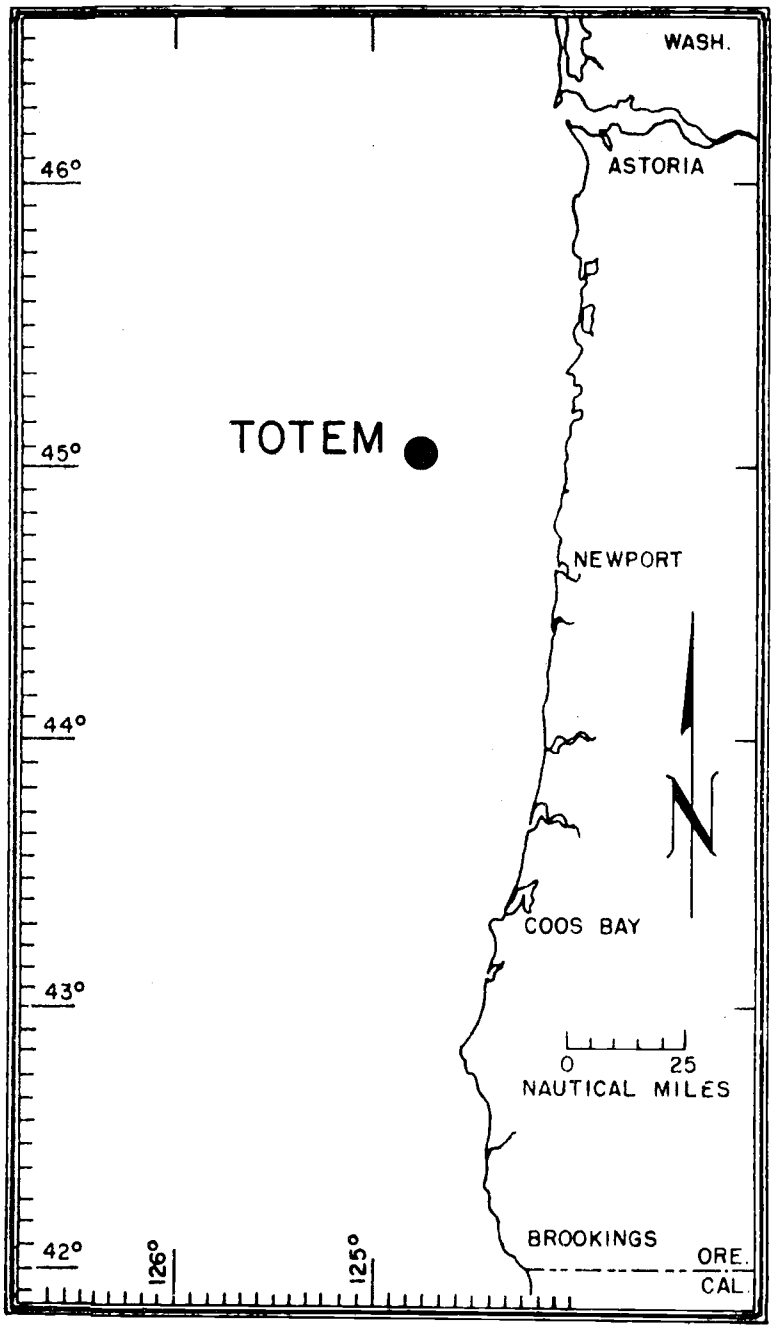

Figure 4. Location of TOTEM buoy.

to be hourly apart. This conversion is done by a moving average scheme with a low-passing Cosine-Lanczos filter which has 73 number of weights and the half-power frequency at 0.5 cycles per hour (CPH) - the Nyquist frequency. This scheme is developed by the Coastal Upwelling Group at the School of Oceanography, Oregon State University. It is able to alleviate the aliasing at the expense of losing six hours data at the both ends of the record (Bottero, 1973). Hence, there are 559 data lines in each data series after the conversion. In addition to the changing of the data interval, the unit of the data is also converted to centimeter per second (cm/sec). Due to the restriction imposed by the Fast Fourier Transform, only 512 data lines in each data series can be used for actual analysis.[10] The edited series are from 1710 July 20-0010 August 21, 1971.

From the edited wind record, a wind stress data series is formed with the following formulae:

$$\tau_u = D \rho_a u S \quad \text{dyne/cm}^2$$
$$\tau_v = D \rho_a v S \quad \text{dyne/cm}^2 \qquad (86)$$

where τ_u, τ_v are the E-W and N-S components of the wind stress,

D is the dimensionless drag coefficient and $D = 2.6 \times 10^{-3}$,

---

[10] Fast Fourier Transform requires that the number of data in each truncation must be power of two.

ρ_a is the mean air density near surface and $\rho_a = 1.25 \times 10^{-3}$ gm/cm^{-3},

u, v are the E-W and N-S components of the wind velocity in cm/sec,

S is the wind speed and $S^2 = u^2 + v^2$.

Equation (86) is derived directly from the well known Quadratic Law applied by Ekman.[11]

The hourly data interval series are called TWIND, TWSTR, TCU14 and TCU34 for the record of wind, wind stress, and currents at 14 and 34 meter depths respectively.

Since all the rotary spectral parameters in this study are calculated from wind stress and currents at the depths of 14 and 34 meters, the data series TWSTR, TCU14 and TCU34 will have their mean removed and will be overlapped to yield higher degrees of freedom when all spectral analysis are applied. The zero mean overlapped data series are called OTWSTR, OTCU14 and OTCU34. Each of them will have seven truncations of 128 data lines with 64 of the data lines overlapped (details of overlapping, see Appendix II). Using the formulae given by Welch (1966), one can find that the resolved frequency band of the spectral estimates of the overlapped

---

[11] The reason, that the Quadratic Law is preferred by many investigators in determining the wind stress, has been discussed by Neumann and Pierson (1966).

data series is 1/128 cycles per hour (0.0078 CPH)[12], and that the equivalent degrees of freedom, EDF, is then 9.8 instead of 8.0 for the non-overlapped data series.

C. Hydrographic Conditions

A hydrographic station, located at 45°00.2' N, 124°49.3' W, about two miles west of the TOTEM site, was made by the R/V CAYUSE of the Oregon State University at GCT 0445 July 31, 1971 (Wyatt, Tomlinson, Gilbert, Gordon and Barstow, 1972). The time of cast is about in the middle of the data series monitored by the TOTEM. Thus, the oceanic conditions around the TOTEM site can approximately be described by this hydrographic data. The vertical profiles of the temperature, salinity, and sigma-t from the surface down to 100 meters depth are shown in Figure 5.

From this figure, one can see that the current at 14 m was measured about at the bottom of the mixed layer; the one at 34 m is measured near the lower end of the thermocline. The Brunt-Vaisala frequencies at these two depths, calculated from the

---

[12] The resolved frequency band of 0.0078 CPH is the roughest possible frequency resolution to show the diurnal tidal-, inertial- and semi-diurnal oscillations in the current spectrum off Oregon coast. The frequencies of these oscillatory components in this region are approximately 0.04, 0.057 and 0.082 CPH respectively (Pillsbury, 1972). The angular frequency, in this study, is expressed in terms of cycles per hour instead of radians per hour for the sake of easy interpretation.

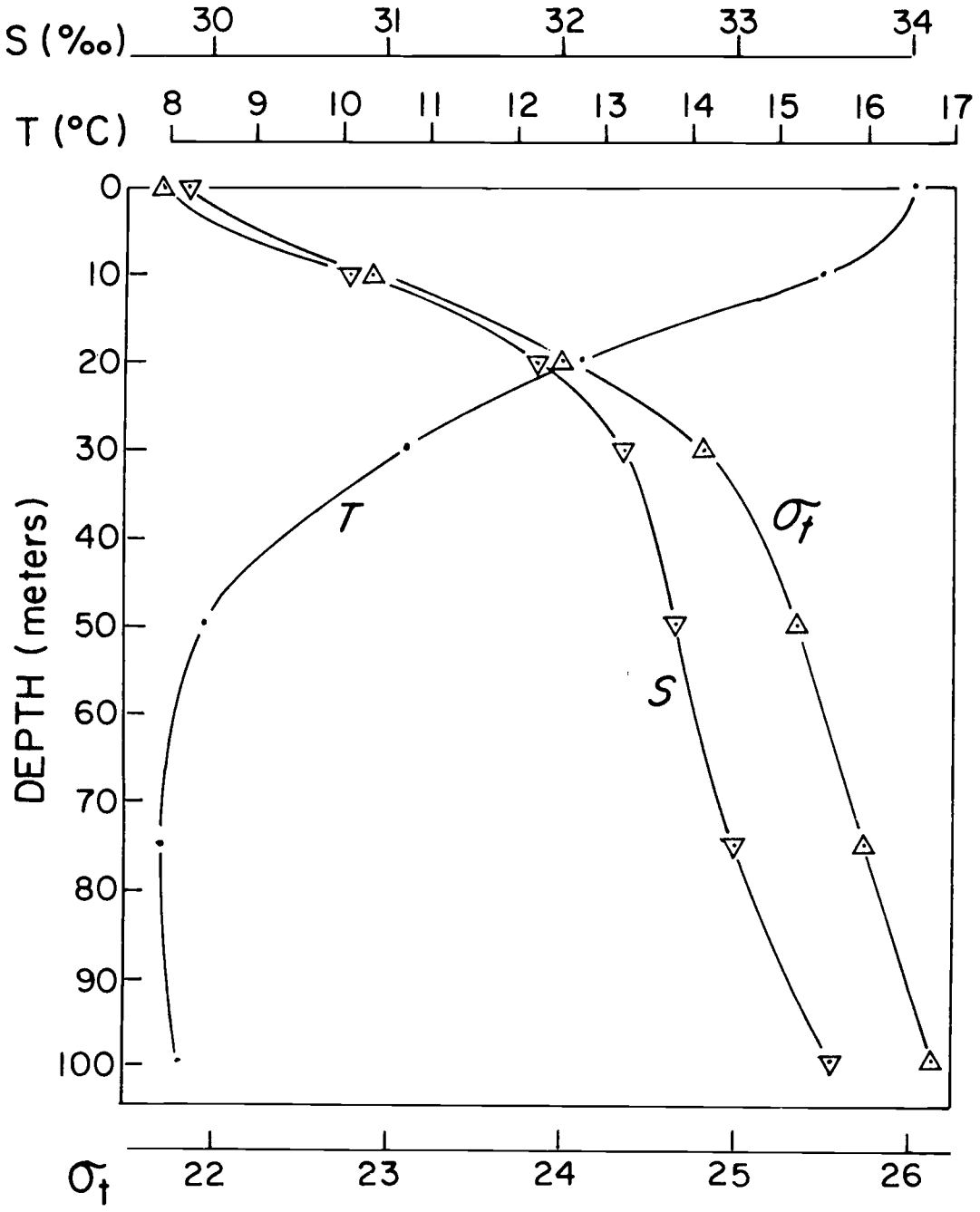

Figure 5. Vertical profile of temperature, salinity and sigma-t at station 10 of Y7107C cruise; lat. 45° 00.2' N, long. 124° 49.3' W, July 31, 1971.

hydrographic data with formulae provided by Phillips (1966), are 20.5 CPH and 7.3 CPH respectively. They are above the Nyquist frequency, and are not included in the frequency domain in this study.

D. Statistical Properties

The statistical properties of the data series, discussed in this section, are their elementary statistics, normality and wide sense stationarity. The elementary statistics are useful either for describing the general features of the wind and current fields, represented by the data series, or for testing the normality of those fields. Since all rotary spectral parameters used in this study will be calculated from the wind stress and the current data series, the normality and wide sense stationary tests are applied to those data series. The importance of these tests has been discussed in Chapter III.

Table 1 gives the summary of those useful elementary statistics of the data series of TWIND, TWSTR, TCU14 and TCU34. The general features of wind and current fields, described by certain statistics, are as follows:

1) The overall mean direction of wind velocity field is toward the southwest as shown by the mean values in its u component (-234 cm/sec) and in its v component (-342 cm/sec). The variance and range is slightly larger in the u component (1.77×10^6 cm^2/sec^2, from 814.5 to -119.30 cm/sec) than in the v component (1.54×10^6 cm^2/

Table 1. Elementary statistics of data series: TWIND, TWSTR, TCU14 and TCU34. (There are 512 data in each series, and the unit of the data is cm/sec except that of TWSTR whose unit is dyne/cm^2.)

Data	TWIND		TWSTR		TCU14		TCU34	
Components	u	v	u	v	u	v	u	v
Mean	-234.55	-343.80	-0.87	-1.08	0.02	-19.33	-10.72	-15.02
Max	814.55	562.74	2.39	1.55	18.52	2.44	4.40	0.05
Min	-1191.03	-1343.39	-6.25	-7.02	-24.99	-53.46	-30.58	-42.51
Median	-159.86	-269.33	-0.15	-0.29	1.80	-19.41	-10.49	-13.75
Variance	177225.14	153723.18	2.35	2.63	59.77	99.60	52.88	102.74
Standard Deviation	420.98	392.08	1.56	1.62	7.73	9.98	7.27	10.36
Cornu	1.46	1.45	1.57	1.54	1.65	1.55	1.47	1.37
DC	-7.20	-7.95	0.16	-1.86	5.31	-1.15	-6.44	-12.74
Skewness	-0.11	-0.35	-1.14	-1.33	-0.80	-0.21	-0.19	-0.39
Kurtosis	2.37	2.35	3.59	3.92	3.40	2.83	2.13	2.11

sec^2, from 562.74 to -1342.29 cm/sec). The overall wind stress field is also toward the southwest as the mean values of its u and v components are -0.87 dyne/cm^2 and -1.08 dyne/cm^2 respectively. However, its variance has a higher value in the v component (2.63 $dyne^2/cm^4$) than in the u component (2.35 $dyne^2/cm^4$) although the ranges of the wind stress in the u and v components appear about the same (from 2.39 to -6.25 dyne/cm^2 vs. from 1.55 to -7.02 dyne/cm^2).

2) The overall mean direction of the current field at 14 m is southward as the mean value of the u component is only 0.02 cm/sec while that of the v component is -19.33 cm/sec. The variance and range of this current field is larger in the v component (99.66 cm^2/sec^2, from 2.44 to -53.46 cm/sec) than in the u component (59.77 cm^2/sec^2, from 18.52 to -24.99 cm/sec). However, the overall mean direction of the current field at 34 m is southwesterly as the mean values of its u and v components are -10.72 cm/sec and -15.02 cm/sec respectively. The variance and range are also larger for the v component (102.74 cm^2/sec^2, from 0.05 to -42.51 cm/sec) than the u component (52.88 cm^2/sec^2). Comparing the two current fields, one can see that there is big difference in their overall mean directions. The variance of the u component decreases as the depth increases while the variance of the v component increases as the depth increases, but the total variance remains about the same

(159.37 cm^2/sec^2 at 14 m vs. 155.68 cm^2/sec^2 at 34 m).

The three normality tests i.e., skewness test, CORNU ratio test and the χ^2 goodness fit test, discussed previously, are applied to the data series of TWSTR, TCU14 and TCU34. The testing statistic of the skewness test is the skewness of the u and v components of each series and the confidence limits of this test are obtained, according to the number of data in each series, from the table given by Crew and Bodvarsson (1971). The testing statistic of the CORNU ratio test is DC which is given as

$$DC = (CORNU - 1.5708)/0.015708$$

and

$$CORNU = (\text{Standard deviation}/<|C'|>)^2 \qquad (87)$$

where C' is the deviation of data from sample mean. The confidence limits are also obtained, according to the number of data in each series. The χ^2 goodness fit test is conducted according to the scheme given by Bevington (1969). The testing statistic is the probability that if the tested data is normally distributed, it will have a true χ^2 value greater than the calculated χ^2 value. The results of these tests are summarized in Table 2. It is shown that none of the components of the data series pass all of the tests at 5% significance level and that all of the components fail the well known χ^2 goodness fit test. Thus the wind stress and current fields, represented by those data series, are not normally distributed random processes, and they are

Table 2. Normality tests of data series (of 512 data values) at 5% significance level.

Data		Skewness Test: Skewness	Skewness Test: Compared with 95% confidence limits ± 0.2147	Cornu Ratio Test: DC	Cornu Ratio Test: Compared with 95% confidence limits +5.801 -3.826	χ^2 Goodness Fit Test: Degrees of freedom	χ^2 Goodness Fit Test: χ^2	χ^2 Goodness Fit Test: Prob.> χ^2 if normal	χ^2 Goodness Fit Test: Test at 5% significance level
TWSTR	u	-1.1400	F	0.1552	P	15	586.55	0.0	F
	v	-1.3284	F	-1.8549	P	13	469.71	0.0	F
TCU14	u	-0.8008	F	5.3068	P	27	139.90	0.0	F
	v	-0.2130	P	-1.1520	P	27	38.76	0.0	F
TCU34	u	-0.2810	F	-6.4383	F	32	96.70	0.0	F
	v	-0.4857	F	-12.7368	F	31	221.10	0.0	F

non-Gaussian in nature.

The testing statistic of the wide sense stationarity is the average value of the coherence squared between the Fourier coefficients at different frequencies, R_{ij}, defined by Haubrich (1965). The confidence limit of such true zero coherence squared is obtained from the standard χ^2 distribution table with its expected value and the equivalent degrees of freedom of the Fourier coefficients. The expected value is given as a function of the EDF and the true coherence squared by Haubrich (1965). This test is applied to the data series of OTWSTR, OTCU14 and OTCU34. The $\hat{R}_{ij}$ is estimated from the Fourier coefficients from the zero mean overlapped data series tapered with Haubrich's (1965) data window which yields an EDF of 11 for the Fourier coefficient estimates. For each component of the data series, there are 65 such Fourier coefficients at frequencies ranging from 0.0 to 0.5 CPH, and the total number of $\hat{R}_{ij}$ is 4160. The result of this test is given in Table 3. It shows that all the components pass this test at 5% significance level. Thus, the wind stress field and the two current fields are wide sense stationary at the 5% significance level at the time the data were taken.

Table 3. Test for wide sense stationarity of data series (512 values) at 5% significance level by comparing the average coherence squared between different frequency components with the 95% confidence limit of the true zero coherence squared value (Haubrich, 1965).

Data		Average $\hat{R}^2_{ij}$	Compared with 95% confidence limit <0.329 ($R^2_{ij} = 0.0$)
TWSTR	u	0.187	P
	v	0.305	P
TCU14	u	0.164	P
	v	0.154	P
TCU34	u	0.154	P
	v	0.169	P

V. THE RESULTS OF DATA ANALYSIS

In addition to the second and third order rotary spectral analysis techniques discussed in Chapter III, the vector progressive diagram is also employed to study general variation of the wind field and current fields represented by data series of TWIND, TCU14 and TCU34. All the rotary spectral analyses use the zero-mean overlapped data series of OTWSTR, OTCU14 and OTCU34. Thus all the rotary spectral parameter estimates have the same equivalent degrees of freedom of 9.8 and a resolved frequency band of 0.007812 CPH as duscussed previously. Due to the restriction of the frequency resolution and the Nyquist frequency, all spectra can only show the variations with an absolute frequency higher than 0.007812 CPH (with a corresponding period less than 128 hours) and lower than 0.5 CPH (with a corresponding period greater than two hours). Hence the frequency domain covers only the intermediate frequency range and a part of the high frequency range defined by Sakou and Neshyba (1972). The results of all the analyses are discussed in the following sections.

A. Progressive Vector Diagram

The progressive diagrams, PVD, of the data series TWIND, TCU14 and TCU34 are shown in Figure 6.

From July 20 to July 26, the wind generally blew towards the southwest but its daily mean speed decreased rather rapidly from about 1555 cm/sec (30 knots) to 620 cm/sec (12 knots). In the following ten days, the wind velocity is light and variable as shown by the PVD. Finally, from August 6 to the end of the data series, the wind shifted back to about 1444 cm/sec (28 knots) in the daily mean speed and southwest in the direction. The PVD of the wind data series gives a general picture of the longer period variation of the wind velocity, but it does not show clearly the variation with period less than 24 hours.

However, from July 20 to July 28, the current at 14 m flowed generally towards south and its daily mean speed was fairly constant around 18.4 cm/sec (0.36 knots). From July 29, about two days after the beginning of the light but variable wind, the direction the current shifted slightly towards southwest and the daily mean speed of which started increasing very slightly and reached its highest value of about 25.5 cm/sec (0.5 knots) around August 1. Then, the direction moved back towards south. The daily mean speed of the current decreased rather substantially after August 6. The variations with periods less than 24 hours are quite discernible from the PVD, it is

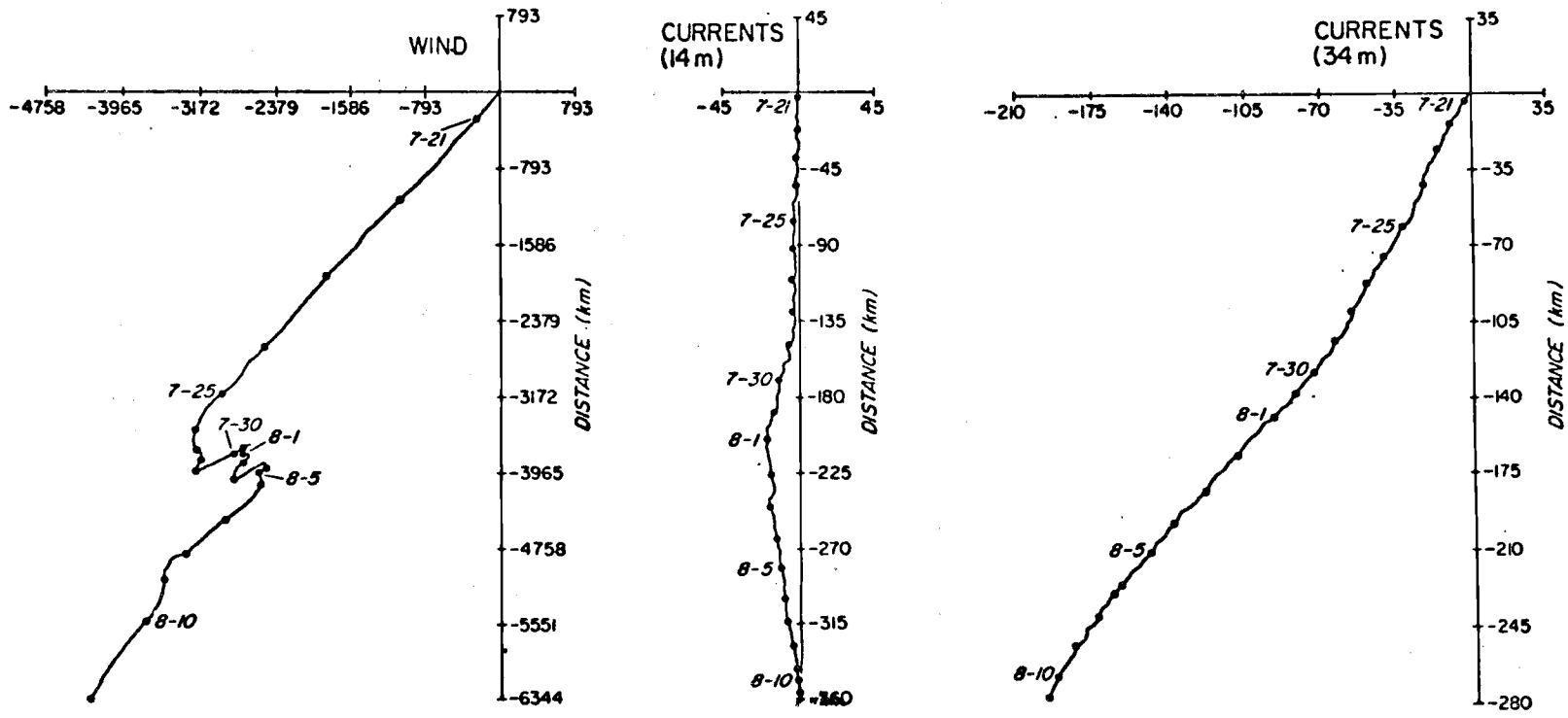

Figure 6. Progressive vector diagram of wind, current at 14 and 34 m at TOTEM site July 20-August 11, 1971.

rather difficult to assess their exact frequencies.

The TCU34 data series gives a different trend of the mean flow. The direction is generally southwest. The change of the daily mean speed is quite variable. The highest daily mean speed is also around August 1 as it was for the TCU14 data series. However, the magnitude of the highest daily mean speed of the current at 34 m is about 40 cm/sec (0.8 knots) which is considerably higher than that at 14 m. The current velocity variations with period less than a day are not so obvious as those at 14 m.

The general directions of the wind and the current fields shown by the PVD are consistent with the overall mean directions of those fields described by the elementary statistics in the previous chapter. The PVD of each field shows discernible evidences of the field variations with periods longer than 24 hours. It appears that the variations of the wind field are more complicated than those of the two current fields. But the PVD does not yield the detailed characteristics of the variations e.g., their frequencies, energy distribution, or trajectory's shape, orientation and sense of rotation. The results of the rotary spectral analysis, discussed in the next section, are able to provide those detailed informations for the variations with periods less than 24 hours.

B. Rotary Spectral Analysis

The rotary spectra of the wind stress, the currents at 14 m and 34 m are shown in Figures 7-9 respectively. For convenience in investigating the amount of energy contained in each frequency component, the spectrum is plotted in terms of energy density i.e., half the value of the spectral density. Also, for convenience in comparing the energy distributions, the spectra of the two counter-rotating components of each data series, as well as the total spectrum, are put into one plot. The significance of each spectral density estimate is assessed by examining whether the lower significance limit of the spectral density estimate is larger than the upper significance limit of the spectral density at the Nyquist frequency. This testing criterion has been discussed previously in Chapter III. The amount of energy contained in any frequency component is equal to the product of the energy density and the resolved frequency band, and the area under the total energy spectrum represents the total kinetic energy of the vector series (half value of its total variance).

Figure 7 shows the energy distribution of the wind stress field (see footnote 4, Chapter III). The significance test shows that no energy density estimate, in both clockwise and counter-clockwise spectra, with a value less than 0.136 $(\text{dyne}/\text{cm}^2)^2 \text{CPH}^{-1}$ is significantly greater than zero at 5% level. Among those significant ones, one can see that distinct peaks exist at -0.04 CPH and $\pm$0.085 CPH, and that less distinct but

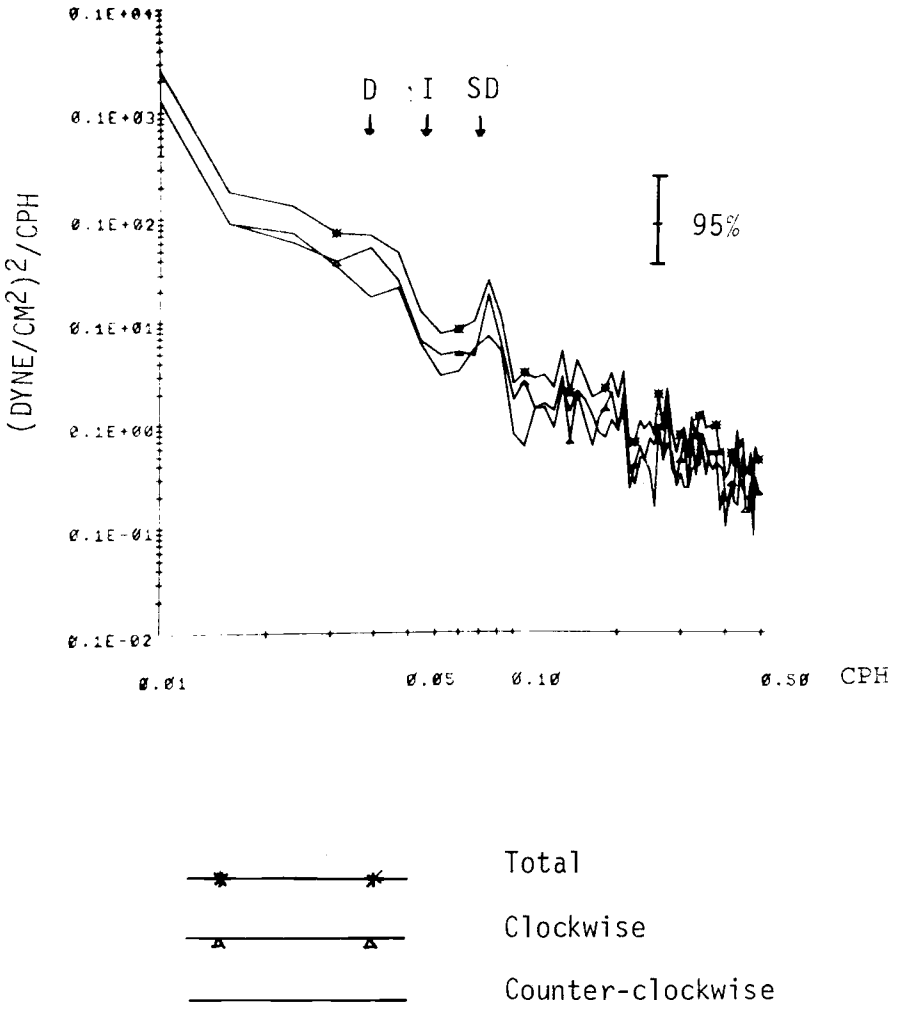

Figure 7. Rotary spectra of wind stress at TOTEM, July 20-August 11, 1971.

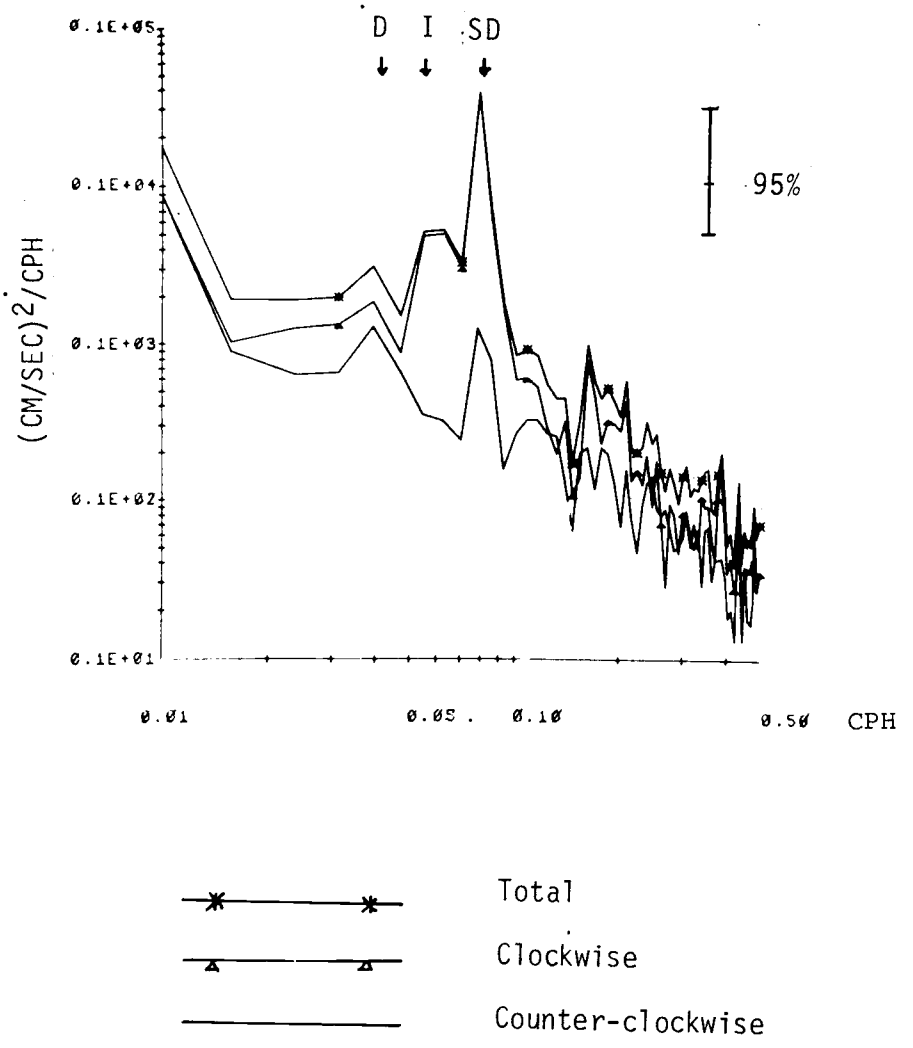

Figure 8. Rotary spectra of current at 14 m at TOTEM, July 20-August 11, 1971.

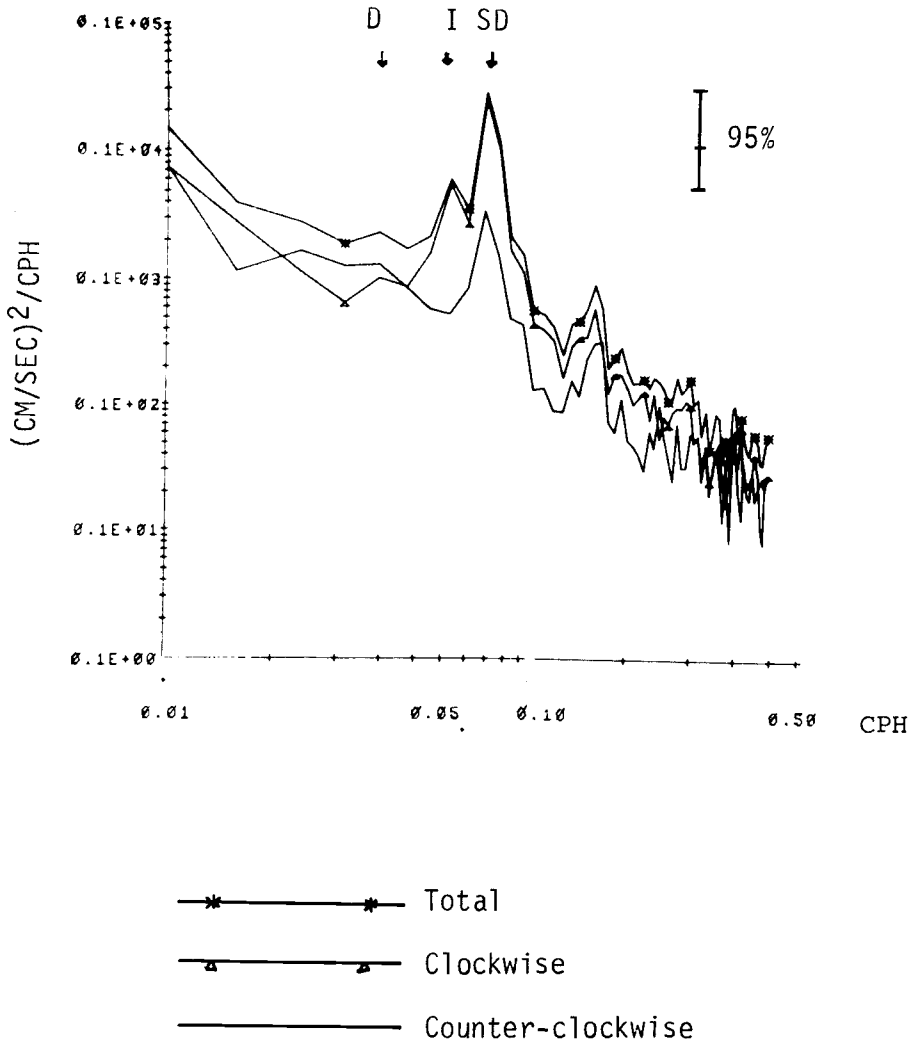

Figure 9. Rotary spectra of current at 34 m at TOTEM, July 20-August 11, 1971.

discernible peaks exist at 0.047 CPH, ± 0.014 CPH and ± 0.016 CPH. It is clear that the predominant intermediate frequency oscillation of the wind stress are the clockwise rotating elliptical motions at absolute daily frequency (0.04 CPH) and semidaily frequency (0.085 CPH). There is no peak shown at positive daily frequency, but there is substantial amount of energy at that frequency and the peak at 0.047 CPH may be the counter-clockwise daily component as the exact absolute daily frequency is 0.042 CPH which cannot be given by the spectra because of the restriction of the frequency resolution. The orientation of the two ellipses' major axes are found along the direction about northeast.[13] The less distinct peaks also denote clockwise rotating ellipses whose major axes are also about along the northeast direction. It is interesting to note that no distinct wind stress variation appears at the inertial frequency (-0.057 CPH). The clockwise rotating components, as a whole, contain about same amount energy as the counter-clockwise rotating ones.

The rotary spectral estimates of the energy distribution of current field at 14 m is shown in Figure 8. Here, the minimum value of the significant energy density estimate is 22.29 $(cm/sec)^2$ CPH^{-1}.

---

[13] The orientation of the major axis of the ellipse is equal to the half value of the phase difference between the two counter-rotating components as discussed in Chapter III. It is calculated with the rotary spectral analysis procedure and is not shown in the spectra plot.

Among the significant ones, distinct peaks exist at diurnal tidal frequency (±0.04 CPH), inertial frequency and semidiurnal tidal frequency (±0.078 CPH); less distinct but discernible peaks exist at frequencies of ±0.11 CPH, ±0.16 CPH and ±0.21 CPH. The semidiurnal tidal oscillation has the largest energy, 97% of which is contained in its clockwise rotating component. The next strong one is the inertial oscillation, but due to the fact that the spectrum does not have a resolved frequency exactly at the inertial frequency at the TOTEM site (0.057 CPH), a broad peak appears at the adjacent frequencies of -0.055 CPH and -0.0625 CPH.[14] Hence, the energy density estimate at the true inertial frequency should have a higher value than the broad peak shows. It is interesting to note that no discernible peak is found either at 0.055 CPH or at 0.0625 CPH as one would expect for the inertial oscillation in the northern ocean. One can see that the semidiurnal tidal oscillation and the inertial oscillation at 14 m are almost circular and rotate clockwise. In contrast, the diurnal tidal oscillation, with about 60% of its total energy in its clockwise rotating component, is a clockwise, very narrow elliptical motion with its major axis in north-south direction. The less distinct peaks are the shorter period oscillations with

---

[14] The broad peak may also be the effect of nonlinear interactions between the wind stress field and the inertial oscillation as the nonlinear interaction will broaden the response spectra as pointed out by Hasselmann (1966).

equivalent periods of about nine, six, four and half hours respectively. They are all clockwise-rotating elliptical motions, and their major axes are also generally in the north-south direction. The predominant clockwise rotation of all the oscillating elements is consistent to the fact that most energy of the current is in its clockwise-rotating components.

Figure 9 shows the rotary spectral estimates of the energy distribution of the current field at 34 m. In the spectra, the minimum value of the significant energy density estimate is 18.36 $(cm/sec)^2$ CPH^{-1}. Among those estimates which pass the significance test, distinct peaks exist at the inertial and semidiurnal tidal frequencies and at a frequency of ±0.16 CPH (corresponding to the period of six hours). The diruanl tidal oscillation at this depth becomes less distinct, with a total energy only 75% of that at 14 m, and it has almost an equal amount energy in its two counter-rotating components. It appears almost a unidirectional oscillation along an axis in the direction of north by northeast. The semidiurnal tidal current at this depth also contains about 8% less energy than that at the 14 m, but its counter-clockwise rotating component has about three times the energy of that at 14 m. Thus, this oscillation is less circular at the 34 m. The inertial oscillation appears at a frequency of -0.0625 CPH with a sharp peak of magnitude 10% higher than the broad peak of inertial oscillation at 14 m. The apparently lower

amount of inertial energy at 14 m is due to that, at that depth, the energy of the inertial oscillation is shown to be spread over two adjacent resolved frequencies, and it is not a real phenomenon. However, the shift of the inertial frequency to a higher value at 34 m is significant. This may be because of that there is about 40% more energy appears in the frequency band centered at 0.0625 CPH of the 34 m spectra than that of 14 m spectra, and consequently, the inertial oscillation at this depth is more like an ellipse. The major axis of this ellipse is found to be along the axis of the mean current at that depth. Thus, along the axis of the mean current, the speed of this elliptical oscillation is higher than that of a circular oscillation whose total energy is the same as the elliptical one, and Doppler effect discussed by White (1972) has a larger effect on the elliptical inertial oscillation. The other elliptical oscillation with an absolute frequency of 0.16 CPH also shows a decrease in its total energy at this depth (it has about 40% of that at 14 m) but only a slight increase of energy in its counter-clockwise rotating component compared with that at 14 m. This ellipse' major axis is also orientated along the axis of the mean current. As a matter of fact, all the major axes of the significant ellipses shown by the three rotary spectra are generally orientated along the axes of the mean direction of their corresponding fields. The total energy of the current field at 34 m, as a whole, is little less than that at 14 m but the energy contained

in the counter-clockwise rotating components is about 30% higher than that at 14 m.

A comparison of the total variance obtained from each field's u and v components versus its two rotary components is given in Table 4. The variance in the u and v components are calculated with standard statistical method, and those in the rotary components are obtained from the rotary spectra. The total variance values by the second method are higher than that by the first method by 16% for the wind stress and by 8% for the currents. However, if only significant rotary components are included in the second method, the differences are reduced to 14%, 2.5% and 0.4% respectively. Thus, the significance test for the rotary spectral density, proposed in this study, seems able to identify the noise in the spectra in most cases.

C. Rotary Cross-spectral Analysis

The results of the rotary cross-spectral analysis between two data series are given in Figures 10-12 in forms of the rotary coherence squared spectrum. By using equation (85), the F-test shows that the 95% confidence limit for the true non-zero coherence squared estimates is 0.53 i.e., any coherence squared estimate with a value less than 0.53 is not significantly greater than zero at 5% level.

Figure 10 gives the rotary coherence squared spectrum between

Table 4. Comparison of the total variance of wind stress and current fields by the rotary spectral method and the statistical method.

	TWSTR	TCU14	TCU34
	$dyne^2/cm^4$	cm^2/sec^2	cm^2/sec^2
Rotary Spectral Method			
All comp.			
Clockwise	3.04	137.20	139.20
Counter-clockwise	2.94	35.20	48.40
Sum	5.98	172.40	167.60
Significant comp. only			
Clockwise	2.86	133.20	113.80
Counter-clockwise	2.86	30.20	43.28
Sum	5.72	163.40	156.08
Statistical Method			
u comp.	2.36	59.80	52.80
v comp.	2.62	99.60	102.74
Sum	4.98	159.40	155.54

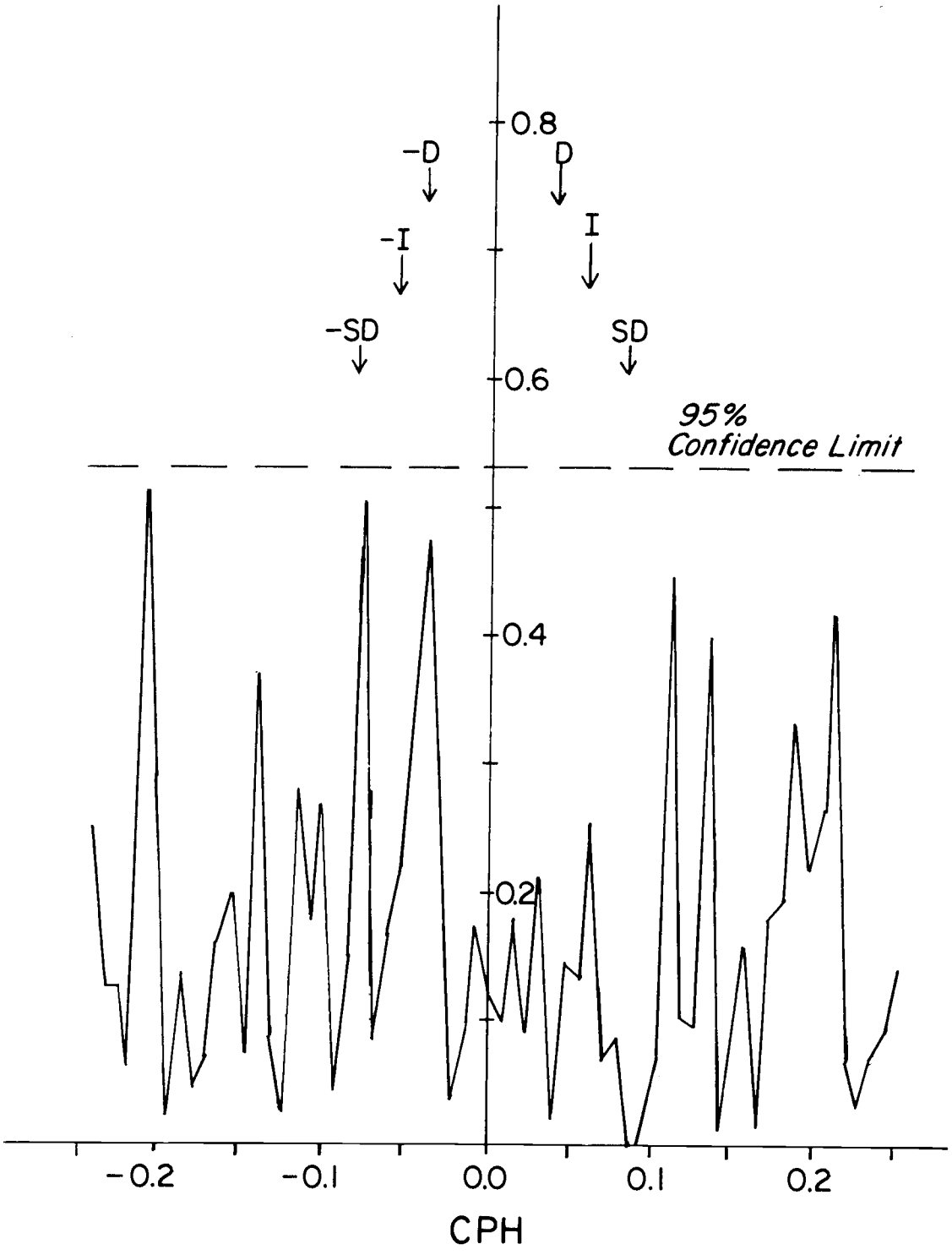

Figure 10. Rotary coherence squared spectrum between wind-stress and current at 14 m.

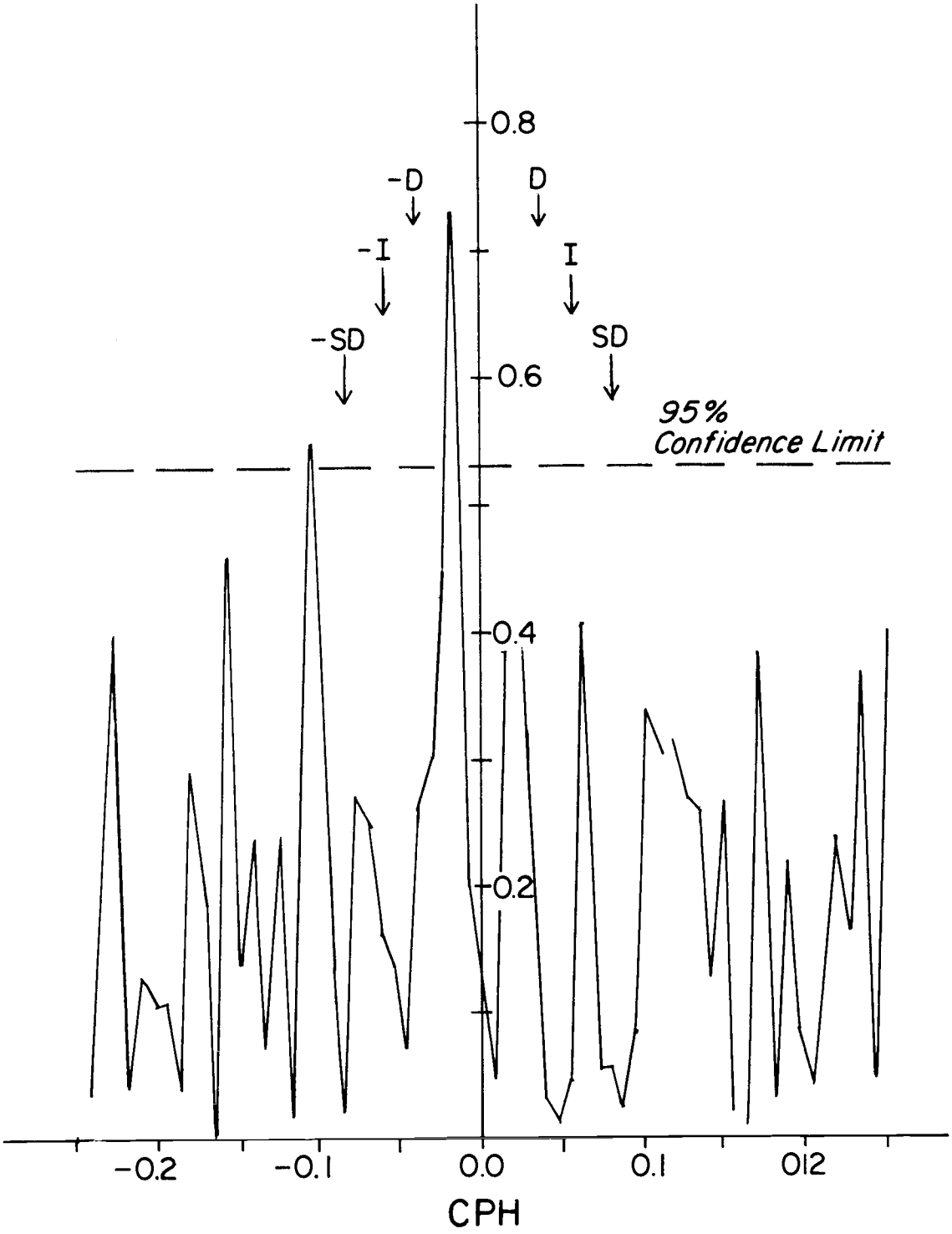

Figure 11. Rotary coherence squared spectrum between wind-stress and current at 34 m.

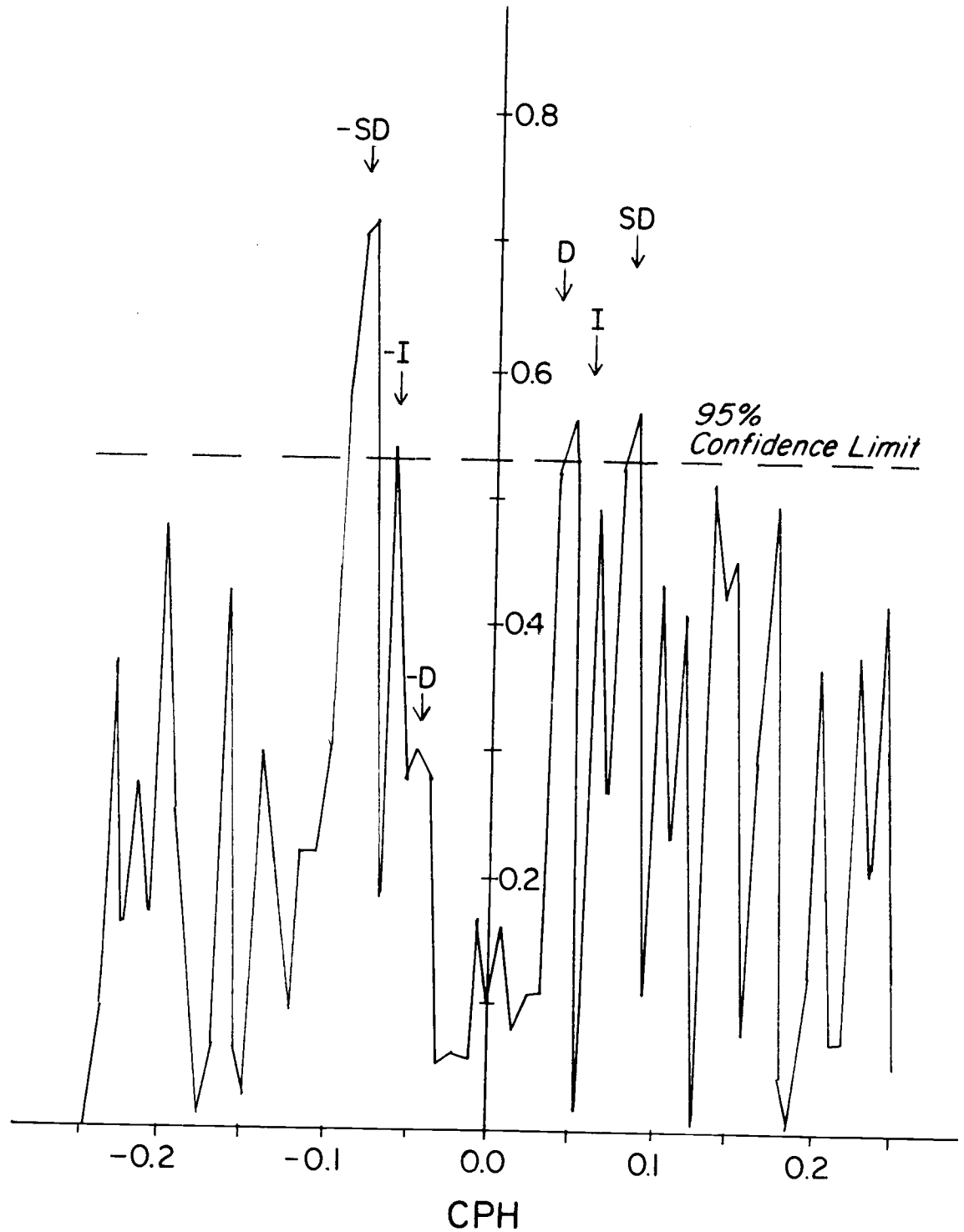

Figure 12. Rotary coherence squared spectrum between currents at 14 m and 34 m.

wind stress field and the current field at 14 m. It is obvious that no rotary coherence squared estimate, in the intermediate frequency range, is significantly greater than zero at 5% level. This phenomenon can be interpreted as that no significant linear relationship exist between the intermediate frequency variations of the wind field and that of the current field at 14 m at the time when the data series were being collected. However, the extremely low value of the rotary coherence squared estimates at the low frequencies may be due to the poor frequency resolution restricted by the data series.

In Figure 11, the rotary coherence squared spectrum between the wind stress field and the current field at 34 m shows significant peaks at -0.016 CPH (64 hours period) and -0.10 CPH (10 hours period). However, no distinct peaks can be found at those frequencies in either the rotary spectrum of the wind stress field or that of the current field at 34 m. No meaningful interpretation can be given to this phenomenon. Pillsbury (1972) reports a similar situation from a location 15 miles off Newport, Oregon in the late summer of 1969. He also found a high coherence squared value at the frequency of -0.10 CPH in the coherence squared spectrum between current fields at 20 m and 80 m, while the rotary spectra of the current fields at these two depths show no distinct energy at that particular frequency. Pillsbury (1972) could offer no explanation of the physical meaning either. Thus, there is no indication of

significant linear relationship between the wind stress field and the current field at 34 m in the intermediate frequency range.

The rotary coherence squared spectrum between the two current fields is given in Figure 12. It again shows extremely low values in the low frequency region, but significant values appear at both positive and negative frequency of semidiurnal tidal oscillation (±0.078 CPH), negative inertial frequency (-0.0625 CPH) and the positive diurnal tidal frequency (+0.04 CPH). The highest peak at negative semidiurnal frequency implies that the semidiurnal tidal oscillations at 14 m and at 34 m are essentially the same. The very low peak at negative diurnal tidal oscillation frequency, on the other hand, indicates the different nature of that oscillation at these two depths as shown by the rotary spectrum. The low but significant peak at the inertial frequency seems consistent with the results found by other investigators, e.g., Sakou and Neshyba (1972). This implies that the inertial oscillations at these two depths are not exactly the same as indicated in the rotary spectrum also. The extremely low coherence squared value at low frequencies may not be due to the poor frequency resolution but may be due that the two current fields are separated by the thermocline (Figure 5) and are indeed two different systems as shown by the PVD diagrams (Figure 6).

D. Rotary Bispectral Analyses

Figures 13-15 show the amplitude distributions of the rotary bispectral density in the frequency domain for the wind stress field and the current fields at 14 m and 34 m. Each topography is presented on four separate tri-frequency planes. These are the two sum-frequency planes $\sigma_1 + \sigma_2 = \sigma_3$ and $-\sigma_1 - \sigma_2 = -\sigma_3$, and the two difference-frequency planes $-\sigma_1 + \sigma_2 = \sigma_3$ and $\sigma_1 - \sigma_2 = -\sigma_3$, on which the counter-clockwise and clockwise rotating components' interaction is shown. Together they compose the half-plane of the frequency domain which uniquely defines the rotary bispectral density of a two-dimensional vector random process. All four computer-produced plots are arranged in identical perspective view, with the origin at the upper right corner of the grid. This imposes an inconvenience in the study of their topography in that the frequency scales of the three axes of the perspective views differ from plane to plane. For example, in the positive sum-frequency plane (for $\sigma_1 + \sigma_2 = \sigma_3$), the directions of all three frequency axes are reversed from that of the master sketch in the center of Figure 13.

Since the significance test shows that, for all three data series, no value of the rotary spectral density estimate with an absolute frequency higher than 0.21 CPH is greater than zero at 5% significance level, the ranges of the interacting frequencies in

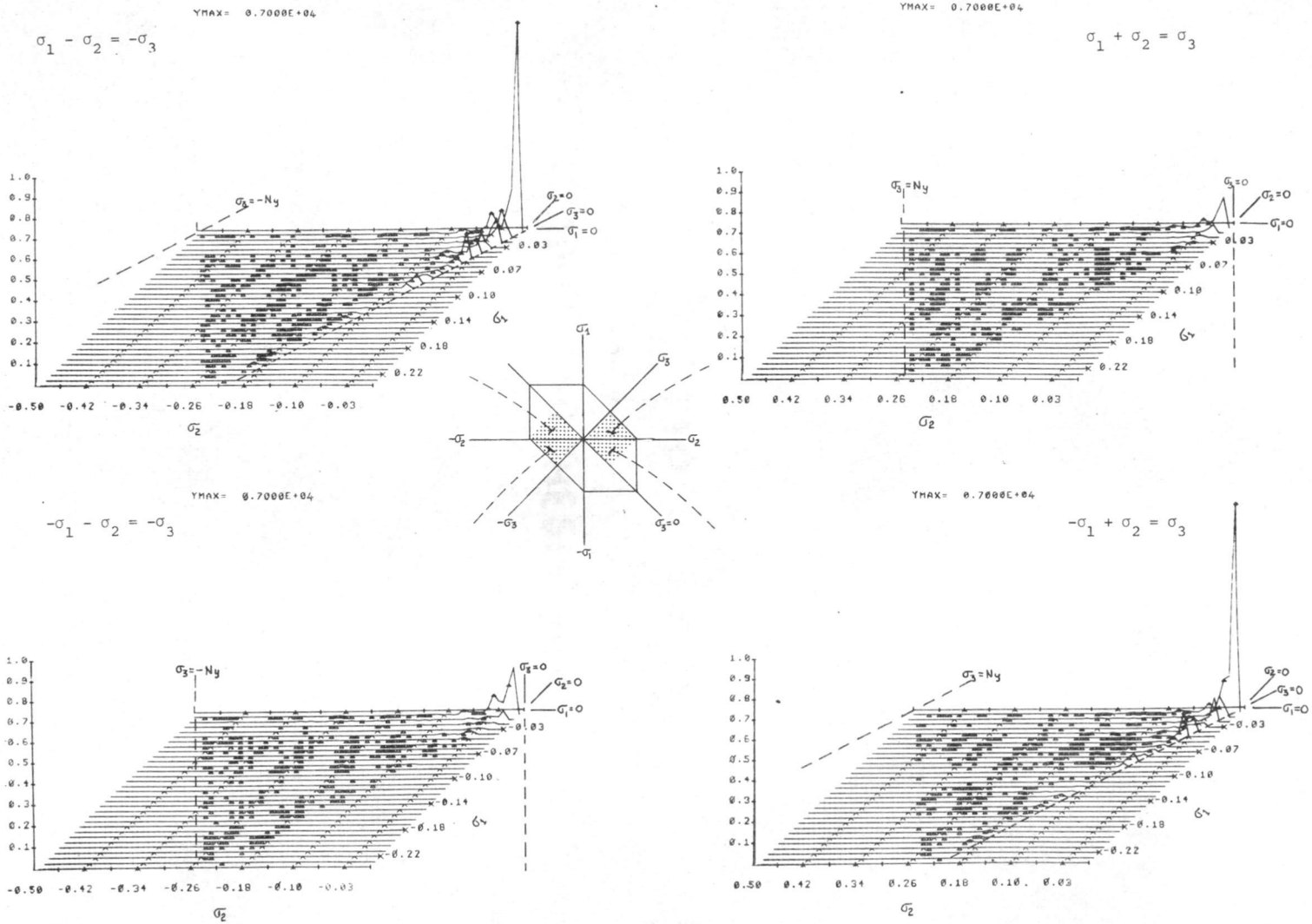

Figure 13. Rotary bispectrum of wind-stress.

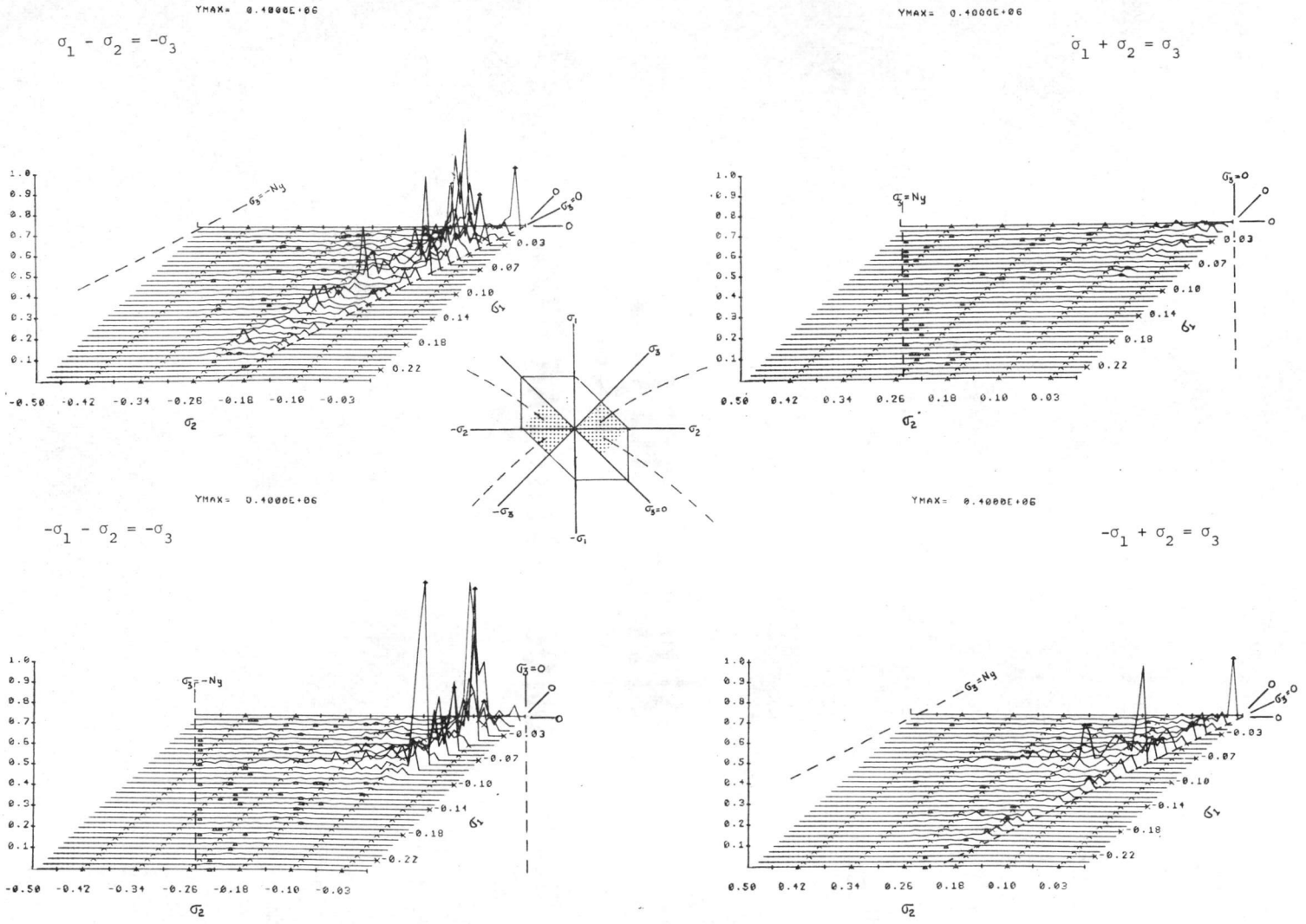

Figure 14. Rotary bispectrum of current at 14 m.

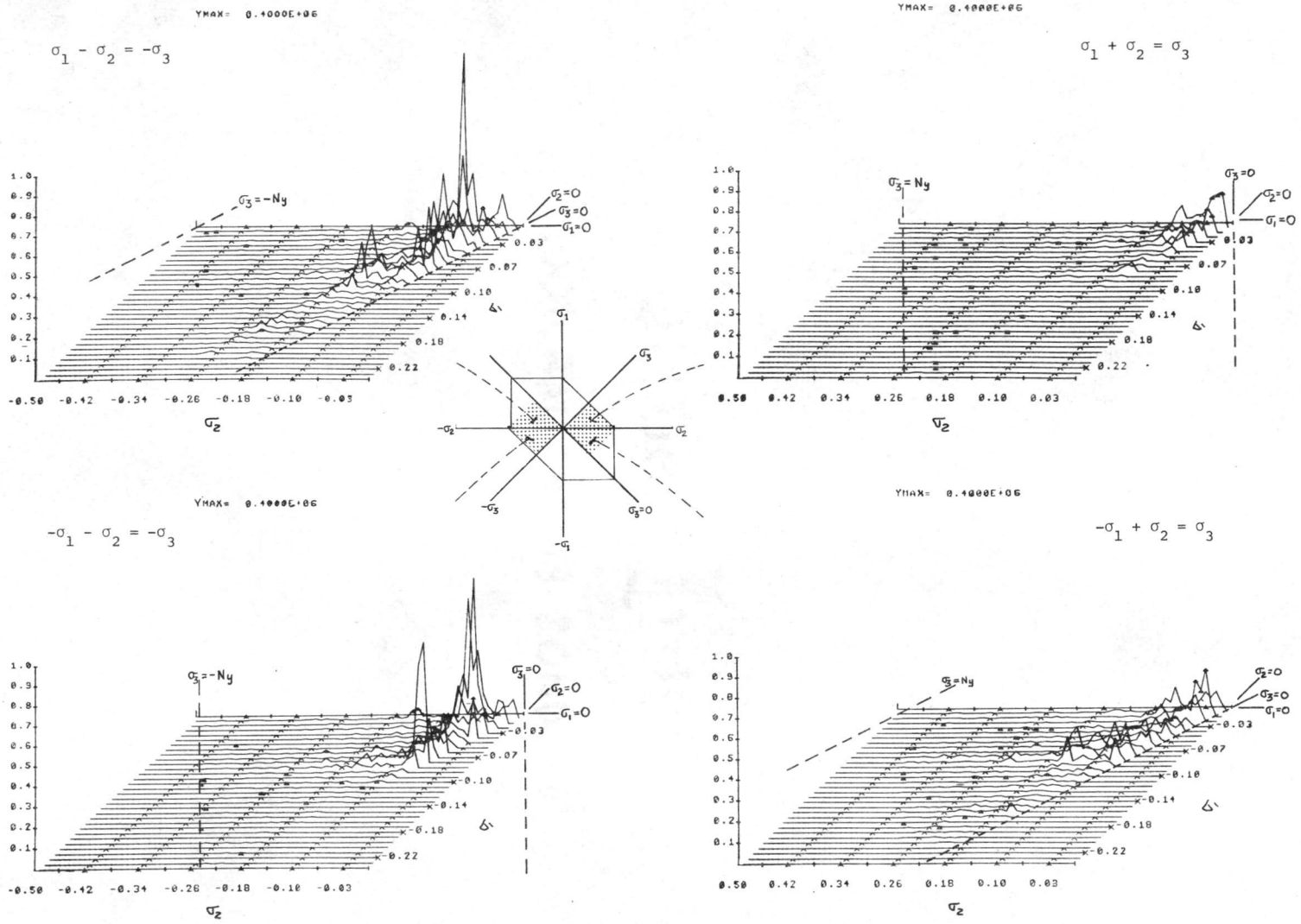

Figure 15. Rotary bispectrum of current at 34 m.

the difference-frequency planes are given as

$$0 \leq |\sigma_1| \leq 0.25 \text{ CPH and } 0 \leq |\sigma_1 + \sigma_2| \leq 0.5 \text{ CPH},$$

which are the same as those in the sum-frequency plane, but occupy only half of the theoretical difference planes shown in Figure 1. Hence all planes presented here have the same size triangular sections in the frequency domain. In all planes, topography features which are statistically significant (i.e., the corresponding bicoherence squared of the bispectral density estimate is greater than 6/EDF as discussed in Chapter III) are marked with a small triangle at their peak. For comparing the relative importance of the interactions appearing in all planes, the amplitudes of all of the estimated bispectral densities are plotted along the vertical Y axis to the same scale, whose maximum value is shown at the top of each plane.

The topography of the rotary bispectra of the wind stress field (Figure 13) shows noticeable quadratic interactions internal to the wind stress field. The conspicuous ridge along the zero σ_3 axis in the two difference-frequency planes indicates the existence of such interactions between the non-oscillatory element of the wind stress and various pairs of counter-rotating components whose frequencies sum to zero. This particular type of quadratic interaction may be interpreted in the following way. When two counter-rotating wind stress components of the same absolute frequency interact, a non-

oscillatory wind stress component is produced. Its amplitude is equal to the product of the amplitudes of the interacting components, and its direction is determined by the phases of the interacting components. Thus, in a non-Gaussian wind stress field, various such non-oscillatory resultants of different amplitudes and directions may be produced by various pairs of interacting counter-rotating components of different absolute frequencies if their phase relations and amplitude products are also different. The relation between each non-oscillatory resultant and the wind stress field's existing non-oscillatory component depends on their amplitudes and directions. If the amplitude of the interactive resultant is relatively high and its direction is parallel to and of the same or opposite sense as that of the existing non-oscillatory component, then the relation indicates strong nonlinear coupling is important. This condition on the direction is analogous to the phase-lock situation discussed in Chapter III. Consequently, this interaction will show a significant feature on the ridge at the intersection of σ_1 and σ_2 lines corresponding to the absolute frequency of the interacting counter-rotating component. In fact, all the quadratic interactions may be interpreted in the same way except that the resultant is an oscillatory component whose frequency is the algebraic sum of the other two components' frequency.

The highest significant elevation of this ridge ($\sigma_3 = 0$) is

related to the pair of counter-rotating components whose absolute frequencies are both 0.0078 CPH (128 hours period). The other parts of the ridge's elevation vary from place to place, but none of them are greater than 15% of the highest significant one, and not all are significant. The ridge becomes undiscernible when the absolute frequency of the interacting pair is higher than 0.10 CPH (10 hours period). The uneven distribution of the ridge's elevation may be because the wind stress field does not have the distinct oscillatory elements at all of the resolved frequencies and that the energy contained in those interacting pairs also varies. Around the origin in all four planes, there are several distinct peaks but they are not all significant. One such non-significant but distinct peak appears in the positive sum-frequency plane at the place where σ_1, σ_2 are equal to 0.0078 CPH (128 hours period) and σ_3 is equal to 0.0156 CPH (64 hours period). It indicates that even though the bispectral density estimates of those three counter-clockwise rotating components is substantial, each of the components also has large amounts of energy; consequently, their bicoherence is too small to vouch for a significant quadratic interaction among them. The same interpretation can be given to another distinct but non-significant peak which appears in the negative sum-frequency plane near the origin. There are also indications of significant but minor interactions existing over all four planes. All the features in this

figure imply that the wind stress field is not a Gaussian process. The concentration of high bispectral density in the lower frequency region is due to the fact that the interacting oscillatory elements at that region contain more energy than at higher frequency region, as shown by the rotary spectra of the wind stress field (Figure 7).

The quadratic interactions internal to the current field at 14 m are more complicated than those within the wind stress field. From Figure 14, one can see that, in addition to the same conspicuous ridge along the zero σ_3 axis as in the wind stress, three other distinct ridges also appear in the frequency domain.

In the two difference-frequency planes, the ridge along the zero σ_3 axis extends from the origin to the place where the absolute value of σ_1 is equal to 0.20 CPH. The ridge has its highest significant elevation near the origin; the other parts of the elevation are generally low and variable and none have an elevation higher than 1/3 of the highest significant peak. This ridge also shows the relation between the non-oscillatory component and the various oscillatory elements of pairs of counter-rotating components (as that discussed in the previous paragraph). In the negative difference-frequency plane, a very distinct ridge appears along the constant σ_3 line of negative inertial frequency (-0.0625 CPH). This ridge shows the interaction between the inertial oscillation and various pairs of counter-rotating components whose difference frequency is equal to

the negative inertial frequency. This ridge extends from a point where σ_1 is equal to zero to one where σ_1 is equal to 0.16 CPH (6 hours period), and its elevation changes rather drastically from place to place. In several places, where σ_1, σ_2 are low, the peaks are high but not significant. The significant peaks along this ridge are related to the rotary components which have been shown to possess significant amounts of energy and which have discernible or minor peaks in the rotary spectra of this current field (Figure 8). However, there is no evidence that the semidiurnal tidal oscillation interacts significantly with the inertial oscillation. It is important to note that no ridge appears in the positive sum-frequency plane along the line where σ_3 is equal to the positive inertial frequency, a phenomenon consistent with the fact that no substantial amount of energy ever exists in the counter-clockwise rotating component at the inertial frequency in the current field at this depth in the northern hemisphere.

The other two ridges that appear in the negative sum-frequency plane and in the positive difference plane are actually two parts of a single ridge along the axis where σ_1 is equal to negative semidiurnal tidal oscillation (-0.078 CPH). This ridge crosses both positive and negative σ_2 frequency lines over a wide range. The highest significant peak on this ridge is at the place where both σ_1 and σ_2 are equal to the negative semidiurnal tidal frequency. This is an indication of

strong quadratic interaction between the semidiurnal tidal oscillation and an oscillatory component at twice the semidiurnal tidal frequency i.e. 6 hours period. Other peaks along this ridge are quite discernible but most are not significant. There are also indications of significant nonlinear interactions between the inertial oscillation and various rotary components in these two planes but they cannot be seen easily in the figure. High peaks in the lower frequency region in these two planes show the interactions among the high energy, low-frequency rotary components. Only scattered and minor peaks can be seen in the positive sum-frequency plane. This is because none of the counter-clockwise rotary components of the current field at this depth have substantial amounts of energy, as shown before (Table 4).

Figure 15 shows different features in the rotary bispectra topography of the current field at 34 m. All of the obvious ridges shown in Figure 14 are also found here, but their elevations are quite different. The ridge along the zero σ_3 axis extends only from the origin to a place at which σ_1 is equal to ± 0.10 CPH. It is an obvious indication that the current field's non-oscillatory component interacts with only a few counter-rotating components (whose frequencies sum to zero). This ridge not only has generally lower elevations than that in Figure 14 (the same vertical scale is used in both figures) but it has no significant peaks. Thus, this particular

type of quadratic interaction is not important to the current field at 34 m. The ridge along the line where σ_3 is equal to the negative inertial frequency is distinct and it cuts through σ_1 lines from 0.0 CPH to 0.18 CPH. Very high elevations are shown at the low frequency region, but they are not significant. The only significant peak appears at the position where σ_1 and σ_2 are equal to 0.10 CPH and -0.16 CPH respectively. The ridge representing the interactions between the negative semidiurnal tidal oscillations and various rotating components is barely discernible in the two difference frequency planes; it has also only one significant peak. This peak appears at the place where σ_2 is equal to -0.14 CPH (7 hours period). In the positive difference-frequency plane there is also a short ridge, barely discernible along the constant σ_3 line of positive inertial frequency. It cuts through the constant σ_1 lines from 0.0 CPH to -0.10 CPH. This feature appears only in Figure 15 and indicates the interactions between the counterclockwise rotating component of an inertial frequency oscillation and various counter-rotating components (whose frequencies sum to the positive inertial frequency). It has only one significant peak at place where σ_1 and σ_2 are equal to -0.11 CPH (9 hours period) and 0.17 CPH (6 hours period), respectively. There is also other evidence of significant nonlinear interactions between the inertial oscillation and various rotary components. But these are not very obvious. In the positive sum-frequency

plane, quite a few significant peaks appear at the lower frequency region. They indicate substantial amounts of energy in the interactions of the counter-clockwise rotating components which have lower frequencies. This phenomenon is consistent with the results shown by the rotary analysis.

E. Rotary Cross-bispectral Analysis

Figures 16-18 show the amplitude distribution of the rotary cross-bispectral density between the wind stress field and the current field at 14 m, between the wind stress field and the current field at 34 m, and between the current fields at 14 m and 34 m. The structure of these figures follows the same pattern as that of Figures 13-15. By using the "cause" and "effect" roles postulated in Chapter III, the topography of the rotary cross-bispectral density can be interpreted as the distribution of the effect on various rotary components of σ_3 (in the second field) by the interaction of various rotary components of σ_1 and σ_2 (in the first field).

In Figure 16 two discernible ridges appear in the negative difference-frequency planes. One of them is along the zero σ_3 axis from the origin to the place where the absolute values of σ_1 and σ_2 are 0.14 CPH. This ridge has only one significant peak - at the place where both σ_1 and σ_2 have an absolute value of 0.024 CPH (43 hours period). The features of this ridge indicate that only one pair

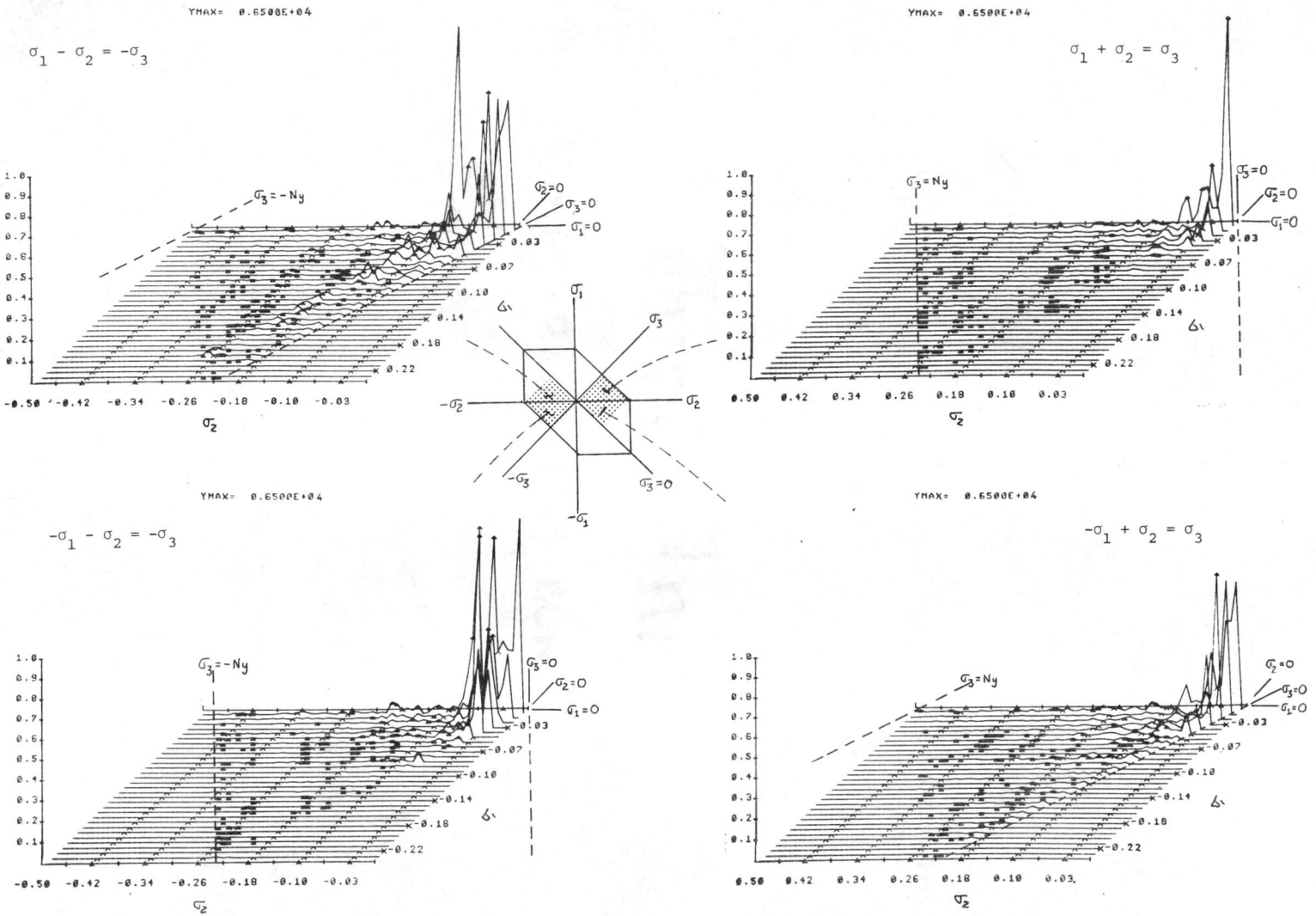

Figure 16. Rotary cross-bispectrum between wind stress and current at 14 m.

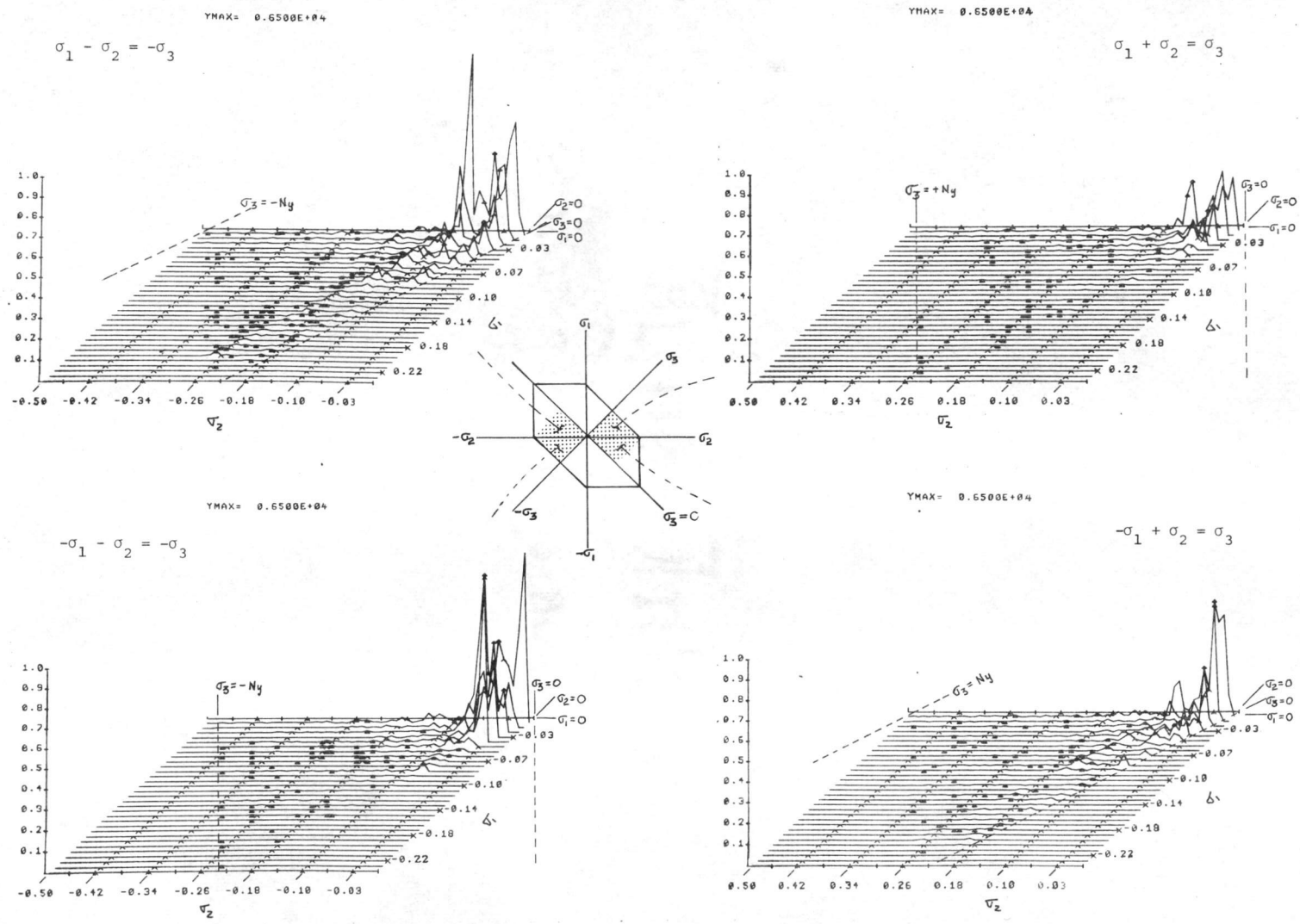

Figure 17. Rotary cross-bispectrum between wind stress and current at 34 m.

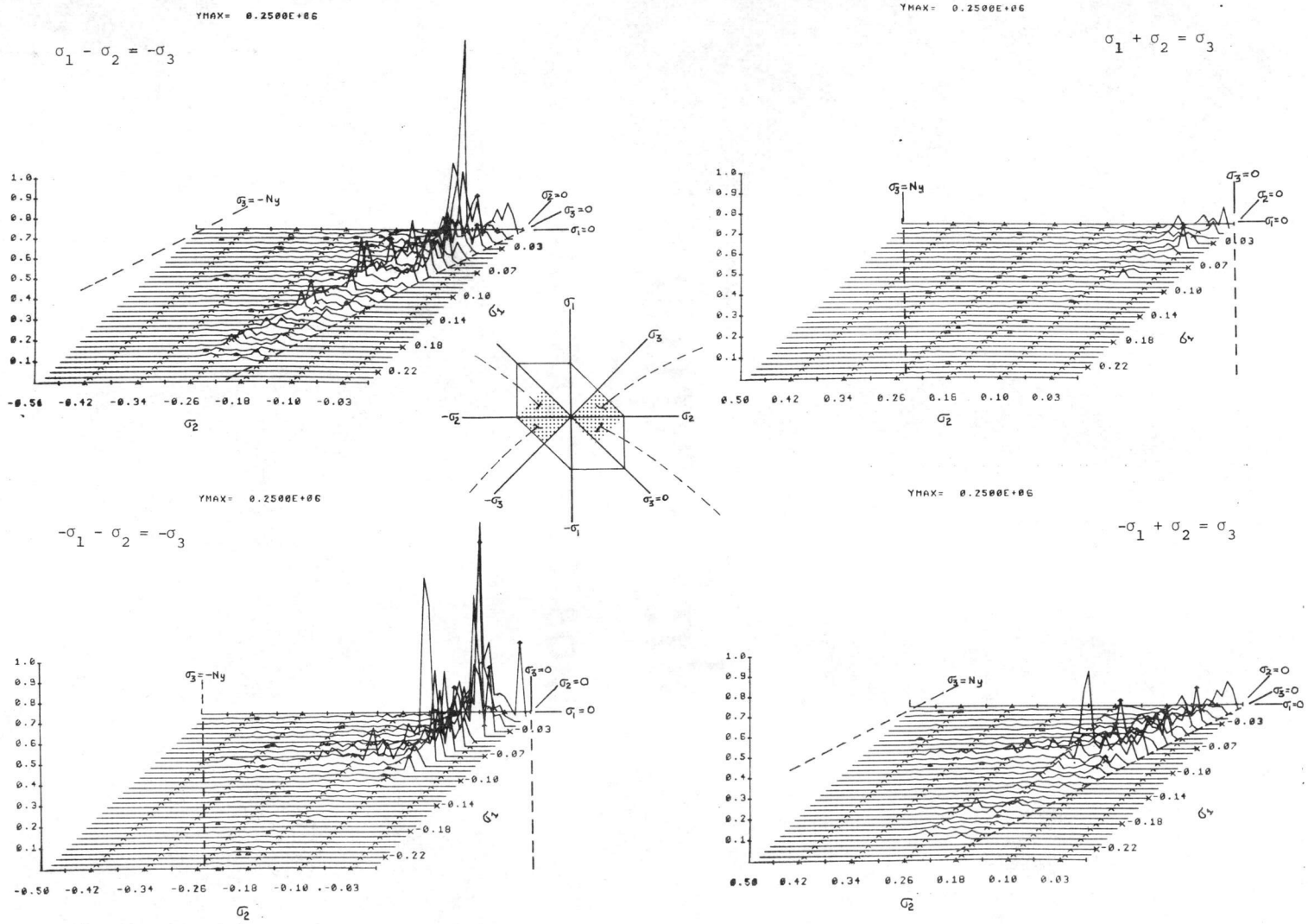

Figure 18. Rotary cross-bispectrum between currents at 14 m and 34 m.

of such counter-rotating wind stress components contributes significantly to the non-oscillatory component of the current field at 14 m. However, the ridge does show other pairs which are related in a non-linear fashion to the non-oscillatory component in that current field. The other ridge in this negative difference-frequency plane is along the constant σ_3 line of negative inertial frequency. It represents the effect on the inertial oscillation at 14 m by the interactions between various pairs of counter-rotating wind stress rotary components (whose difference frequency is equal to the negative inertial frequency). However, only five of such pairs yield significant effects. Their frequencies are 0.000 CPH and -0.0625 CPH; 0.008 CPH and -0.070 CPH; 0.094 CPH and -0.156 CPH; and 0.125 CPH and -0.186 CPH, respectively. Very high significant elevations exist in the lower region in all four planes. They clearly indicate the strong effect on the low frequency components of the current field at 14 m caused by the interactions between the components in the wind stress field.

Figure 17 shows that the topography features of the rotary cross-bispectra between the wind stress field and the current field at 34 m are different from those in the previous figure. One can still see the two ridges in the negative difference-frequency plane. However, the ridge along the zero σ_3 axis extends only from the origin to the point where the absolute values of σ_1 and σ_2 are both 0.086 CPH, and it shows no significant peaks i.e. the interactions between the wind

stress field's counter-rotating components has no significant effects on the non-oscillatory component in the current field at 34 m. The other ridge, which implies the effect on the inertial oscillation at 34 m by the interactions between the wind stress field's counter-rotating components, is discernible, but it has only two significant peaks: at 0.018 CPH and -0.014 CPH; and at 0.125 CPH and -0.186 CPH, respectively. This figure also shows the high significant peaks in the lower σ_3 region of all four planes. One notices that the elevations of this topography are generally lower than those in Figure 16. This indicates that, in this case, the effect of the interactions between the wind stress field's rotary components have less effect on the current field at 34 m than on the current field at 14 m.

The topography shown in Figure 18 represents the distribution of the effect on the rotary components of the current field at 34 m by the interactions between various components in the current field at 14 m. At least six ridges can be seen in the four planes of this figure. In the two difference-frequency planes, the two symmetric ridges along the zero σ_3 axis are quite distinct, but they do not show any significant peaks. Thus, no significant effect on the non-oscillatory component in the current field at 34 m can be expected from the interactions between the counter-rotating components in the current field at 14 m. Distinct ridges appear along the constant negative σ_3 line of the inertial frequency in the negative difference-frequency

plane as well as along the constant positive σ_3 line of the same frequency in the positive difference-frequency plane. But only the former one shows a significant peak to indicate the significant effect on the inertial oscillation at 34 m by the interaction between the counter-rotating components of the current field at 14 m, whose frequencies are 0.10 CPH and -0.164 CPH. Two distinct ridges appear along the constant σ_1 line of semidiurnal (negative) frequency in the negative sum-frequency plane and in the positive difference-frequency plane. They represent the effect on the clockwise rotating components and counter-clockwise rotating components at 34 m by the interactions between the semidiurnal tidal oscillations clockwise rotating component and various other components in the current field at 14 m. But this effect is not important as no significant elevation can be found on these two ridges. High significant elevations can be seen in the lower frequency region in the negative sum-frequency plane, but there are no indications of their existence in the positive sum-frequency plane. This topography, as a whole, shows that the interactions between various rotary components in the current fields at 14 m affect mostly the clockwise components in the current field at 34 m.

The interpretation of the rotary cross-bispectrum, with the postulated roles of "cause" and "effect" and with the emphasis on the significance of the estimated values, is qualitative in nature. The

quantitative analysis is done with the transfer functions developed in Chapter III. The results of that analysis will be discussed in the next section.

F. Energy Transfer

Using the transfer functions defined in Chapter III (see equations 75, 76, 79, 80 and 81), the amount of energy transferred linearly and quadratically from the "cause" field's rotary components to the "effect" field's various rotary components can be calculated in the way described by equation (82). This quantitative analysis, with the postulated roles of "cause" and "effect", is applied first to the wind stress field and 14 m current field and then to the two current fields. The transfer functions and the amount of energy transferred are calculated only from the significant rotary spectral parameter estimates, i.e., only the significant linear and quadratic cases are calculated. The results of this quantitative analysis are summarized in Figures 19-21. In each figure, in addition to the distribution of the transferred energy densities, the significant part of the rotary spectra (in terms of energy density) of the two fields are also given for comparison.

Figure 19 shows the distribution of the energy density transferred from the wind stress field to the current field at 14 m. One can see that not all the energy in the current field is transferred

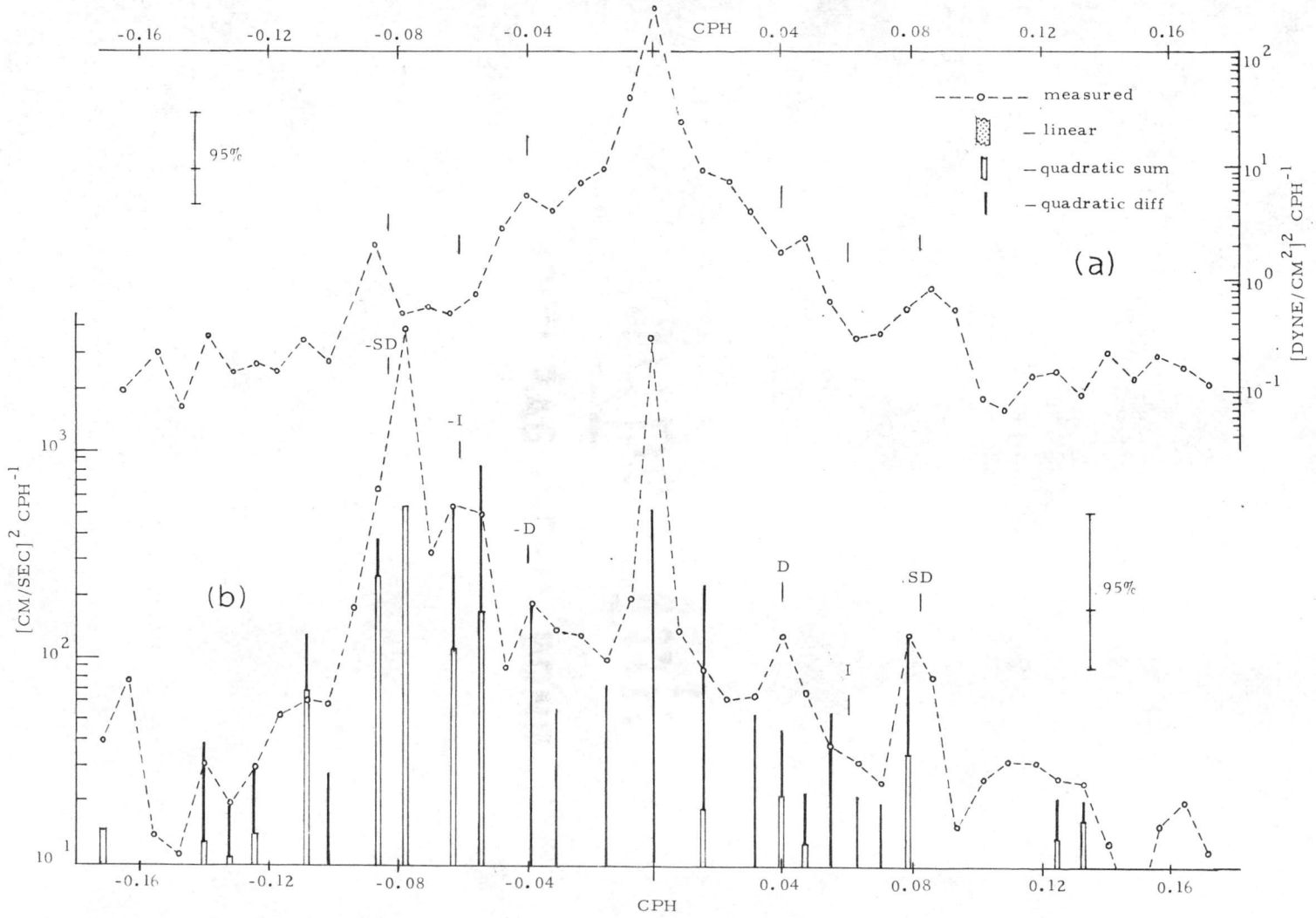

Figure 19. a) Measured rotary spectra of wind stress, b) measured rotary spectra of current at 14 m, compared with the distribution of energy calculated by the energy transform functions.

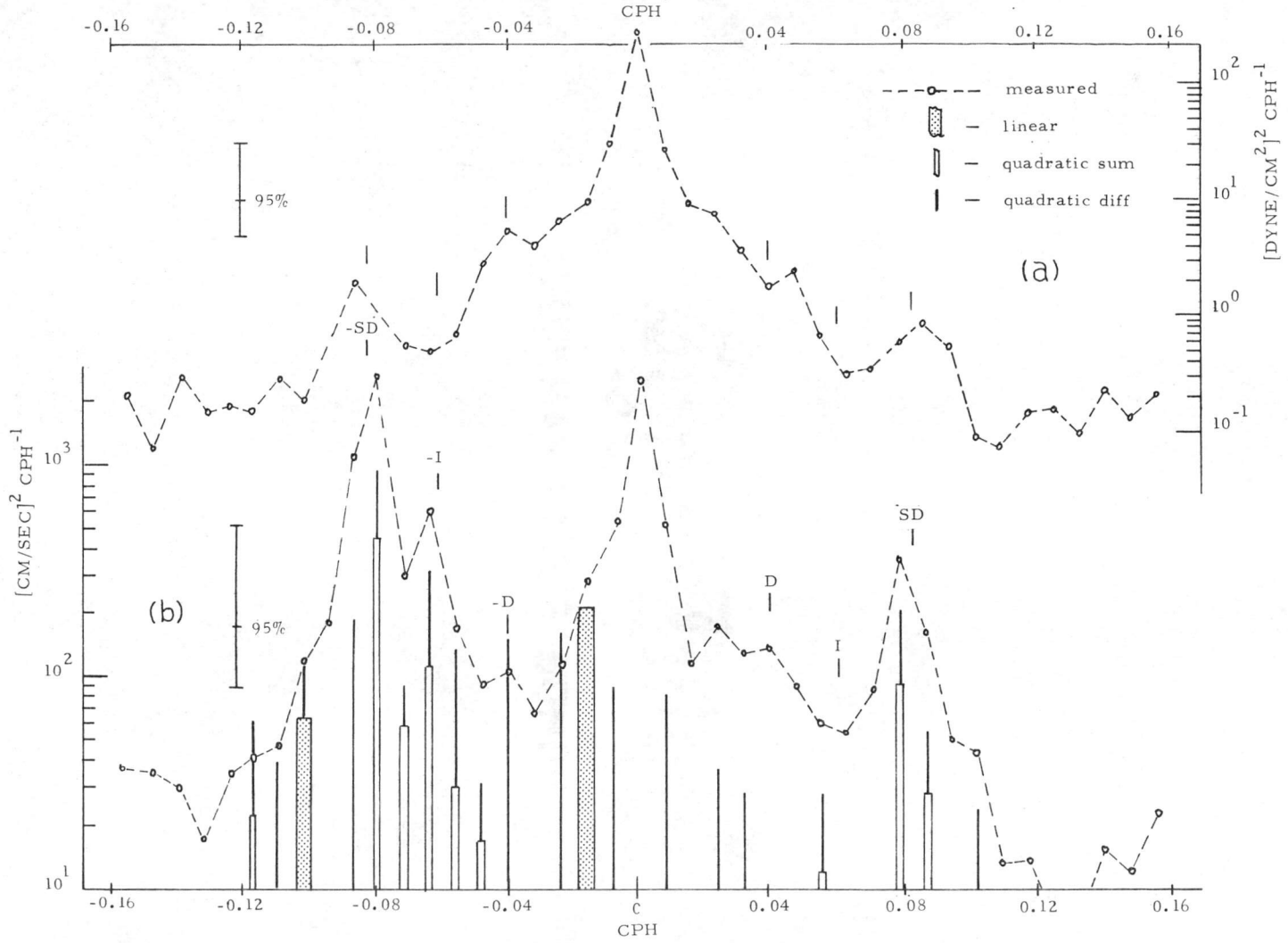

Figure 20. a) Measured rotary spectra of wind stress, b) measured rotary spectra of current at 34 m, compared with the distribution of energy calculated by the energy transform functions.

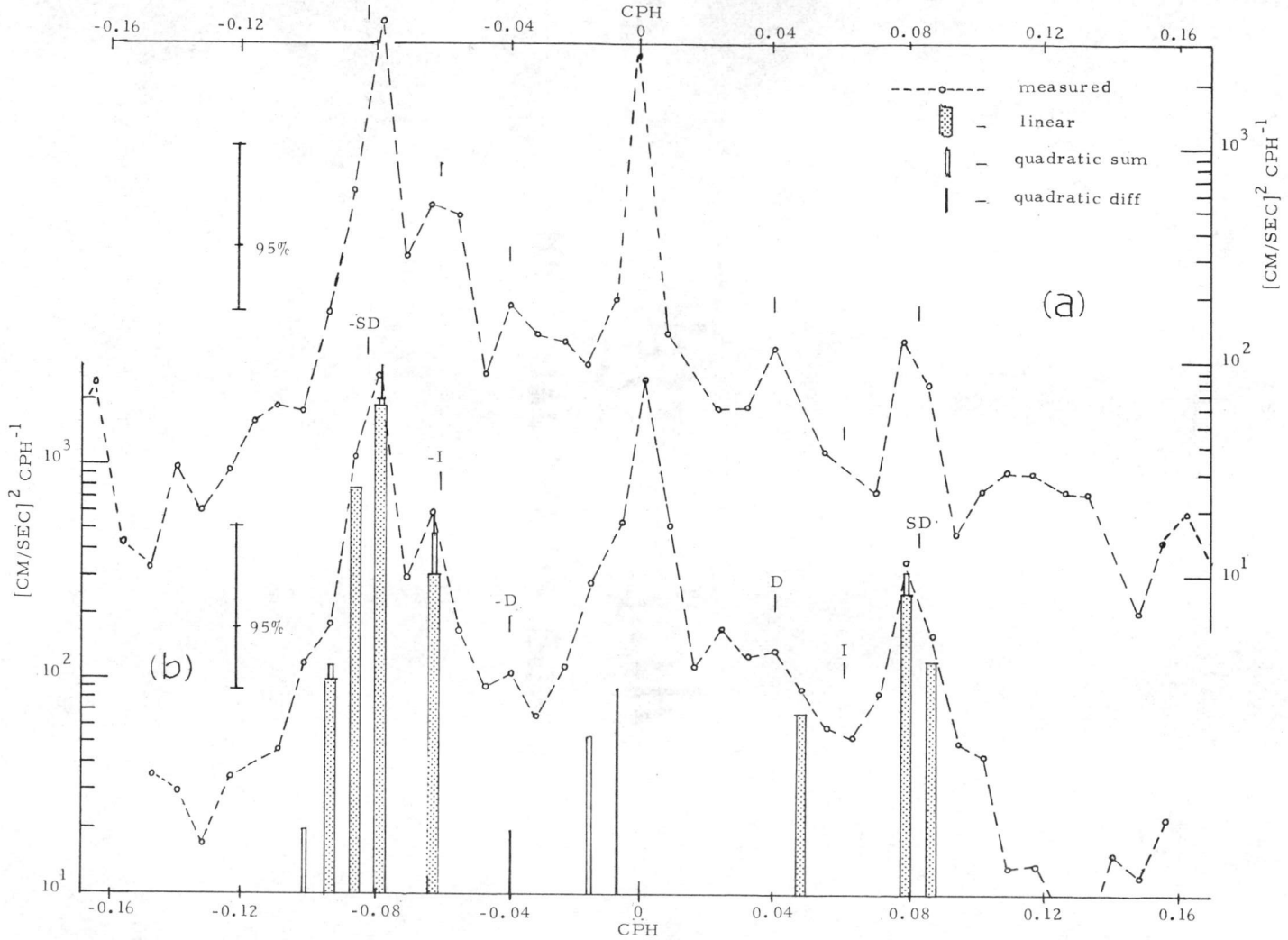

Figure 21. a) Measured rotary spectra of current at 14 m, b) measured rotary spectra of current at 34 m, compared with the distribution of energy calculated by the energy transform functions.

from the wind stress (only 63% of the total energy in the current field can be accounted for as being transferred from the wind stress field), and that no energy is transferred linearly to the current field in the frequency range of interest in this study. At some frequencies, the values of the transferred energy appear higher than those measured. However, they are all in the 95% confidence limit of the measured one. Thus, both calculated and measured energies can be considered to be equal in these cases.

The current components which have the same amount of measured and calculated energies may be said to obtain their energy from the interacting components in the wind stress field. For instance, at the inertial frequency (both positive and negative), the measured and calculated energy densities appear the same (6% of the total energy measured in the current field at 14 m). The result is compatible with the previously discussed hypothesis that inertial oscillations in the upper layers of the ocean are locally generated by wind (see Chapter I). However, one should note that, here, the energy in the inertial oscillation components derives from several pairs of interacting components in the wind stress field; further, no part of the calculated energy density is transferred linearly from the wind stress component at the inertial frequency, as the rotary spectral analysis shows no such component existing distinctly in the wind stress field, and the rotary cross spectral analysis shows no significant linear relationship

between the two fields at such frequency. Thus, a linear transfer function cannot be established between these two fields. These results do not agree with Belyaev and Koleniskov's hypothesis (1966) that the inertial oscillation is the resonance response of the current to the wind stress component whose energy is constant at the inertial frequency and is linearly transmitted to the current field through a "sharp transmission function". Besides, both the wind stress field and current field, as well as the relation between them, have been shown previously to be non-Gaussian in nature. This is in contrast to the assumption of Gaussian process upon which their hypothesis is based.

Table 5 gives a breakdown of the total energy transferred from the wind stress field to the inertial oscillation at 14 m. It shows that seven pairs of the interacting wind stress components contribute 96.4% of the total to the oscillation's clockwise rotating component (-0.063 CPH), and that another three pairs contribute only 3.6% of the total to its counterclockwise rotating component (0.063 CPH). Since the inertial oscillation rotates clockwise in the northern hemisphere, the small contribution (to its counter-clockwise rotating component) from the last three pairs can be considered as the noise part and will not be further discussed here. The first seven pairs are grouped and discussed as follows:

1) Interactions involving the non-oscillatory component

Table 5. Contributions of the wind stress components to the calculated energy density of the inertial oscillation at 14 m, in $(cm/sec)^2\ CPH^{-1}$.

Components	Interacting Frequency Triplets, CPH	Amount	%	Sub-total	Total
Clockwise					
1) Linear		0.0	0.0	0.0	
2) Quadratic Sum	0.000 - 0.063 = - 0.063	22.7	3.7		
	-0.023 - 0.039 = - 0.063	88.6	15.3	111.3	
3) Quadratic Diff.	0.000 - 0.063 = - 0.063	22.7	3.7		
	0.008 - 0.070 = - 0.063	97.0	16.7		
	0.078 - 0.141 = - 0.063	160.0	27.2		
	0.094 - 0.145 = - 0.063	88.0	15.3		
	0.125 - 0.187 = - 0.063	87.0	15.0	455.7	567.0
Counter-clockwise					
1) Linear		0.0	0.0	0.0	
2) Quadratic Sum	0.031 + 0.031 = 0.063	8.9	1.5	8.9	
3) Quadratic Diff.	-0.023 + 0.086 = 0.063	6.0	1.0		
	-0.063 + 0.125 = 0.063	6.7	1.1	12.6	21.6
			100 %		588.6

Three pairs comprise this group. Two of these, at frequencies 0.000 CPH and -0.063 CPH, represent the effect of the interacting non-oscillatory wind stress component and the wind stress component of inertial frequency. The third pair, whose frequencies are 0.008 CPH and -0.070 CPH, may also be considered to be the same as above because of the rough frequency resolution at low frequencies (they do not appear distinctly in the rotary spectra). This particular type interaction may be interpreted as follows. In the wind stress field, the variation at the inertial frequency is not distinct, i.e., such variation is not persistent. It still can affect the inertial oscillation in the ocean if it interacts with the non-oscillatory component in such a way that, at some time, it is in phase lock with the inertial oscillation in the ocean. Since this type interaction is not distinct, one would not expect that substantial amounts of energy can be transferred. In this case, only about 23% of the total transferred energy to the inertial oscillation is accounted for as being from this wind stress variation at the inertial frequency. Thus, it further shows that the inertial oscillation in upper layer ocean does not obtain all its energy from such wind stress variation in contrast to what Belyaev and Kolesnikov (1966) imply in their hypothesis.

2) Other pairs

The other four pairs from which the inertial oscillation derives

a significant amount of energy are the wind stress components with periods ranging from near two days to one quarter of a day. It is interesting to note that about 42.5% of the energy transferred to the inertial oscillation results from the interacting wind stress components with periods of half-day and a quarter of day. This phenomenon is compatible with the conclusion given by Pollard and Millard (1970). They say that one of the features in the wind stress field which is most efficient in changing the amplitude of the inertial motion is a strong wind blowing in one direction for up to half an inertial period. Their statement accurately describes the interaction seen here between the significant half-day period and the quarter-day period components. The amount of energy transferred to the inertial oscillation can either destroy or enhance the oscillation depending on the phase relation among the interacting components and the existing inertial oscillation. However, in this study, it is not possible to identify the actual phase relation because only the modified components can be estimated from the sampled data.

Figure 19 also shows that other current components derive energies from various interacting wind stress components. The current field's non-oscillatory component has about 10% of its energy derived from the interacting of two counter-rotating wind stress components of same period, of 43 hours, as shown in the previous rotary cross-bispectral analysis (1.5% of the total energy measured

in the current field at 14 m). Also, the energy contained in the various components of the tidal oscillation appears to result solely or partly from the interacting wind stress components. The counter-clockwise rotating tidal current components can be considered as the noise part of the tidal currents as the tidal currents are expected to rotate clockwise in the northern hemisphere. However, the clockwise components are not the sole effect of the wind stress components, linearly or nonlinearly. An explanation may be given in the following way for the case that the measured and calculated energy densities appear the same for the diurnal tide current's clockwise component. In this component, half of the original energy caused by the celestial tidal forces is destroyed by an out-of-phase clockwise component induced by the interacting wind stress components whose algebraic sum frequency is equal to the negative diurnal tidal frequency, and the modified component with half of the original diurnal energy appears to have all its energy derived from the interacting wind stress components. One also may use this explanation to interpret the apparent indication that the rotary spectra of the current field at 14 m show less energy in the diurnal tidal component than in the semidiurnal. On one hand, larger semidiurnal energy could be attributed to an enhancement by addition of energy nonlinearly from the wind stress. On the other hand, the smaller diurnal energy could be attributed to the degeneration by the energy from the wind

stress, again by the nonlinear process.

Figure 20 shows the distribution of the energy density transformed from the wind stress field to the current field at 34 m. It again shows that not all the energy in the current field is transferred from the wind stress field (in this case, 52% of the total energy in the current field can be accounted for as being transferred from the wind stress field). But it shows small amounts of energy (2.4% of the total) being transferred linearly at frequencies of -0.024 CPH and -0.10 CPH. However, this phenomenon is insignificant not only because of the small amount of energy involved but also because the linear relationship between these two fields at these frequencies have no real physical meaning. Thus, one can still assume that wind stress field's energy is transferred nonlinearly to the current field at 34 m. However, this current field (below the mixed layer) is not subject to the direct influence of the wind stress field either, linearly or nonlinearly. It can be considered as a modified version of the current field at 14 m, i.e., modified by the other processes in the ocean. Thus, both the qualitative and quantitative analyses between the wind stress field and this current field do not yield any subjective information because of the unsound postulated roles of "cause" and "effect". Nevertheless, the results of those analyses may still be used heuristically to infer the remaining characteristics, induced by the wind stress, of the current field at 14 m, in that at 34 m.

Compared to Figure 19, Figure 20 shows a different distribution of the calculated energy densities, and it shows less numbers of the current components having the same measured and calculated energy densities. These imply that a different nonlinear relationship exists between the wind stress field's interacting components and various components in the current field at 34 m which are also affected by other processes in the ocean. For instance, the inertial oscillation at this depth appears to derive only 64% of its energy from the wind stress through nonlinear process, and the computation shows it nonlinearly related to fewer and different interacting wind stress components than that at 14 m. From Table 6, one can see that 1) some pairs shown in Table 5 are not here, e.g., those involving the non-oscillatory wind stress components; 2) new pairs not shown in Table 5 appear here, and 3) the pairs shown in both tables have different calculated energy densities. From these features, it is concluded that only the effect of the distinct interacting wind stress components, e.g., the pair with periods of half a day and quarter of a day, still remains in the inertial oscillation after it has been influenced by other processes in the ocean. It is also interesting to note that the interacting wind stress components do not have any effect on the non-oscillatory component in the current field at 34 m as discussed previously.

Figure 21 gives the distribution of the energy densities

Table 6. Contributions of the wind stress components to the calculated energy density of the inertial oscillation at 34 m, in $(cm/sec)^2$ CPH^{-1}.

Components	Interacting Frequency Triples, CPH	Amount	%	Sub-total	Total
Clockwise					
1) Linear					
2) Quadratic Sum	-0.031 - 0.031 = - 0.063	123.2	35.0	123.2	
3) Quadratic Diff.	0.078 - 0.140 = - 0.063	107.7	31.0		
	0.125 - 0.197 = - 0.063	101.5	29.0	209.2	332.4
Counter-clockwise					
1) Linear		0.0	0.0	0.0	
2) Quadratic Sum	0.031 + 0.031 = 0.063	17.0	5.0	17.0	
3) Quadratic Diff.		0.0	0.0	0.0	17.0
			100 %		349.4

transferred from the current field at 14 m to that at 34 m. It is obvious that not all the energy in the latter current field is derived from the former, and that, compared with the wind stress field to current field cases, fewer current components at 34 m derive their energies from the "cause" field, i.e., current field at 14 m. Here, the computation shows that of all the energy derived from the current components at 14 m (50% of the total measured energy in the current field at 34 m), two-thirds is transformed linearly at frequencies of semidiurnal tidal frequency and negative inertial frequency or near to these frequencies. One notes that at these frequencies, the measured and calculated energy densities appear to be the same, and the linear transfer process is predominant. For instance, at the negative and positive semidiurnal frequencies, the linear process accounts for 67.5% and 81% of the transferred energy, respectively; at the negative inertial frequency, it accounts for 53.4%. These features indicate that, at these frequencies, the current components are really the common part of the two current fields separated by the thermocline. One can also say that the field below the thermocline has been modified by nonlinear processes in the ocean as shown by the portion of energy transferred nonlinearly.

A breakdown of the transferred energy density at the inertial frequencies (positive and negative) is given in Table 7. There are three pairs of interacting current components at 14 m which transform

Table 7. Contributions of the current components at 14 m to the calculated energy density of the inertial oscillation at 34 m, in $(cm/sec)^2\ CPH^{-1}$.

Components	Interacting Frequency Triples, CPH	Amount	%	Sub-total	Total
Clockwise					
1) Linear		313.3	53.2	313.3	
2) Quadratic Sum	-0.016 - 0.047 = - 0.063	52.5	8.9*		
	-0.031 - 0.031 = - 0.063	108.8	18.5	161.3	
3) Quadratic Diff.	0.102 - 0.164 = - 0.063	112.2	19.4	112.2	586.8
Counter-clockwise					
1) Linear		0.0	0.0	0.0	
2) Quadratic Sum		0.0	0.0	0.0	
3) Quadratic Diff.		0.0	0.0	0.0	0.0
			100 %		586.8

* By second path only

energy nonlinearly to the clockwise-rotating component of the inertial oscillation at 34 m. The first pair, at frequencies of -0.016 CPH (two pendulum days period) and -0.047 CPH (21 hours period), contribute energy to the inertial oscillation at 34 m by the second path discussed in Chapter III (see Figure and discussion on page 58). These components show no distinct peaks in the rotary spectrum, and they are not significantly nonlinearly related to the inertial oscillation at 34 m. However, the resultant of their interaction is linearly related to that oscillation. The process is not distinct, and, consequently, transfers only a small amount of energy. The second pair shows an interaction involving two clockwise-rotating components at 14 m each with the same period of one pendulum day. However, on the resolved frequency scale of the rotary spectrum, the estimated energy density at this frequency appears adjacent to that of the clockwise-rotating diurnal tidal current; at 14 m, the latter shows a somewhat distinct peak on the rotary spectrum. Thus, it is rather difficult to assess the distinctness of one-pendulum day oscillations. The third interacting pair includes the current components at 14 m with frequencies of -0.10 CPH (10 hours period) and -0.163 CPH (quarter-day period). They are distinct components, but are not the direct effect of the wind stress variation (see Figure 19). Their existence at 14 m is due to the nonlinear interactions internal to the current field at that depth.

Therefore, this interacting pairs' effect on the inertial oscillation at 34 m is an oceanic nonlinear process.

It is interesting to note that the amount of 34 m current energy which is related nonlinearly to the wind stress field is about the same as that (50% of its total) which is related nonlinearly and linearly to the current field at 14 m. One cannot say that this is the amount of wind stress energy actually transferred to the current field below the thermocline (at 34 m) as one has to exclude the part of energy transformed by pure oceanic processes. If one makes such a calculation using only the parts which can be considered as being transformed from the wind stress field, i.e., parts linearly transformed at or near the negative inertial and positive tidal frequencies, the result shows only 7% of the total measured energy of the current field at 34 m can be considered as being from the wind stress field (about 10% of the amount of the energy transferred from wind stress field to the current field in the mixed layer at 14 m).

VI. SUMMARY AND CONCLUSIONS

A. Summary

Much of the current literature on the generation of inertial oscillations by local wind are based on the assumption that these are Gaussian fields. It is shown here that the fields are not Gaussian, and therefore that cause and effect analysis should include the non-linearity. Bispectral and cross-bispectral statistics are ways of examining nonlinearity in the wind-current momentum transfer. When they are applied to rotary components of the fields of wind and current, these statistical techniques produce new and interesting insights of the complex energy transfer process.

The use of four tri-frequency planes is an effective means of viewing the distribution of all possible nonlinear interactions internal to a two dimensional field or between two such fields. This is particularly true for those involving a wide range of triples of frequencies, as in the case of the non-oscillatory component, inertial oscillation and tidal components. Postulating "cause" and "effect" roles on the basis of physical nature, the effects of all possible interacting components of the "cause" field on the vaious components in the "effect" field can be examined qualitatively from the cross-

bispectra features shown in these four planes. Statistical tests can identify the significance of each nonlinear interaction presented there.

Quantitative analysis of the energy transferred from one field to another, linearly and nonlinearly, are calculated with linear and quadratic transfer functions. The linear transfer function at each frequency is computed from significant rotary cross-spectral density estimates between the two fields and the rotary spectral density estimate in the "cause" field. The quadratic transfer function at each frequency triple is computed from the significant rotary cross-bispectral density estimate between the two fields and the significant two rotary spectral density estimates at the interacting frequencies in the cause field. The nonlinear interaction internal to the "cause" field concerning the components at the two interacting frequencies is accounted for with the significant rotary bispectral density estimate at this frequency triple and the first order linear transfer function at the frequency which is the algebraic sum of the two others in the triple.

The postulated "cause-effect" relation between the wind stress and the current within the well-mixed layer at 14 m has a firm physical foundation for those current oscillations at the negative inertial frequency. Accordingly, all of the 14 m inertial frequency energy is considered to derive directly from the wind. Results show that the

transfer is only by nonlinear process.

The transfer computation also shows relations between the wind stress and 14 m current fields at frequencies other than the inertial, e.g., the tidal frequencies. In this case, "cause-effect" should not exist by physical argument. However, since finite transferred energy is found in the current field at the tidal frequencies, it is possible that the "pure" tidal oscillation is modified. At the diurnal tidal frequency, the calculated energy transferred nonlinearly from wind stress appears equal to measured energy. It is necessary then to interpret the "measured" diurnal tidal current energy as being highly modified by the wind field. It is argued that the modification effect can be either enhancement or degeneration of the "pure" tidal oscillation depending on its phase relationship to the diurnal oscillation transferred from the wind fields, but that this analysis technique is unable to distinguish which case obtains.

The energy transferred linearly between the two current fields is considered as common to the two current fields; of this linearly transferred part, that which is the result of the wind stress field is the measure of the effect of the wind on the current field below the mixed layer.

B. Conclusions

Examining the results of the data analysis, the conclusions of

this study are as follows:

1. In the intermediate frequency range, no energy is found to be transferred linearly to the ocean.

2. In the mixed layer at the TOTEM site, 63% of the total energy measured in the current field at 14 m can be accounted for as being transferred nonlinearly from various interacting wind stress components. Of this amount, less than two percent (1.5%) goes to the current field's non-oscillatory component but accounts for 10% of its measured value, and 9% goes to the inertial oscillation and accounts for 100% of its measured value; the rest, 89.5%, goes to other components, e.g., tidal current components, etc.

3. In the frequency range with corresponding periods longer than 7 hours, various pairs of counter-rotating wind stress components of like period are shown to be nonlinearly related to the non-oscillatory current component in the mixed layer at 14 m, but only the pair with period of 43 hours can significantly transfer energy nonlinearly to that component. None of these pairs are significantly related with the non-oscillatory component just below the mixed layer at 34 m.

4. Over a wide frequency range, various pairs of wind stress components are shown nonlinearly related to the inertial oscillation in the mixed layer at 14 m. But only few such interacting pairs can significantly transfer any energy to this oscillation. The most

effective pair has periods of half-day and quarter-day, and 43% of this oscillation's measured energy is derived from this pair. Its effect is also shown on the inertial oscillation just below the mixed layer at 34 m.

5. Spectrally indistinct wind stress variation at the inertial frequency can still transfer energy to the inertial oscillation in the mixed layer if the phase lock situation can be established between the wind stress field's interacting inertial and non-oscillatory components and the current field's inertial oscillation. In this study, 23% of the inertial oscillation's measured energy is attributed to this particular type of interaction. This fact does not support Belyeav and Kolesnikov's hypothesis (1966) that inertial oscillation is the resonant linear response of the ocean to the wind stress variation at the inertial frequency.

6. The inertial oscillation in the mixed layer at 14 m is a nonlinear interaction response of the ocean to the wind stress variation in the intermediate frequency range. Hasselmann (1966) suggests that nonlinear interactions have the effect of broadening the response spectra. This suggestion is supported by the existence of the broad peak shown at the inertial frequency in the rotary spectra of current field at 14 m.

7. The current field just below the mixed layer at 34 m represents a different water movement compared to that in the

mixed layer at 14 m. Their common parts are in the inertial oscillation and tidal currents. However, these common parts are shown as being subjected to nonlinear interactions internal to the ocean. Only 7% of the total measured energy of the current field at 34 m is shown as being derived from the wind stress.

BIBLIOGRAPHY

Barnett, T. P., et al. 1971. Bispectrum analysis of electroencephalogram signals during waking and sleeping. Science 172(3981): 401-402.

Belyaev, V. S. 1967. The dependence of the spectra of the velocity components of a wind-driven current on the spectrum of tangential wind forces. Atmospheric and Oceanic Physics 3(11): 715-719. (Translated from Fizika Atomosfery I Okeana)

Belyaev, V. S. and A. G. Kolesnikov. 1966. On the reason for the formation of inertial oscillations in connections with pure drift currents. Atmospheric and Oceanic Physics 2(10): 665-667. (Translated from Fizika Atomosfery I Okeana)

Bendat, J. S. and A. G. Piersol. 1966. Measurement and analysis of random data. New York, John Wiley and Son. 390 p.

Bevington, P. R. 1969. Data reduction and error analysis for the physical sciences. New York, McGraw-Hill. 336 p.

Bingham, C., M. D. Godfrey and J. W. Tudey. 1967. Modern techniques of power spectrum estimation. IEEE Transactions on Audio and Electroacoustics 15(2): 56-66.

Bottero, J. 1973. Research Assistant, Oregon State University, School of Oceanography. Personal communication. Corvallis, Oregon.

Brillinger, D. R. and M. Rosenblatt. 1966a. Asymptotic theory of estimates of K-th order spectra. In: Proceedings of Advanced Seminar on Spectral Analysis of Time Series, ed. by B. Harris. New York, John Wiley and Son. p. 153-188.

_____. 1966b. Computation and interpretation of K-th order spectra. In: Proceedings of Advanced Seminar on Spectral Analysis of Time Series, ed. by B. Harris. New York, John Wiley and Son. p. 189-232.

Burt, W. 1973. Use of on-line computers in environmental research. Corvallis, 7 numb. leaves. (Oregon State University. School of Oceanography. Final Report to Office of Naval Research Contract N00014-68-A-0148 Project NR 083-230)

Collins, C. A. 1968. Description of measurements of current velocity and temperature over the Oregon continental shelf, July 1965-February 1966. Doctoral dissertation. Corvallis, Oregon State University. 154 numb. leaves.

Crew, H. and G. Bodvarsson. 1971. Testing data for normality. Corvallis, Oregon State University, Department of Oceanography. 6 numb. leaves. (Informal memorandum)

Crow, E. L., F. A. Davis and M. W. Maxfield. 1960. Statistic manual. New York, Dover. 288 p.

Dewan, E. M. 1969. Nonlinear cross-spectral analysis and pattern recognition. L. G. Hanscom Field, Bedford, Massachusetts. 7 p. (U. S. Air Force. Cambridge Research Laboratories. Data Science Laboratory. Physical and Mathematical Research Paper no. 367)

Ekman, V. W. 1905. On the influence of the earth's rotation ocean currents. Arkiv för Matematik, Astronomi och Fysik 2(11): 1-52.

Endoh, M. and T. Nitta. 1971. A theory of non-stationary oceanic Ekman boundary layers. Journal of the Meteorological Society of Japan 49(4): 262-266.

Faller, A. J. and R. Kaylor. 1969. Oscillatory and transitory Ekman boundary layer. Deep-Sea Research Vol. 16, sup., p. 54-58.

Fofonoff, N. P. 1969. Spectral characteristics of internal waves in the ocean. Deep-Sea Research Vol. 16, sup., p. 58-71.

Fomin, L. M. 1968. The spectral density of distribution of drifting current velocity in ocean. Atmospheric and Oceanic Physics 4(12): 735-738. (Translated from Fizika Atomosfery I Okeana)

Granger, C. W. J. and M. Hatanaka. 1964. Spectral analysis of economic time series. Princeton, Princeton University Press. 299 p.

Godfrey, M. D. 1965. An exploratory study of the bispectrum of economic time series. Applied Statistics 14: 48-69.

Gonella, J. 1972. A rotary-component method for analyzing meteorological and oceanographic vector time series. Deep-Sea Research 19(12): 833-846.

Hasselmann, K. 1966. On nonlinear ship motions in irregular waves. Journal of Ship Research 10(1): 64-68.

Hasselmann, K., W. Munk and G. J. F. McDonald. 1963. Bispectrum of ocean wave. In: Proceedings of Symposium on Time Series Analysis, ed. by M. Rosenblatt. New York, John Wiley and Son. p. 125-139.

Haubrich, R. A. 1965. Earth noise, 5 to 500 millicycles per second. 1. Spectral stationarity, normality and nonlinearity. Journal of Geophysical Research 70(6): 1415-1427.

Henry, R. F. and P. W. U. Graefe. 1971. Zero padding as a means of improving definition of computed spectra. Ottawa. 10 p. (Canada. Marine Science Branch. Manuscript Report Series no. 20)

Hinich, M. J. and C. S. Clay. 1968. The application of the discrete Fourier transform in the estimation of power spectra, coherence, and bispectra of geophysical data. Reviews of Geophysics 6(3): 347-364.

Huber, P. J., et al. 1971. Statistical methods for investigating phase relations in stationary stochastic processes. IEEE Transactions on Audio and Electroacoustics 19(1): 78-86.

Jenkins, G. M. and D. G. Watts. 1968. Spectral analysis and its application. San Francisco, Holden-Day. 535 p.

Kraus, E. B. 1972. Atmosphere-ocean interaction. Oxford, Clerendon Press. 275 p.

Kraus, W. 1972. On the response of a stratified ocean to wind and air pressure. Deutsche Hydrogrophische Zeitschrift 25(2): 447-472.

Lumley, J. L. 1970. Stochastic tools in turbulence. New York, Academic Press. 199 p.

McDonald, G. J. F. 1963. The bispectra of atmospheric pressure records. In: Proceedings of IBM Scientific Computing Symposium on Statistics. Oct. 21-23, 1963. White Plains, IBM Data Processing Division. p. 247-363.

Mooers, C. N. K. 1970. The interaction of an internal tide with the frontal zone of a coastal upwelling region. Doctoral dissertation. Corvallis, Oregon State University. 480 numb. leaves.

_____. 1973. Cross spectrum analysis of pairs of complex valued time series with application to horizontal velocity time series. Deep-Sea Research 20(12): 1129-1141.

Murty, T. S. and R. F. Henry. 1972. Some Tsunami studies for the west coast of Canada. Ottawa, 79 p. (Canada. Marine Sciences Directorate. Manuscript Report Series no. 28)

Munk, W. and N. Phillips. 1968. Coherence and band structure on inertial motion in the sea. Reviews of Geophysics 6(4): 447-472.

Nagata, Y. 1970. Lag joint probability, higher order covariance function and higher order spectrum. La mer 8(2): 10-25.

Neumann, G. and W. J. Pierson, Jr. 1966. Principles of physical oceanography. New Jersey, Prentice-Hall. 545 p.

Pandolfo, J. P. 1969. Motions with inertial and diurnal period in numerical model of the navificial boundary layer. Journal of Marine Research 24(3): 301-317.

Perkins, H. 1970. Inertial oscillations in the Mediterranean. Doctoral dissertation. Cambridge, Massachusetts Institute of Technology. 123 numb. leaves.

Phillips, O. M. 1966. The dynamics of the upper ocean. Cambridge, Cambridge University Press. 261 p.

Pillsbury, R. D. 1972. A description of hydrography, wind and currents during the upwelling seasons near Newport, Oregon. Doctoral dissertation. Corvallis, Oregon State University. 163 numb. leaves.

Plutchak, N. B. 1972. 1970 TOTEM wind and current data. Corvallis. 61 numb. leaves. (Oregon State University. Department of Oceanography. Reference 72-13)

Pollard, R. T. 1970. On the generation by winds of inertial waves in the ocean. Deep-Sea Research 17(4): 795-812.

Pollard, R. T. and R. C. Millard, Jr. 1970. Comparison between observed and simulated wind-generated inertial oscillation. Deep-Sea Research 17(4): 813-821.

Roden, G. I. and D. J. Bendiner. 1973. Bispectra and cross-bispectra of temperature, salinity, sound velocity and density fluctuations with depth off Northeastern Japan. Journal of Physical Oceanography 3(3): 308-317.

Rosenblatt, M. and J. W. Van Ness. 1965. Estimation of the bispectrum. Annals of Mathematical Statistics 36: 1120-1136.

Sakou, T. 1970. Inertial-period oscillation in response to local atmospheric motion. La mer 8(4): 235-239.

Sakou, T. and S. Neshyba. 1972. The temporal structure of oceanic motion off Oregon Coast, Northeastern Pacific, 1969. Journal of Marine Research 30(1): 1-14.

Tukey, J. W. 1961. What can data analysis and statistics offer today? In: Proceedings of Conference on Ocean Wave Spectra, May 1-4, 1961. Easton, Maryland. New Jersey, Prentice-Hall. p. 347-351.

Van Ness, J. W. 1966. Asymptotic normality of bispectral estimates. Annals of Mathematical Statistics 37: 1257-1272.

Veronis, G. 1956. Partition of energy between geostrophic and non-geostrophic motions. Deep-Sea Research 3(3): 157-177.

Webster, F. 1968. Observations of inertial-period motions in the deep sea. Reviews of Geophysics 6(4): 473-489.

Welch, P. D. 1967. The use of fast Fourier transform for the estimation of power spectra: A method based on time averaging over short, modified periodograms. IEEE Transactions on Audio and Electroacoustics 15(2): 70-73.

White, W. B. 1972. Doppler shift in the frequency of inertial waves observed in moored spectra. Deep-Sea Research 19(8): 595-600.

Wyatt, B., et al. 1972. Hydrographic data from Oregon waters 1971. Corvallis, 77 numb. leaves. (Oregon State University. Department of Oceanography. Reference no. 72-14)

APPENDICES

APPENDIX I

Scalar Representation of the Third Order Spectral Densities of Two-dimensional Random Vector Processes

A. The Fourier Transform of Two-dimensional Vector Time Series

Let $\vec{x}(t)$ be the vector time series representing a two-dimensional vector stationary random process. If $x_1(t)$ and $x_2(t)$ are the scalar component series of $\vec{x}(t)$ resolved along rectangular coordinates ox_1, ox_2, then

$$\vec{x}(t) = x_1(t) + i\, x_2(t) .$$

The Fourier Transform of $\vec{x}(t)$ is (Fofonoff, 1969)

$$\vec{Z}_x(\lambda) = \frac{1}{T} \int_0^T [x_1(t) + i\, x_2(t)]\, e^{-i2\pi\lambda t} dt \qquad \text{(AI-1)}$$

$$= Z_{x1}(\lambda) + i\, Z_{x2}(\lambda) \qquad \text{(AI-2)}$$

where T is the duration of the time series,

λ is the frequency,

$Z_{x1}(\lambda)$ and $Z_{x2}(\lambda)$ are the complex Fourier Coefficients of the scalar component series $x_1(t)$ and $x_2(t)$ respectively.

B. Cross-bispectral Density

If the cross-bispectral density among the vector time series

$x(t)$, $y(t)$ and $z(t)$ is denoted as $VB_{xyz}(\lambda_1, \lambda_2)$, one obtains[15]

$$VB_{xyz}(\lambda_1, \lambda_2)d\lambda^2 = \langle \vec{Z}_x(\lambda_1)\vec{Z}_y(\lambda_2)\vec{Z}_z(\lambda_3) \rangle$$

$$\lambda_1 + \lambda_2 + \lambda_3 = 0 . \qquad \text{(AI-3)}$$

By equations (2) and (3), one can see

$$VB_{xyz}(\lambda_1, \lambda_2)d\lambda^2$$

$$= [\langle Z_{x1}(\lambda_1)Z_{y1}(\lambda_2)Z_{z1}(\lambda_3)\rangle - \langle Z_{x1}(\lambda_1)Z_{y2}(\lambda_2)Z_{z2}(\lambda_3)\rangle$$

$$- \langle Z_{x2}(\lambda_1)Z_{y2}(\lambda_2)Z_{z1}(\lambda_3)\rangle - \langle Z_{x2}(\lambda_1)Z_{y1}(\lambda_2)Z_{z2}(\lambda_3)\rangle]$$

$$+ i[-\langle Z_{x2}(\lambda_1)Z_{y2}(\lambda_2)Z_{z2}(\lambda_3)\rangle + \langle Z_{x1}(\lambda_1)Z_{y1}(\lambda 2)Z_{z2}(\lambda_3)\rangle$$

$$+ \langle Z_{x2}(\lambda_1)Z_{y1}(\lambda_1)Z_{z1}(\lambda_3)\rangle + \langle Z_{x1}(\lambda_1)Z_{y2}(\lambda_2)Z_{z1}(\lambda_3)\rangle]$$

$$\lambda_1 + \lambda_2 + \lambda_3 = 0 . \qquad \text{(AI-4)}$$

Using the definition of cross-bispectral density, it follows that

$$VB_{xyz}(\lambda_1, \lambda_2)$$

$$= [B_{x1y1z1}(\lambda_1, \lambda_2) - B_{x1y2z2}(\lambda_1, \lambda_2)$$

---

[15] In manner analogous to the definition of cross-spectral density among real random process (see equation (26) of Chapter III), except that the Fourier coefficients are used in place of the Fourier Stieltjes Integrals. A similar replacement as been used by other authors in their estimation of bispectral density (Hinich and Clay, 1968; Huber et al., 1971; etc.)

$$- B_{x2y2z1}(\lambda_1, \lambda_2) - B_{x2y1z2}(\lambda_1, \lambda_2)]$$

$$- i [B_{x2y2z2}(\lambda_1, \lambda_2) - B_{x1y1z2}(\lambda_1, \lambda_2)$$

$$- B_{x2y1z1}(\lambda_1, \lambda_2) - B_{x1y2z1}(\lambda_1, \lambda_2)]$$

$$\lambda_1 + \lambda_2 + \lambda_3 = 0 \ , \qquad \text{(AI-5)}$$

where $B_{xjyjzj}(\lambda_1, \lambda_2)$, $j = 1, 2$, are the cross-bispectral densities among the scalar component series of $\vec{x}(t)$, $\vec{y}(t)$ and $\vec{z}(t)$ and they are all independent functions.

C. Bispectral Density

If all the three vector random processes are the same, equation (AI-5) is the scalar representation of the bispectral density of the vector random process and has the following form

$$VB(\lambda_1, \lambda_2)$$

$$= [B_{111}(\lambda_1, \lambda_2) - B_{122}(\lambda_1, \lambda_2) - B_{212}(\lambda_1, \lambda_2) - B_{221}(\lambda_1, \lambda_2)]$$

$$- i[B_{222}(\lambda_1, \lambda_2) - B_{112}(\lambda_1, \lambda_2) - B_{211}(\lambda_1, \lambda_2) - B_{121}(\lambda_1, \lambda_2)]$$

$$\lambda_1 + \lambda_2 + \lambda_3 = 0 \qquad \text{(AI-6)}$$

where $B_{111}(\lambda_1, \lambda_2)$ and $B_{222}(\lambda_1, \lambda_2)$ are the bispectral density of the

scalar component series the rest are the cross bispectral densities among the various scalar component series. Due to the symmetrical relation of the cross-bispectral density discussed in Chapter III, equation (AI-6) has only six independent terms, i.e.,

$$VB(\lambda_1, \lambda_2) = [B_{111}(\lambda_1, \lambda_2) - 2B_{122}(\lambda_1, \lambda_2) - B_{221}(\lambda_1, \lambda_2)]$$

$$- i[B_{222}(\lambda_1, \lambda_2) - 2B_{211}(\lambda_1, \lambda_2) - B_{112}(\lambda_1, \lambda_2)]$$

(AI-7)

APPENDIX II

Estimation Procedures of the Rotary Spectral, Rotary Cross-spectral, Rotary Bispectral and Rotary Cross-bispectral Functions

A. Editing the Data

For practical reasons, the existing data of two-dimensional vector random process are often recorded in the form of a finite length discrete time series of their resolved scalar components or of their magnitude and directions. Since rotary Fourier coefficients are obtained from the linear combinations of the cosine and sine Fourier coefficients of the scalar components and since their amplitudes are independent of the coordinates along which the scalar components are resolved, data should be in the form of resolved scalar component series along E-W (ox_1) and N-S (ox_2) directions with E, N designated as the positive axes. The choice of coordinates is arbitrary; to be consistent, conventional notation is used. For the sake of saving computation effort, the cosine and sine Fourier coefficients are computed with the help of the relatively new, fast Fourier transform algorithm (Welch, 1967). Also, in order to increase the number of degrees of freedom of the estimates of various functions, (i.e., to ensure the proper statistical stability), each data record is broken into several truncations, from which the averaged

estimated functions are obtained (Haubrich, 1965; Hinich and Clay, 1968; Huber et al., 1971). Therefore, the data records have to be edited to achieve the proper estimation with less computational expense.

1. Rearranging the data interval and removal of the mean

The data sampling interval should be of proper length so that the Nyquist frequency will not be excessively higher than the upper limit of the frequency range of interest. This can be done with either a block average of several closely spaced data values or with a weighted moving average technique. The latter method is a combination of low pass filtering and averaging. With properly chosen weighting coefficients, the aliases can be avoided. However, certain data points on both ends of the record will be sacrificed. Then the mean of the data should be removed in order to be consistent with the assumption that the random process has zero mean.

2. Adjusting the data record

The data record may have to be adjusted to provide the proper number of truncations so that the averaged function estimates can have proper equivalent degrees of freedom. Because of the requirements of the Fast Fourier transform, the number of data points in each truncation must be a power of two. In order to have the proper

number of truncations, it may be necessary to adjust the data length by either adding zeros at the end of each truncation (Henry and Graefe, 1971) or by overlapping a part of data in each truncation (Haubrich, 1965; Welch, 1967; Huber et al., 1971). The latter method is proposed in this study because the equivalent degrees of freedom EDF of the spectral estimates from the overlapping truncated data can be calculated explicitly (Welch, 1967). Let $x(t)$, $t = 0, \ldots N-1$ be the finite discrete time series of a random process $x(t)$. If $x(t)$ has a record length of T and a data interval of Δt, the total number of data points N is $T/\Delta t$. Overlapping can be done by taking truncations of length $m\Delta t$ (m data points in each truncation) with the starting point D data points apart. Then the truncated data is represented as

$$x(k, j) = x(j + (K-1)D) \quad j = 0, \ldots N-1$$
$$k = 1, \ldots K \qquad \text{(AII-1)}$$

where k is the total number of the truncations.

$$K = \left(\frac{N}{M} - 1\right)\frac{M}{D} + 1 \qquad \text{(AII-2)}$$

There are M-D data points overlapped in each truncation. If no overlapping is allowed, one simply lets D equal M. Then equation (AII-2) becomes $K = N/M$ (Welch, 1967).

3. Applying weighting function to the truncated data

This modification can reduce the leakage of spectral power from a spectral peak to frequencies far away (Haubrich, 1965; Welch, 1967; Huber et al., 1971). However, weighting the data not only will degrade the frequency resolution but also changes the expectations and the variances of the spectral estimates (Huber et al., 1971). Since the data available for this study are already limited in length this technique will not be used for the sake of keeping adequate frequency resolution.

B. Approximating the Rotary Fourier Coefficients of the Truncated Data

For each truncation of M data values, $(1 + M/2)$ number of the rotary Fourier coefficients, with the frequencies ranging from zero up to Nyquist, can be obtained from the linear combinations of the sine and cosine Fourier coefficients of the resolved scalar components in that truncation.

Let $u_1(k, j)$ and $u_2(k, j)$ be the scalar components of the kth truncation. Then the discrete fast Fourier transform is

$$Z_p(k, \lambda) = \frac{1}{M} \sum_{j=0}^{M-1} u_p(k, j) W(j) e^{-i2\pi jq/M}$$

$$p = 1, 2 \quad ; \qquad q = 0, \ldots, \frac{M}{2} \qquad \text{(AII-3)}$$

(Welch, 1967)

where, $Z_p(k, \lambda)$ is the complex Fourier coefficient; λ is the frequency of cycle per data interval CPH and $\lambda = q/M$; $W(j)$ is the weighting function or data window. If no weighting function is used, then $W(j) = 1$, for $j = 0, \ldots, M-1$. Physically $Z_p(k, \lambda)$ represents the amplitude and the phase of the qth frequency component of the scalar components; the resolved frequency band of the component is $1/M\Delta t$ CPD if no data window is applied[16]. The cosine and sine coefficients of $u_p(k, j)$ are the real and imaginary parts of $Z_p(k, \lambda)$ respectively by definition. Thus

$$A_p(k, \lambda) = \mathrm{Re}[Z_p(k, \lambda)]$$

$$B_p(k, \lambda) = \mathrm{Im}[Z_p(k, \lambda)] \qquad \text{(AII-4)}$$

By equation (35), the rotary Fourier coefficients of the truncated data $u(k, j)$ are

$$U_+(k, \lambda) = [A_1(k, \lambda) + B_2(k, \lambda)] + i[A_2(k, \lambda) - B_1(k, \lambda)]$$

$$U_-(k, \lambda) = [A_1(k, \lambda) - B_2(k, \lambda)] + i[A_2(k, \lambda) + B_1(k, \lambda)]$$

(AII-5)

---

[16] The definition of the discrete Fourier transform is not uniform in the literature. Some authors use a quantity equivalent to $Z(\lambda)M\Delta t$ or $Z(\lambda)(M\Delta t)^{1/2}$, others use a positive exponent instead of a negative one (Jenkins and Watts, 1968; Hinich and Clay, 1968). These variants appear not only in magnitude but also in physical meaning. For example, the quantity $Z_p(\lambda)(M\Delta t)$ represents the distribution of $u_p(t)$ per resolved frequency band, and $Z_p(\lambda)(M\Delta t)^{1/2}$ represents the distribution of $u_p(t)$ per square root of the resolved frequency band. For the purpose of consistency with the derivation, the coefficients of DFT defined as given in equation (AII-3).

C. Computing the Spectral Estimates

Once the rotary Fourier coefficients are calculated, computing the spectral estimates is fairly straightforward. Using the definitions given before, the formulae for computing various spectral estimates are given in the following equations.

For a single vector random process, x(t)

$$\hat{P}_{x\pm x\pm}(\lambda)d\lambda = \frac{1}{K}\sum_{k=1}^{K}\left| U(k,\lambda)\right|^2 \qquad \text{(AII-6)}$$

$$\hat{R}B(\pm\lambda_1, \pm\lambda_2)d\lambda^2 = \frac{1}{K}\sum_{k=1}^{K} U_{x\pm}(k,\lambda_1)\, U_{x\pm}(k,\lambda_2)\, U_{x\pm}{}^{*}(k,\pm\lambda_3)$$

$$\pm\lambda_1 \pm\lambda_2 = \pm\lambda_3 \qquad \text{(AII-7)}$$

$$\hat{R}B(\pm\lambda_1, \pm\lambda_2) = \left|\hat{R}B(\pm\lambda_1, \pm\lambda_2)\right| e^{iR\phi(\lambda_1, \lambda_2)} \qquad \text{(AII-8)}$$

$$\hat{R}bic^2(\pm\lambda_1, \pm\lambda_2) = \frac{K\left|\sum_{k=1}^{K} U_{x\pm}(k,\lambda_1)\, U_{x\pm}(k,\lambda_2)\, U_{x\pm}{}^{*}(k,\lambda_3)\right|^2}{\sum_{k=1}^{K}\left|U_{x\pm}(k,\lambda_1)\right|^2 \sum_{k=1}^{K}\left|U_{x\pm}(k,\lambda_2)\right|^2 \sum_{k=1}^{K}\left|U_{x\pm}(k,\lambda_3)\right|^2} \qquad \text{(AII-9)}$$

where ^ denotes estimating value.[17]

[17] More sophisticated average procedures are suggested by Huber et al. (1971) for their study of ordinary bispectral analysis. But these procedures need too lengthy a data record and too much computing time to be used in this study.

In the case of multiple random processes, let $U_{x\pm}(k, \lambda)$, $U_{y\pm}(k, \lambda)$, $U_{z\pm}(k, \lambda)$ represent the rotary Fourier coefficients of their truncated data. Then

$$\hat{P}_{x\pm y\pm}(\lambda)d\lambda = \frac{1}{K}\sum_{k=1}^{K} U_{x\pm}(k, \lambda)\, U_{y\pm}^{*}(k, \lambda) \qquad \text{(AII-10)}$$

$$\hat{R}B_{xyz}(\pm\lambda_1, \pm\lambda_2)d\lambda^2$$

$$= \frac{1}{K}\sum_{k=1}^{K} U_{x\pm}(\lambda_1)\, U_{y\pm}(\lambda_2)\, U_{z\pm}^{*}(\lambda_3)$$

$$\pm\lambda_1 \pm\lambda_2 = \pm\lambda_3 \qquad \text{(AII-11)}$$

$$\hat{R}bic^2{}_{xyz}\pm\lambda_1, \pm\lambda_2)$$

$$= \frac{K\left|\sum_{k=1}^{K} U_{x\pm}(k, \lambda_1)\, U_{y\pm}(k, \lambda_2)\, U_{z\pm}^{*}(k, \lambda_3)\right|^2}{\sum_{k=1}^{K}\left|U_{x\pm}(k, \lambda_1)\right|^2 \sum_{k=1}^{K}\left|U_{y\pm}(k, \lambda_2)\right|^2 \sum_{k=1}^{K}\left|U_{z\pm}(k, \lambda_3)\right|^2}$$

(AII-12)